UNIVERSIDAD POLITÉCNICA DE CARTAGENA
Departamento de Electrónica, Tecnología de Computadores y Proyectos

Organic solar cells: life cycle assessment as a research tool to reduce payback time and environmental impacts

Nieves Espinosa Martínez

Junio 2012

UNIVERSIDAD POLITÉCNICA DE CARTAGENA
Departamento de Electrónica, Tecnología de Computadores y Proyectos

Organic solar cells: life cycle assessment as a research tool to reduce payback time and environmental impacts

Nieves Espinosa Martínez

Dirigida por:

Dr. Antonio Urbina Yeregui
Dr. Rafael García Valverde

Junio 2012

A mi madre, *in memoriam*

Acknowledgements

I am grateful to the people that have helped me in the last four years. I want to first acknowledge very deeply Antonio Urbina Yeregui for the outstanding opportunity he has given to me, his unconditional support whenever I needed, scientifically but personally as well. Despite difficulties, he has wisely advised me in taking decisions, and struggled to smooth the way for me. Thanks Antonio.

Rafael García Valverde, cosupervisor of this work, deserves a big thank. He helped me to discover by myself the most important skills in research to succeed: steadfastness, effort and good planning of resources and time. He has been always there as a Telemachus, as a colleague but as a friend too.

The UPCT team with Rafa, Jose, Javi, Antonio, Lucía and Juan Gabriel made my PhD period easier and happier. I would like to show my gratitude to them, they have helped me to work out many times; thanks for this high level support. Technical and administrative supports, as well as warmth, were given from Mamen and David, who I want to remember here.

At UMU, there have also been people such as Cati, Juani and Jose that shared with me fun, happiness but also concerns in our PhD periods.

The LCA part of this thesis, the core actually, has been possible to the stay in Denmark at Risø DTU in 2010. It was a privilege to be there, where I

also felt warmly received from Frederik C. Krebs team. Thanks to his generosity, that I couldn't be grateful enough, I took off and learnt that mankind problems related to energy have to be undertaken, that it is necessary to give back the society the resources invested in research, and that we all owe it.

A mi familia, abuelos, tíos y hermana, muchas gracias por vuestro cariño, y por apoyarme incondicionalmente en cualquier proyecto en que me embarco. Este trabajo está dedicado a la memoria de mi madre.

A Paco un gracias muy especial por ser capaz de hacerme sentir optimismo en todas las situaciones de mi vida. Es una suerte poder vivirlas contigo.

Finally, this thesis has been realized thanks to the support of the -extinct now- Spanish Ministry of Science and Innovation through the Consolider Project HOPE (CSD2007-00007), and thanks to support of the Comunidad Autónoma de la Region de Murcia through the project CARM-D429-2008).

Nieves Espinosa

Cartagena, April 2012

Abstract

In view of the world energy panorama, modern societies are urged to rethink and redesign the energy model into a more sustainable one if they want to preserve an ecological balance. Renewable energies as low-carbon technologies can tackle climate change targets. Sunlight in particular, as the most abundant resource and sustainable resource, is a possible solution.

Among the existing photovoltaic technologies, organic photovoltaics (OPV) has evolved in an exponential way in the last five years exhibiting a large potential. Despite that there are still important challenges to overcome, there is an active research in this subject that has enabled for example that the efficiency of the devices has increased by a factor of 10 during the last decade. These progress lead to expect fast, cheap and low environmental impact production methods.

In this thesis, OPV devices have been prepared by different methods and the great potential of this technology has been quantified through life cycle assessment (LCA) methods. LCA studies on production of printed polymeric modules at semi industrial scale have been carried out, showing promising results.

The studies have sought to establish the parameters that are critical for the beneficial use of polymer solar cells in society and to firmly demonstrate where the potential of the polymer solar cell technology is.

Contents

List of Figures

List of Tables

Nomenclature & Units

AM: Air Mass

AZO: aluminium zinc oxide

EPBT: energy payback time

EPE: equivalent primary energy

EPIA European Photovoltaic Industry Association

ERF: energy return factor

EROI: energy return of investment

ETL: electron transport layer

EU: European Union

EQE: external quantum efficiency

ITO: Indium Tin oxide

FF: filling factor

FTO: Fluor tin oxide

GDP: gross domestic product

GWP Global Warming Potentials

HIL: hole injector layer

IEA: International energy agency

IPCC Intergovernmental Panel on Climate Change

I_{sc}: short circuit current

ITO: indium tin oxide

GJ: gigajoule (1 joule x 10^9)

GW: gigawatt (1 Watt x 10^9)

GWh: gigawatt-hour

Ktoe: kilo tonne of oil equivalent

kV: kilovolt

kW: kilowatt (1 Watt x 10^3)

kWel: kilowatt electrical capacity

kWh: kilowatt-hour

kWth: kilowatt thermal capacity

J_{sc}: short circuit density (I/Area)

LCA: life-cycle analysis

LCI: life-cycle inventory

LCIA: life-cycle impact assessment

LED: led emitting diode

MW: megawatt (1 Watt x 10^6)

MWh: megawatt-hour

n: ideality factor

OPV: organic photovoltaics

OSC: organic solar cells

PEDOT: polyethylene dioxythiophene

P3HT: poly-3-hexylthiophene

PCBM: phenyl-C61-butyric acid methyl ester

PET: polyethylene terephthalate

P_{mpp}: Maximum power point

PV: photovoltaics

R2R: roll-to-roll

TJ: terajoule

toe: tonne of oil equivalent

TW: terawatt (1 Watt x 10^{12})

TWh: terawatt-hour

UN: United Nations

V_{oc}: open circuit voltage

QE: Quantum Efficiency

CHAPTER 1
Proem

Planet Earth reached 7 billion people in 2011, and population will go up by 1.5 billion by 2030, and energy's supply and availability are among the most challenging problems mankind will have to face. The depletion of the main energy source, fossil fuels, is a serious problem: once they are completely used up we cannot produce more, they have no replacement as such. Moreover, as a consequence of the use of fossil fuels, emissions are released to the environment that can accelerate climate change. Energy Renewable sources provide a feasible solution to overcome these problems.

1.1. Motivation

Energy is a growing problem and it will therefore be top of the list of man's challenges over the next several decades will be therefore the energy. We need a world that has enough energy to provide growth and development; that this energy comes from sources we can rely on, and make it safely compatible with health and environment. We need energy that is affordable, secure and sustainable. The solutions are not secret or mysterious. Globally we get $4 \cdot 10^{18}$ joules of primary energy from the sun. Solar energy and in particular photovoltaics can certainly be part of a real sustainable alternative to conventional electricity production.

1.2. World energy panorama

The projected increase in the world energy demand (in Figure 1.1) will cause a severe shortage in the reserves of fossil fuels since it will require an increase in energy production capacity, but this can imply as well uncertainty concerning the supply. World energy demand especially under the form of electricity is expected to grow more sharply than any other final form of energy (*World Energy Outlook*, 2010).

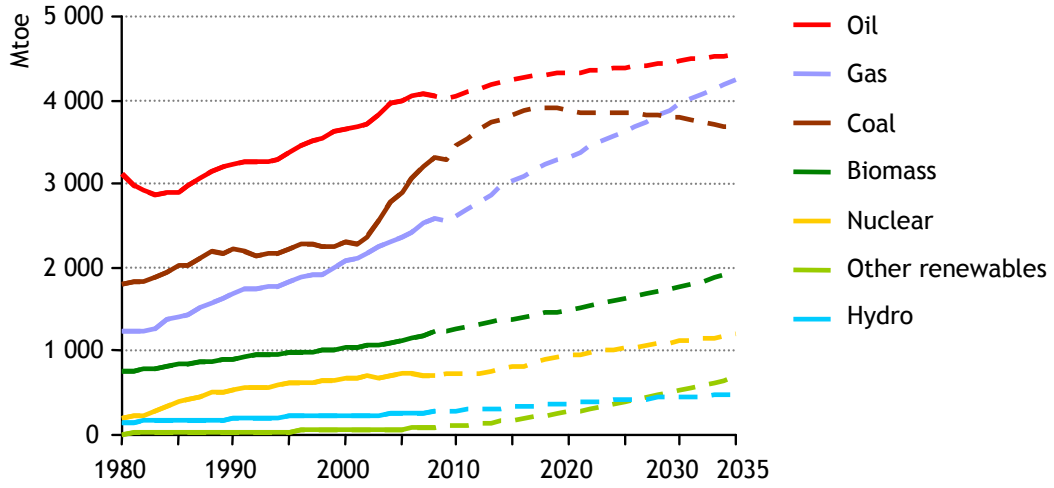

Figure 1.1. World primary energy demand by fuel projected by 2035 from IEA, assuming GAS Scenario[1] ("The Golden Age of Gas Scenario," 2011).

Global energy consumption grows every year, having had in 2010 the strongest growth since 1973: a 5.6%, where a remarkable 20.3% is China's share in this global consumption. World population is increasing but it is not responsible for such growth in energy consumption, as can be seen in Figure 1.2. By 2030, a 40% increase in energy demand is expected globally, where 96% will be from emerging economies, and fossil fuels will provide around 80% of this world's energy (BP Statistical Review of World Energy, 2011).

[1] GAS Scenario adopts the same population and economic growth assumptions as the New Policies Scenario in WEO-2010.

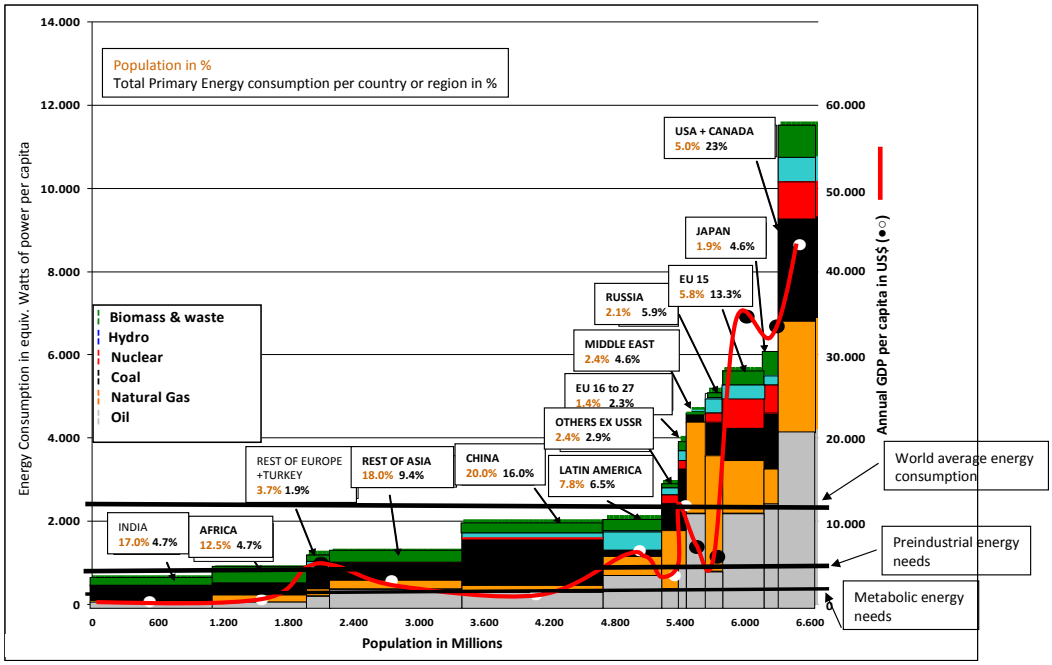

Figure 1.2. Worldwide energy consumption versus population in 2007. Source: BP Statistics 2007.

Oil represents globally 33% of the primary energy according to IEA. Particularly, in Spain, where $5.98 \cdot 10^{18}$ joules of primary energy were consumed in 2010, oil and derivatives represent around 50% of the total primary energy, of which, more than 90% is imported (Figure 1.3).

There are nevertheless some estimates indicating that oil consumption rate is decreasing in developed countries. We are in a situation of rapid lowering in energy consumption, neither searched nor planned, but forced and driven by the ever-growing prices. A roadmap towards GDP growth with less energy intensity is strongly needed, and some countries have already achieved this goal: energy intensity growth has been reduced, contrary to general assumption, in the two main economies of the world: USA and China. In this latest case, energy intensity has been reduced by 4.6% from 2005 to 2010 (Brown et al., 2012)

1.2.1. The need for replacing fossil fuels

Three main reasons explain the need for replacing fossil fuels. First, fossil resources are limited and in some cases scarce. In the second place they contribute to climate change because their combustion release greenhouse gases, and last –but not least- they provoke geopolitical issues since they are not a distributed energy source.

Finitude

The combustion of limited fossil fuels represents approximately 85% of global energy use today -IEA (*World Energy Outlook*, 2010). To cover part of such consumption, EU imports oil to a value of approximately 1 billion € every day (based on oil price Feb. 2012). The time when fossil fuels will run out is highly uncertain; however, it is likely to occur that it becomes unaffordable due to the fact that costs of extractions will enormously increase.

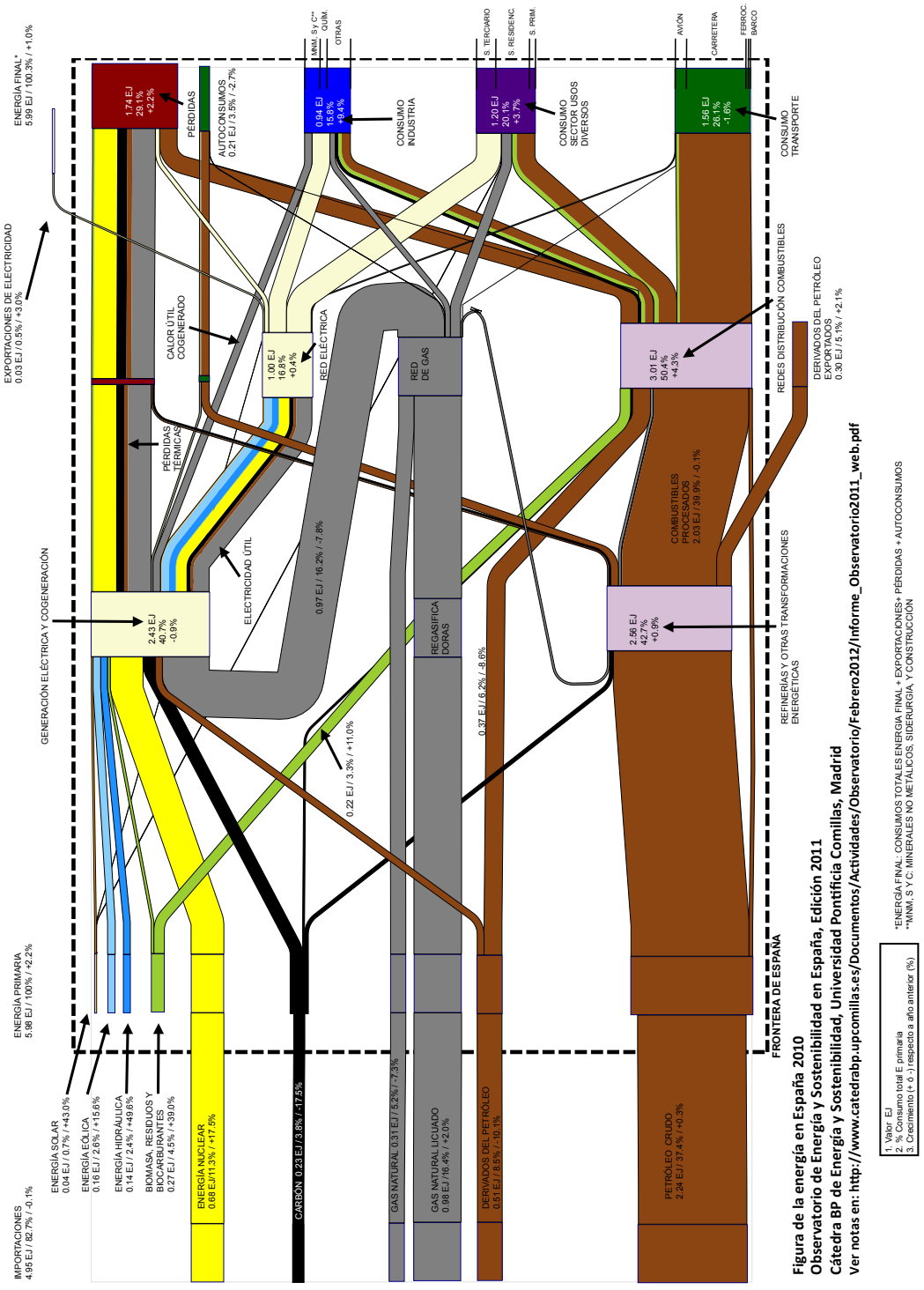

Figure 1.3. Sankey diagram for energy flux in Spain in 2010, elaborated by (López-Peña et al., 2012).

Oil is getting more and more expensive and scarce. In the 1980s for the first time, humanity started to consume more oil than was discovered per year. According to the Association of Peak Oil (ASPO), there is a peak in the production of oil and this peak has already been surpassed in many countries. From 2005 onwards, conventional crude-oil production has not risen to match the increasing demand. In Figure 1.4, the dropping rate at which oil is discovered globally is shown -in

blue- and the projections -in green-, point out that it will drop off even more sharply in future years. However, the rate of worldwide oil consumption is still rising -red line.

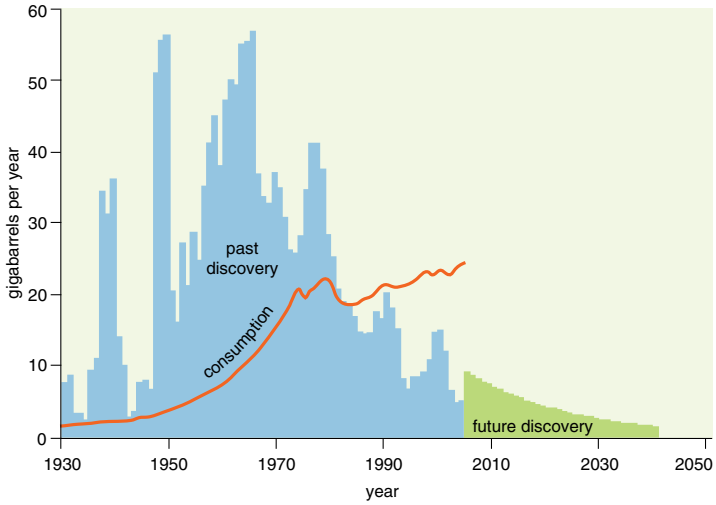

Figure 1.4. Discovered oil histogram globally (blue), and projected drop off of future discoveries (green). The rate of worldwide consumption, in red line is rising (Hall et al., 2009).

Economy and energy consumption have, despite particularities, a large number of similitudes. When in the 1990s scarcity started to be felt in the oil market, the price correction mechanism reacted, as shown in Figure 1.5. Therefore, prices have risen according to the standard economic theory that they stimulate production, but for crude oil the price mechanism has failed: the higher prices made production profitable, but the production costs rose. Over a certain price, production didn't respond any more: it became "inelastic" (Murray et al., 2012). That explains why, despite the new and more sophisticated extraction technologies, the gap between oil supply and demand is today widening. Nevertheless, increasing prices make it profitable to exploit oil fields in remote areas, deep ocean platforms or heavy oil reserves, all of which poses much higher environmental risks for its extraction.

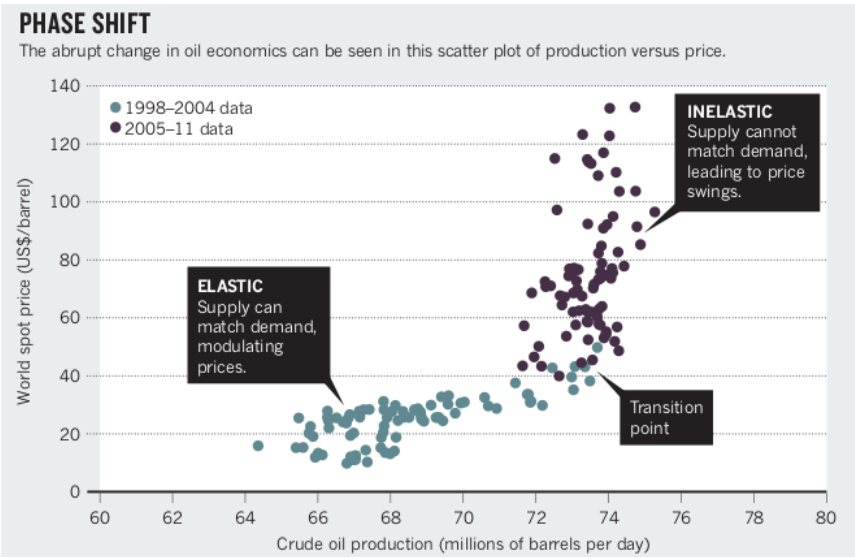

Figure 1.5. Phase shift in oil economics, world's oil price versus crude production. Source: (Murray et al., 2012).

Global warming issues

Climate change and fossil fuels are closely linked as well. As a consequence of the use of fossil fuels, emissions are released to the environment. Global emissions are expected to rise 30% by 2030 (BP Statistical Review of World Energy, 2011).

Climate protection plays a particularly important part in the transformation towards sustainability, as it is a condition *sine qua non* for sustainable development. But international post-Copenhagen climate policies are in *crisis*. In Copenhagen Accord, adopted at the UN Climate Change Conference (December 2009), an overwhelming majority of countries reaffirmed that climate change is one of the greatest challenges of our time and that the increase in average global temperature should be kept below 2 degrees Celsius.

Skepticals of anthropogenic global warming contend that these claims are not sufficiently demonstrated. However, the prediction models that serve as a foundation for the previous statement have been run many times. Actual temperature increases have been predicted and then compared for two cases accounting for all sources including anthropogenic changes (case 1) and accounting for natural sources alone (case 2). This experiment, described in the Fourth Assessment Report of the Intergovernmental Panel on Climate Change (IPCC) (*Climate Change 2007*, 2007), has been performed many times using climate models. The results show that the projections of climate models are consistent with recorded temperature trends over recent decades, but only if human impacts are included. The divergent trend is especially pronounced after 1980. By 2005, calculations using natural sources alone underestimate the actual temperature increases by about 0.7ºC, while the calculations including human sources match very closely the actual temperature trend.

Some institutions have projected that consequences and social costs will appear in less than three decades if we do not replace fossil fuels; if we continue as such with this carbonisation level. As shown in Figure 1.6, the goal of the transformation is a low-carbon society. Central to the transformation is the decarbonisation of energy systems. Proactive states and change agents are the key players that must move away from a marginalised existence and increase their impact through widespread inclusion in social routines, it is therefore a global cooperation. Furthermore, the cost of a transition to a low-carbon society will be large, but less than the cost of climate change consequences if the business as usual model is kept for the next decades (Stern, 2006).

Geopolitical issues

Today, energy is an instrument of geopolitical rivalries, like nuclear power during the Cold War. Gas and oil are in competition and influence countries relationships. In EU, 85% of gas is imported from Norway, Russia and Algeria. Crude oil comes to EU from the Middle East, Africa, South and Central America, mainly. This is known as monopsony: a market situation in which there is only one buyer. This situation has created a new *energetic diplomacy* that has to deal with political tensions, which could risk the security in the supply. At the beginning of 2012, EU has formally adopted an "unprecedented" oil embargo

against Iran over its nuclear programme, banning all new oil contracts with the country ("EU approves Iran oil imports ban," 2012).

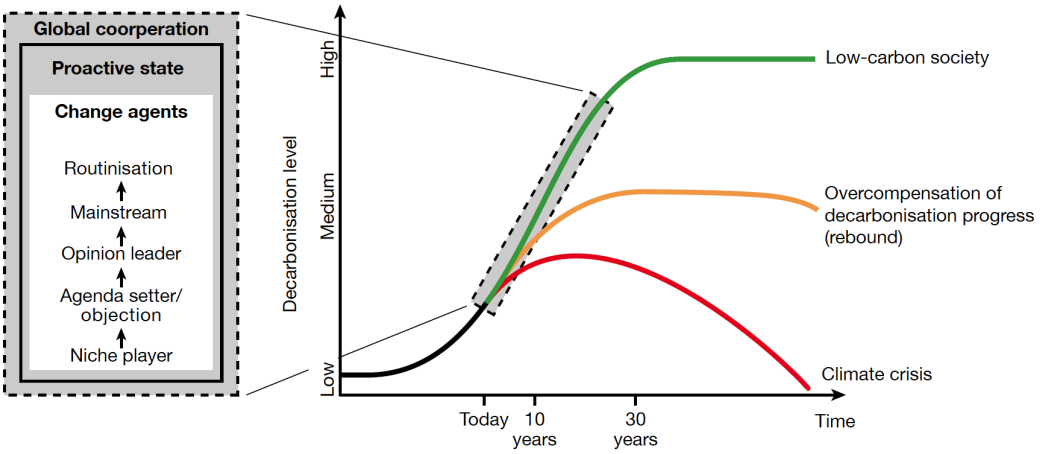

Figure 1.6. Transition costs as a function of the decarbonisation level. The sustainable path (green) with a transition to low-carbon society. A failed transformation, with overcompensation for decarbonisation advances could lead to ineffective climate protection measures (yellow). Moderate endeavours carry the risk of leading to a global climate crisis (red). Source: (German Advisory Council on Global Change (WBGU), 2011).

China's hunger for energy is enormous; its energy consumption is 50% based on coal (International Energy Agency, 2011), but it has also entered recently in gas battles in Central Asia, by financing Iranian pipelines; it will start importing Iranian gas supplies by 2015.

Africa is struggling with these issues as well, immersed in the middle of international interests in its *black gold*, since new oilfields that accounted for 9.5% share of total oil reserves at the end of 2010, have been discovered in e.g. Libya, Nigeria and Angola (BP Statistical Review of World Energy, 2011).

In view of all these reasons, we are urged to rethink and redesign the energy model into a more sustainable one; starting from seeking for secure resources, the use of low-carbon technologies and the employ of more efficient technologies. Renewables are low-carbon technologies that can tackle climate change targets and play a central role in reducing the uncertainty due to the fact they are distributed resources that are available worldwide.

1.3. The renewable revolution

The European Union has committed to increase the total renewables share to 20%, to cut greenhouse gas emissions by 20%, and achieve 20% more energy efficiency by 2020 with the 20-20-20-20 initiative. The renewable energy share would be as depicted in Figure 1.7. The 20% target for renewable energy sources (RES) should be developed further with a view to achieving 100% electricity provision by mid-century: renewables shares of 85–100 % in the electricity sector (Krewitt et al., 2009; Coopers, 2010) and 60 % of primary energy (Krewitt et al., 2009) covered by RES are feasible.

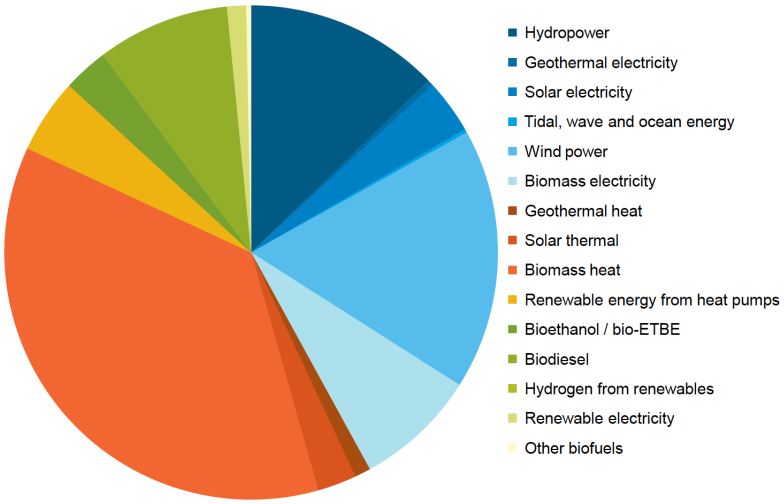

Figure 1.7. Renewable energy share in EU-27 by 2020: 20.7% (target 2020: 20%). Source: (Beurskens et al., 2011) European Environmental Agency.

As seen in Figure 1.8, in 2010, hydro, wind, solar and geothermal quota of the electricity generation span from 95.7% from hydro in Norway -where 2 million barrels of oil are produced yearly- to 5% of Korea, where 46% of electricity is produced from coal (International Energy Agency, 2011).

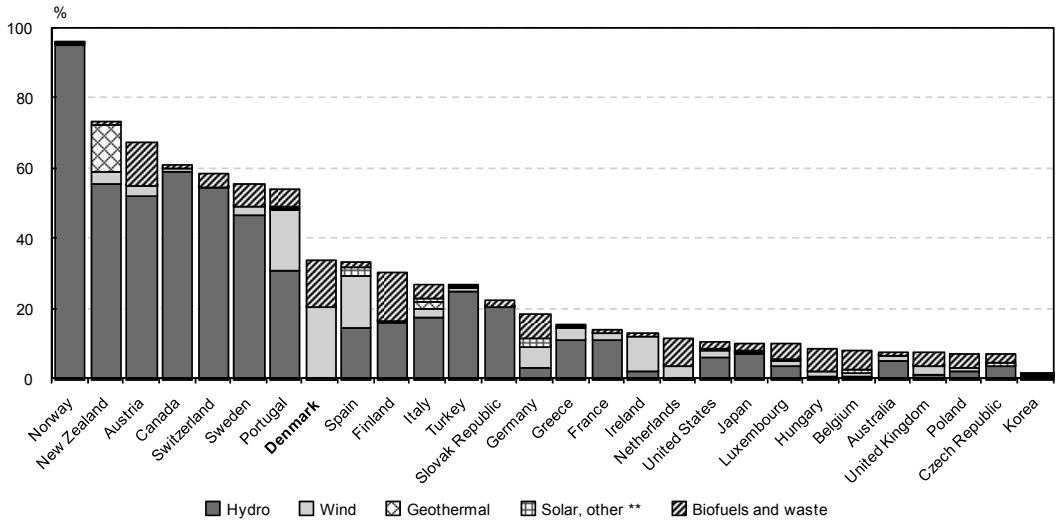

* Estimates.

Source: *Energy Balances of OECD Countries*, IEA/OECD Paris, 2011.

Figure 1.8. Electricity generation from renewable energy as a percentage of all generation in IEA member countries in 2010.

The systems are installed where there are premium tariffs, subsidies, tax exemptions, tax holidays or fiscal benefits: nearly $66 billion in economic incentives were spent worldwide on renewable energy in 2010, less than a fifth of the $409 billion in fossil-fuel subsidies the same year (International Energy Agency, 2011). While 92% of the installed RES power has taken place in developed countries, a scarce 8% has been in emerging countries. Still, 1,600 million people in the world lack access to electricity. This figure, even for an increasing access to electricity scenario, will still be high by 2020 (around 1,400 million) because of population growth (Legros et al., 2009).

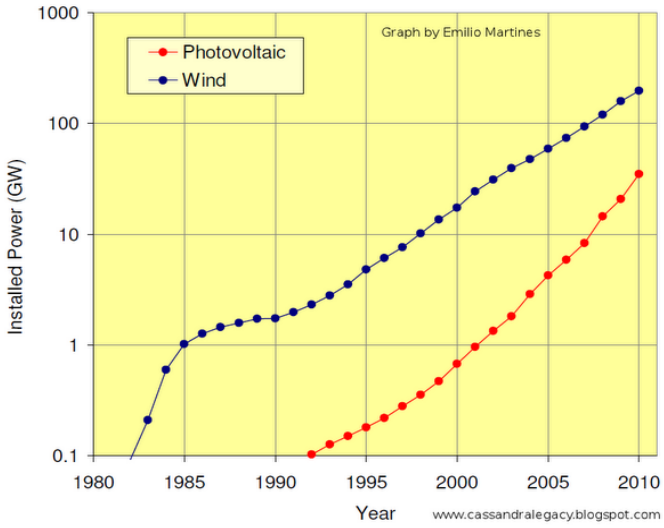

Figure 1.9. Worldwide growth of PV and wind energy installed power per year. Data from IEA Photovoltaic Power Systems Programme, by Emilio Martines. Note the log scale in the Y-axys.

From all renewable sources, solar energy has experienced the largest growth in the past 50 years. As shown in Figure 1.9, the growth of photovoltaic and wind energy has been impressively fast during the past three decades. According to the graph, wind power has grown as a factor 10 in less than 10 years; PV power takes around 5 years.

Following these trends, wind and photovoltaics could reach around 2020 one terawatt (TW) each. Despite the capacity factor of PV, or wind, it is smaller than that of conventional sources -so that one TW of renewable power can produce considerably less energy than one TW of a conventional fuel plant- the data are impressive, considering that the total electric power installed in the world today is around 2 TW.

The strength of RES is as mentioned before, their availability; but it also demand's matching. Wind and solar energy are difficult to predict, although sophisticated short-term weather broadcast models are being developed. PV matches better -when available- with the daily peak consumption in commercial and industrial electric sectors.

There is an energy revolution going on: renewable power has a market and it is growing.

1.4. Photovoltaic energy

The total installed capacity in the world now amounts to around 40 GW_p, producing some 50 terawatt-hours (TWh) of electrical power every year. Over the last 10 years, progress has been impressive (Figure 1.10). The total installed PV capacity in the world has multiplied by a factor of 27, from 1.5 GW in 2000 to 39.5 GW in 2010 -a yearly growth rate of 40%.

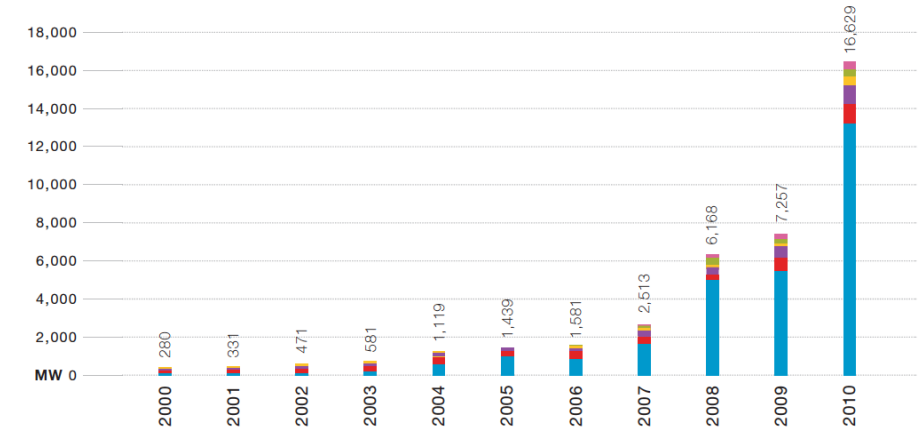

	2000	2001	2002	2003	2004	2005	2006	2007	2008	2009	2010
China	0	11	15	10	9	4	12	20	45	228	520
APEC	5	5	7	8	10	13	33	59	300	258	473
Rest of the world	88	56	80	77	29	10	118	63	115	130	417
North America	23	31	46	65	92	117	149	212	349	539	983
Japan	112	135	185	223	272	290	287	210	230	483	990
EU	52	94	139	199	707	1,005	983	1,950	5,130	5,619	13,246
Total	**280**	**331**	**471**	**581**	**1,119**	**1,439**	**1,581**	**2,513**	**6,168**	**7,257**	**16,629**

Figure 1.10. Evolution of global PV power installed from 2000 to 2010. Source: European Photovoltaic Industry Association (EPIA), 2011.

2010 was the record year, where Europe's photovoltaic sector installed more capacity than any other renewable source, with 13 GW_p of new installed power in the EU, where 7.4 GW_p were installed in Germany (Figure 1.11). The country continues to dominate the PV market world-wide (European Photovoltaic Industry Association (EPIA), 2011, Observer, 2011).

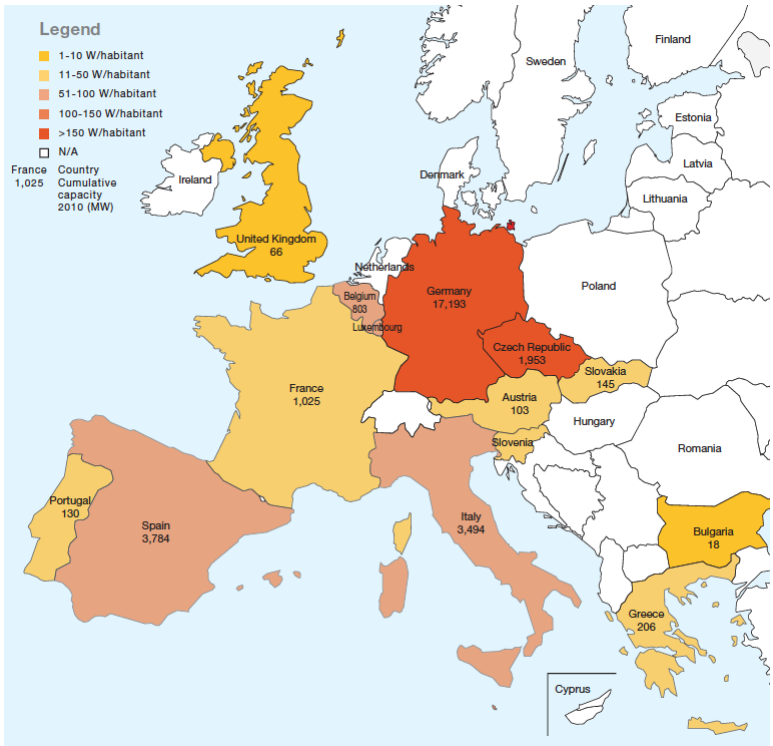

Figure 1.11. Europe PV power map. (European Photovoltaic Industry Association (EPIA), 2011).

Switching to PV is not just a realistic option for tomorrow's energy mix; it is also a desirable solution for society as a whole. PV markets are stronger than ever, and PV now appears on the energy map of several countries as a real alternative to conventional electricity sources. For example in Spain, PV provided up to 4% of the electricity demand during the summer in 2010 (REE, 2012) .

Next reports in European PV sector will not contain so impressive figures. Sadly all these improvements in Europe have been feed-in-tariff guided and policy driven. Now, Spain, United Kingdom, Germany and Italy have reduced or supressed the incentives to PV electricity. But these subsidy cuts in EU show as well that RES are coming of age.

Global crystalline silicon cell production capacity has been 27 to 28 GW_p in 2010. Although installed worldwide, cell production and module manufacturing is located primarily in China, Taiwan and USA. Almost 50% of this capacity is located in China, where 1 GW_p is expected to be installed in 2011 ans 5 GW_p are the official target by 2015, with a longer-term target of 20 to 30 GW_p by 2020. This target could be easily even exceeded if the right market conditions and regulatory frameworks are in place (European Photovoltaic Industry Association (EPIA), 2011).

Chinese competitive prices have driven down 1€/W_p silicon technologies ("Solar Module survey 2012," 2012). This impressive decrease of the prices (4 years ago it was about 4-5€/W_p) has led grid-connected PV very close to the grid-parity (prices of PV generation electricity equal or even lower than typical customer grid prices).

In spite of this recent price revolution, PV research must be addressed to reduce even more the price of kWh generated from PV, making PV growth independent from subsidies and also independent from the production site, freeing PV production from current extremely low-salaries.

Organic photovoltaics (OPV) appeared in the first decade of 21st century as an alternative that offers, as well as other thin-film technologies, a combination of low-cost and low-weight. The low-cost may reflect the fewer materials used in comparison with silicon PV. But the low-cost also reflects new manufacturing processes that employ roll-to-roll (R2R) and printing technology.

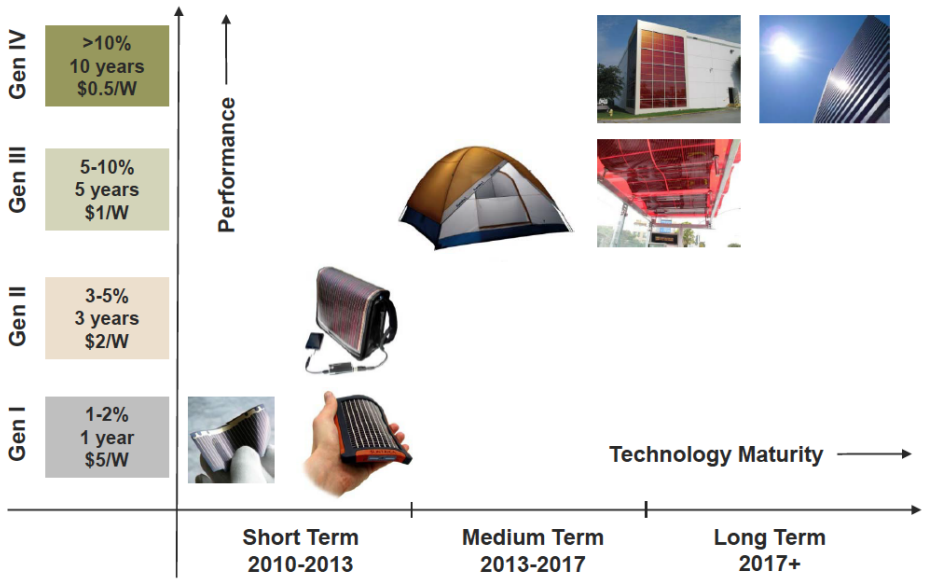

Figure 1.12. Organic photovoltaics roadmap where efficiency, lifetime and price determine the deployment this technology. Source: Organic Electronics Association (OE-A).

The fact that OPV is much lighter than conventional PV is also a key advantage, since OPV panels are much easier to integrate on roofs and walls. The PV functionality could be embedded in building materials; window glass, roof tiles or even applications not yet explored are also possible: integration in canopies, umbrellas, or indoor applications, such as curtains or blinds. The roadmap in Figure 1.12, show there are still goals to accomplish such as increasing the lifetime to 5 and then 10 years, rising up efficiency towards 12% in long term, reduce manufacturing costs through large area R2R production technology and moving to more transparent materials.

OPV modules manufacturing requires moderated capital investment, as seen in Table 1.1, that could enable an international diffusion of the technology in a distributed horizontal technology transfer mechanism. Horizontal transfer of technology occurs when technology used in one place is transferred including intellectual property issues, and used in another country, breaking dependencies between developing and developed countries. This can constitute a solution for access to the electricity in remote places as well as an economic driving force for development.

Table 1.1. Capital and equipment investment for an OPV factory with 450 MW_p per year capacity. Source: (Shrotriya, 2011).

Parameter	Value
Coating Speed	30 m/min
Web Width	1m
Coater Runtime (3 x 5)	6000 hrs/yr
Yield	90%
Total Area	9.0 million m^2/yr
Efficiency	5%
Total Annual Capacity	450 MW_p/yr
Total estimated capital Investment	$30 million

1.5. Aim and scope of the thesis

The main goal of this work is to study routes and materials typically used in the production of polymer solar cells, in order to provide a better understanding of the way this technology is impacting the environment, by establishing the parameters that are critical for the beneficial use of polymer solar cells in society. This has thus allowed us to propose improvements to optimize the fabrication of OPV module having a lower carbon footprint.

There are some questions that will remain open since OPV has still some limitations, like low efficiency short lifetimes due to degradation mechanisms, and decommissioning issues. These important issues should be addressed in the future, but they are beyond the scope of this thesis.

The structure of the present dissertation is organised as follows: chapter one has presented the global energetic situation and the role of photovoltaic technologies in a transition towards a cleaner energy production system. Chapter 2 presents photovoltaic principles and which are the working mechanisms of a photovoltaic device, analysing the particularities for different semiconductors; organic semiconductors and the physics of organic solar cells will also be reviewed. Materials, processing and device characterization of polymer solar cells are presented in Chapter 3, this Chapter focuses on the developments, at a lab-scale and a medium-scale, that are impacting the success of OPV; experimental data of device fabrication will be herein detailed, as well as roll-to-roll processing techniques towards a continuous manufacturing of organic solar cells; the characterization techniques that have been used to characterize both the layers and the devices, are also presented in Chapter 3.

The following chapter, Chapter 4, deals with life-cycle assessment methodology and it will reveal the results of the conducted studies where it has been applied to several OPV systems: to OPV modules manufactured at a semi industrial scale, to a product integrating polymer solar module, and to a new set of alternative routes to fabricate low-environmental impact OPV modules.

Finally, conclusions and future implications of this thesis are discussed in Chapter 5.

References

Beurskens, L. W. M., Hekkenberg, M., & Vethman, P. (2011). *Renewable Energy Projections as Published in the National Renewable Energy Action Plans of the European Member States*. European Commission.

BP Statistical Review of World Energy. (2011). *BP Statistical Review of World Energy June 2011*. London.

Brown, T., Riahi, K., Schulz, N., Faist, M., Foster, S., Jennings, M., Munuera, L., et al. (2012). *China's 2050 Energy Technology Pathway*. Grantham Institute for Climate Change- Imperial College London.

Climate Change 2007: The Physical Sciences Basis. (2007). IPCC.

Coopers, P. W. C. P. (2010). *100% renewable electricity. A roadmap to 2050 for Europe and North Africa*. PwC, Londres.

EU approves Iran oil imports ban. (2012, January 23).*BBC*.

European Photovoltaic Industry Association (EPIA). (2011). *Global Market Outlook for Photovoltaics until 2015*.

German Advisory Council on Global Change (WBGU). (2011). *World in Transition: A Social Contract for Sustainability*. Berlin.

Hall, C. A. S., & Day, J. W. (2009). Revisiting the Limits to Growth After Peak Oil. *American Scientist*, *97*(3), 230.

International Energy Agency. (2011). Key World Energy Statistics 2011, 82.

Krewitt, W., Teske, S., Simon, S., Pregger, T., Graus, W., Blomen, E., Schmid, S., et al. (2009). Energy [R]evolution 2008—a sustainable world energy perspective. *Energy Policy*, *37*(12), 5764–5775.

Legros, G., Havet, I., Bruce, N., & Bonjour, S. (2009). *The Energy Access Situation in Developing Countries*. United Nations Development Programme.

López-Peña, Á., Danesin, A., Linares, P., Pérez-Arriaga, I., Lascorz, M. C., & Rodrigues, R. (2012). *Informe sobre Energía y Sostenibilidad en España 2011* (No. Ed. 2011). Universidad de Comillas. Cátedra BP Energía y Sostenibilidad.

Murray, J., & King, D. (2012). Climate policy: Oil's tipping point has passed. *Nature*, *481*(7382), 433–435.

Observer. (2011). *11ht EuroObserver Report: The state of renewable energies in Europe*. Paris.

REE, D. (2012). Demanda de energía electrica tiempo real.

Shrotriya, V. (2011). Driving down the cost of Flexible Panels. Presented at the SEMICON West, San Francisco.

Solar Module survey 2012. (2012).*Photon International*, *2*.

Stern, N. (2006). Stern Review on the Economics of Climate Change.

The Golden Age of Gas Scenario. (2011). International Energy Agency. World Energy Outlook.

World Energy Outlook. (2010). International Energy Agency.

CHAPTER 2
Photovoltaic principles and technologies

Earth receives solar energy at the rate of approximately 10^5 TW in a continuous and distributed manner. This energy vastly exceeds the current annual worldwide energy consumption rate of ~15 TW and that of any energy scenario that can be contemplated for this century. It would be naïve to think in satisfying it all, but would not be tremendously attractive to harvesting a good part of it directly from the Sun? In this Chapter the working mechanisms of a photovoltaic device, analysing the particularities for different semiconductors, in special the organic-based family will be reviewed.

2.1. Principles of operation of a photovoltaic device

Solar cells when exposed to light are, able to convert the incident radiation into electricity in two major steps: first the absorption of incoming light inside the photoactive material generates an electron-hole pair –or exciton- and, secondly, it comes the dissociation and extraction of this pair in carriers due to an internal asymmetry in the device (Markvart et al., 2005). This is known as *photovoltaic effect*. In conventional silicon technology, a thick p-type layer forms the bulk of a solar cell, where the absorption of most of the incident light takes part. After light absorption, the minority carriers (electrons) diffuse to the junction with an n-type material (the p-n junction), where the carriers are swept across by the strong built-in electric field (Nelson, 2003; Wenham et al., 2007).

So first of all, a junction of two materials with different nature is required. In a conventional semiconductor diode, majority carriers (electrons in n-type material, holes in p-type) are the main players. By initial diffusion across the p-n junction they set up a depletion layer and create an internal electrical field. This field equilibrates the diffusion processes by drifting the carriers in opposite direction, therefore building a potential barrier throughout the junction. Forward-biasing the diode reduces the height of the barrier, making it easier for them to cross the junction and produce substantial current; while in reverse bias the barrier increases and current flow is severely inhibited. Diode action is mainly due to the behaviour of majority carriers under the influence of an applied external voltage. Shockley equation for the diode in dark, in Eq 2.1, defines the I-V characteristic of the device.

Eq 2.1

$$I = I_0\left(e^{\frac{qV}{n\cdot k_B T}} - 1\right)$$

Where, k_B is the Boltzmann constant, T is the absolute temperature, q is the electron charge, V is the voltage at the terminals of the cell, I_o corresponds to the diode saturation current and n is the ideality factor, that depends on the fabrication process and semiconductor material that varies from 1 to 2.

In solar cells, light-generated minority carriers break the equilibrium. Photogenerated carriers take centre stage. The basic reason can be simply stated: a potential barrier that inhibits transfer of majority carriers across a p–n junction, positively stimulates the transfer of minority carriers. Whereas majority carriers experience ‘a hill to climb’, minority carriers see ‘a hill to roll down’. The latter will luckily be swept down this hill, be collected at the cell terminals, and they will produce an output current proportional to the intensity of the incident light.

When the new equilibrium is reached, the excess of photogenerated carriers can a) flow through an external contact which short circuits the device producing a photogenerated current, or b) build a potential difference throughout the device that can be externally measured at open circuit; in all intermediate situations,

both current and potential external to the device can be measured and used to make useful work (at an electrical power rate given by P=I×V at any point of the IV characteristic curve of the device). This electrical power is collected by metal contacts at the front and back of the cell.

Figure 2.1 illustrates the main features of a typical photovoltaic cell, both in side schematic view (top left) and in band diagram (top right and bottom). The band model describes the behaviour in terms of energy levels between the valence (E_V) and the conduction (E_C) bands. The difference between these levels is the bandgap energy (E_g). When light falls into a semiconductor, photons with energy greater than the bandgap will promote electrons to the valence band, creating electron-hole pairs.

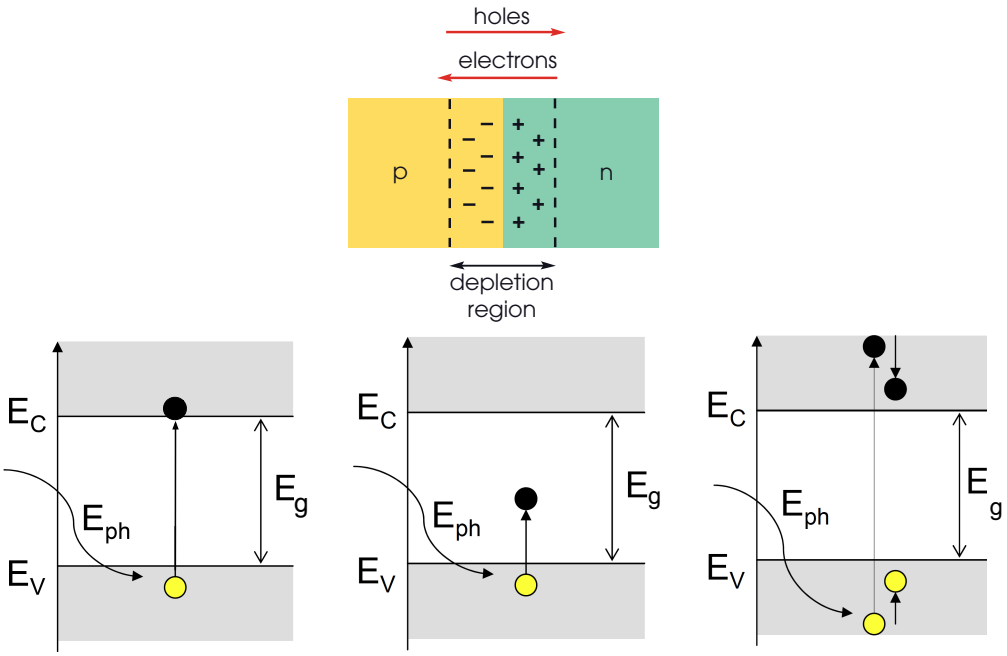

Figure 2.1. Top, the structure of a p-n junction in a solar cell. Bottom left, the promotion of an electron from the valence to the conduction band in a band scheme. Bottom left the case where E_{ph} is lower than E_g and the opposite case with thermalization (bottom right).

Carriers are generated by photon absorption, but unfortunately, not every photon absorbed generates an electron-hole pair, actually in real physical systems about 55% of solar energy is not usable (Nelson, 2003). If we consider the simplified scheme in Figure 2.2, there are just three photons that successfully create electron–hole pairs in the crystal lattice. And this might be due to several factors:

- *Reflection losses*: a certain fraction of photons of all energies are reflected on hitting the surface of the semiconductor, as photons 2, and 3 in Figure 2.2, while photon 1 is reflected by the metallic grid contact. Reflection losses can be reduced by using anti-reflecting coatings.

- *Non-absorption losses*: photons with energy E_{ph} below the E_g of the material cross it without being absorbed (photon 6 in Figure 2.2 and Figure 2.1 bottom left). The opposite case when E_{ph} is larger than E_g causes thermalization of photons (Figure 2.1 bottom right), only E_g energy is useful, while the excess energy is lost by heating the device.

• *Transmission losses*: due to the finite value of the absorption coefficient and the finite thickness of the semiconductor, a certain fraction of photons of energy greater than E_g cross the device without being absorbed (photon 6 in Figure 2.2). Thus, the absorbance or absorptivity, a(E), is the probability of absorption of a photon of energy E_{ph}, and it is determined by the absorption coefficient and by the optical path length through the device.

• *Recombination losses*: The free electron does not immediately experience 'a hill to roll down', but instead starts wandering randomly through the material lattice. But the journey is a dangerous one: it may instead encounter a hole and be annihilated by recombination. There is bulk recombination which is unavoidable. Although such recombination is not illustrated in the figure, unfortunately it not only occurs in the main body of the cell (bulk recombination), but even more importantly at the edges due to defects and impurities in the crystal. Part of the surface recombination can be avoided by selective doping.

• *Collection losses*: some electrons can be lost at metal electrodes; selective doping around the contacts can reduce this loose, improving carrier collection from the semiconducting material to the metallic electrodes.

However, there are some successful photons, for example photon number 4 in Figure 2.2, which produces an electron-hole pair in the p-type region, close to the junction. Its free electron, a minority carrier in p-type material, is easily swept across the junction and collected. So that is the hole, produced in the n-type region by photon number 5, which is swept across the junction in the opposite direction. Both carriers will contribute to the photo-generated current if they can be extracted out by the external contacts.

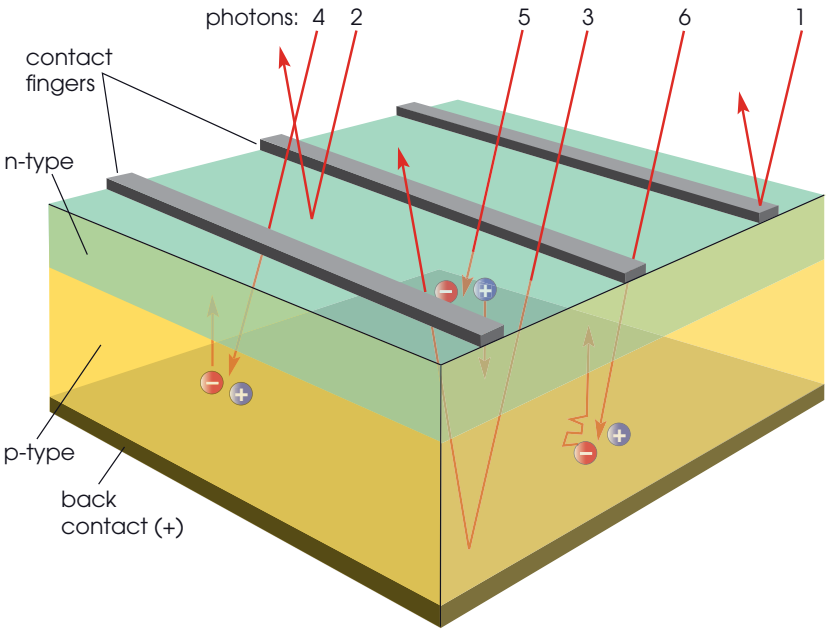

Figure 2.2. A simplified scheme of a crystalline solar cell. Source: (Lynn, 2010).

The parameters that limit solar cell performance are shown in Figure 2.3. They describe the following losses: non-absorption, thermalization, active area, reflexion, transmission, recombination, voltage limit and fill factor.

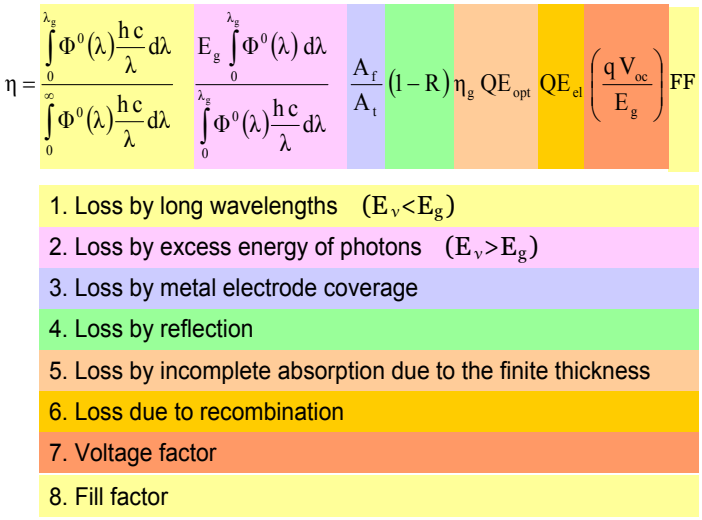

Figure 2.3. Solar cell performance parameters are limited by the losses: non-absorption, thermalization, active area, reflexion, transmission, recombination, voltage limit and fill factor. Source: (Overstraeten et al., 1986) and own elaboration.

PV modelling

The most simplified equivalence of an ideal solar cell in dark is a rectifying diode connected in parallel with a current source, as shown in Figure 2.4.

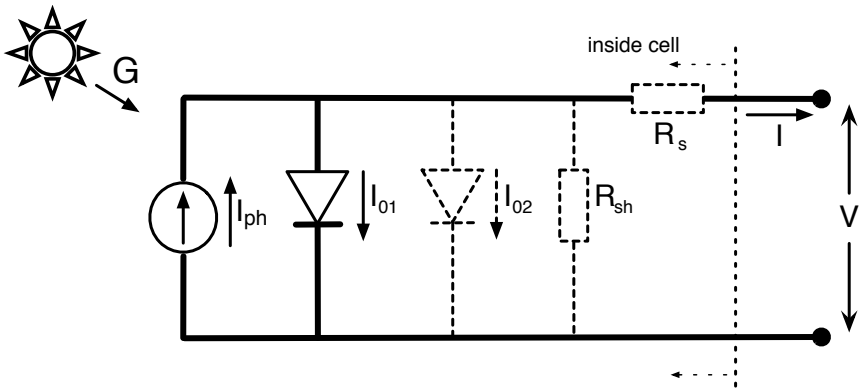

Figure 2.4. Equivalent circuit model of a simple-junction solar cell. In dashed line are shown non-ideal components, necessary to fit the behaviour of a cell more accurately.

Then, adding the photocurrent to the Shockley equation for the ideal diode in dark (Eq 2.1), the I-V characteristic of the solar cell given by Eq 2.2:

Eq 2.2

$$I = \underbrace{I_{sc}}_{I_{ph}(G,T)} - \underbrace{I_0\left(e^{\frac{qV}{n\cdot k_B T}} - 1\right)}_{I_{dark}(V,T)}$$

Where all parameters have been previously described except the photogenerated current, I_{ph}, which is closely related to the photon flux incident on the cell. This

dependence on the wavelength of light is frequently discussed in terms of the quantum efficiency, or spectral response. The photogenerated current is usually independent of the applied voltage, with few exceptions in the case of amorphous silicon (a-Si:H) and some other thin film materials (Hegedus, 1997)[1].

In most cases, this simplified first-level model is not enough to represent the behaviour of a solar cell. It is thus needed to account for losses as contact resistances or low conductivity in semiconductors and electrodes, as well as for unwanted leakages of current through the device, which can be shunted by pinholes, impurities or crystal defects. Series resistance, R_s, and shunt resistance, R_{sh}, as shown in Eq 2.3, model all these losses respectively. Recombination effects, or non-idealities are introduced by the ideality factor of the diode, n.

Eq 2.3

$$I = \underbrace{I_{ph}}_{I_{ph}(G,T)} - \underbrace{I_{01}\left(e^{\frac{q(V+IR_s)}{k_B T}} - 1\right)}_{I_{dark}(V,T)} - \frac{V+IR_s}{R_{sh}} - \underbrace{I_{02}\left(e^{\frac{q(V+IR_s)}{2 \cdot k_B T}} - 1\right)}_{I_{dark}(V,T)} - \frac{V+IR_s}{R_{sh}}$$

These features are shown in the equivalent circuit of Figure 2.4 by the dashed lines. The effect of the second diode is useful to fit the curve of the cell, and further information about the series and parallel resistances, on the I-V characteristic of the solar could be extracted from the dark I-V characteristic.

The solar cell under operation

The maximum power that the device can deliver, P_{max}, is given by the product $I_{mp}V_{mp}$, and it is called *maximum power point, as* shown in Figure 2.5, which can be obtained empirically as the point for which d(IV)/dV equals zero. Therefore, the shape of the I-V curve contains all useful information about the device under consideration. Important parameters can be easily identified on this curve.

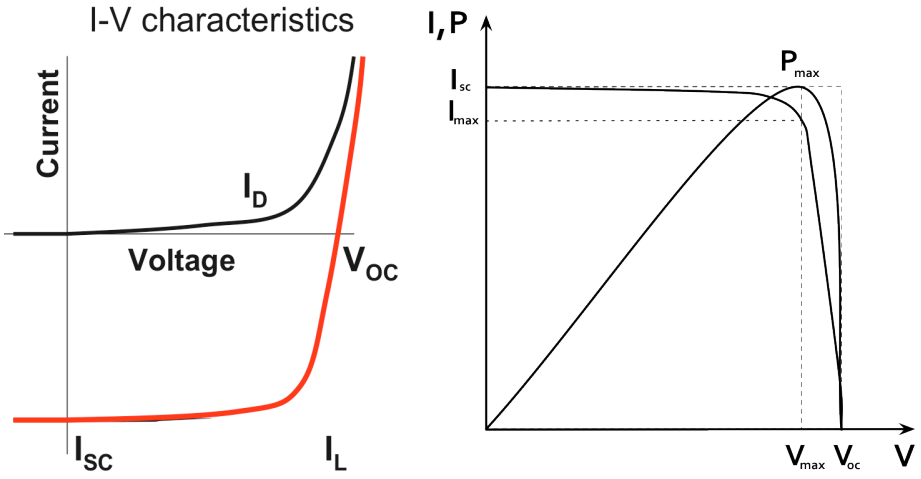

Figure 2.5. I-V curve of a solar cell, from where main parameters can be extracted. In the fourth quadrant in the left, since it is as "shift" in diode curve. At the right, maximum power point is indicated by I_{max} and V_{max} at the point where d(IV)/dV=0 or P_{max}.

[1] To collect the photocurrent, a-Si:H depends almost exclusively on field-aided drift rather than diffusion of minority carriers. The electric field in the intermediate layer is strongly dependent on the voltage bias across the device, which makes the photocurrent collection dependent on the operating bias of the cell.

There is an electric current flowing through the device under illumination, when no external voltage is applied (V=0V), I_{sc}. Since the short-circuit current depends on the active area of a photovoltaic device, it is often more common to list it as a current density, J_{sc}(A/cm²). The open-circuit voltage V_{oc} can be identified as the point for which I=0A. At open circuit voltage no current flows across the device, and all photogenerated charge carriers recombine within the solar cell.

The I-V curve can be plotted in the fourth quadrant. As I_{max} and V_{max}, I_{sc} and V_{oc} coordinates build two rectangles (see Figure 2.5). It can be seen from this figure that the closer the rectangles are, the more rectangular shaped is the IV curve. The ratio of the areas of the two rectangles can therefore be regarded as a measure of the quality of the device; it is called the fill factor *FF* (Eq 2.4).

Eq 2.4

$$FF = \frac{I_{mp} \cdot V_{mp}}{I_{sc} V_{oc}}$$

The power conversion efficiency (*PCE*) of a solar cell, η, is defined as the ratio between the power at the maximum power point (in *standard conditions*[2]) and the power at an incident radiation per area unit, P_{rad}, falling into the solar cell of area A; as shown in Eq 2.5.

Eq 2.5

$$\eta = \frac{\mathrm{P_{max}}}{\mathrm{P_{rad}A}} = FF \cdot \frac{I_{sc} V_{oc}}{\mathrm{P_{rad}A}}$$

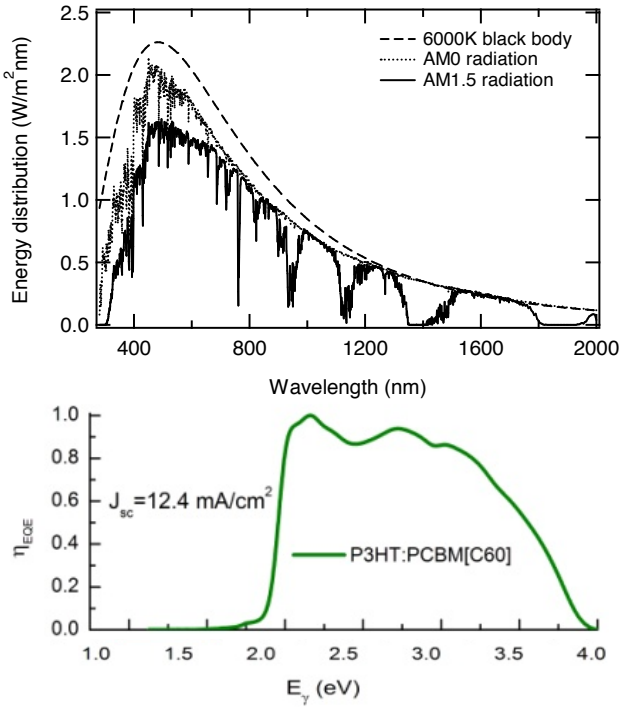

Figure 2.6. a) The photon flux radiation of solar radiation reaching earth's surface at Air Mass zero (AM0), or extra-terrestrial spectrum, and at AM1.5, standard conditions. b) Comparison of the spectral response for P3HT:PCBM devices. J_{sc}= 12.4 mA/cm² calculated from the normalized EQE.

[2] *Standard conditions* are 1000 W/m², at 25°C, 1 m/s wind speed and solar spectrum AM1.5 that is the A*ir Mass* that solar radiation must pass through -equivalent to a sun angle of 48.2°.

If we consider the spectral distribution of solar photons (Figure 2.6), we can study the response o the cell at a particular wavelength, which is called quantum efficiency (*QE*) of a solar cell. It is used to enable fair comparisons among incident lights falling over the same device and stands for the ratio of the number of electrons in the external circuit produced by an incident photon of a given wavelength.

Optimal device design

To extract the current generated by the solar cell, conducting top contacts are necessary. Good top contact design makes possible to optimise current collection against losses due to internal resistances and must prevent cell shadowing, whatever the technology is. A simple grid spacing design is shown in Figure 2.7a). *Busbars* are connected directly to the external leads, while *fingers* are narrower areas of metallisation that collect current to be delivered to the busbars.

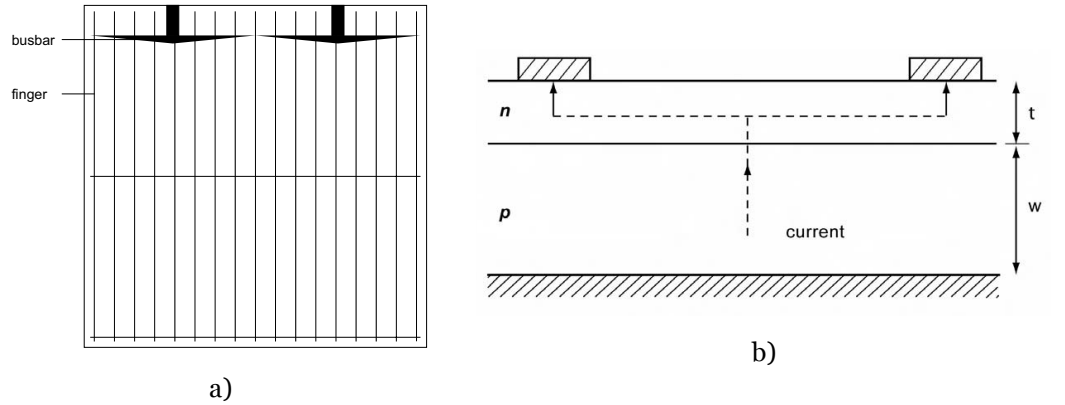

Figure 2.7. a) Top contact design to collect current in a silicon solar cell, busbars and fingers, and b) Typical flow of the generated current in a silicon based cell.

Other design strategies to maximize the extraction of the current are i) to minimize the surface reflection and ii) avoid recombination at the surface. The former can be solved with antireflection coating layers application as SiO_2, or by texturing the surface. A passivation layer can usually prevent the second problem: carrier recombination. Titanium dioxide has been used so far as passivation, but Silicon nitride is now being rapidly replacing TiO_2 because of its versatile properties: it can solve both problems since it prevents reflection and provides passivation. Selective extra doping in silicon cells is also another strategy to avoid surface recombination.

Contact design must also enable for series connection in solar cells. This is widely used in thin film solar cells, including OPVs, to boost the voltage of the module. Voltage increasing is generally favoured over current boosting because lower ohmic losses are expected for higher voltages. However, increasing the number of connections per unit area, either in series or in parallel, implies a reduction in the photoactive area because a substantial area is required to connect the adjacent cells. It will be considered again in Chapter 3 and Chapter 4, when dealing with geometry and layer deposition methods of this emerging technology.

Generated current typically flows as shown in Figure 2.7b), perpendicular to the cell surface; from the bulk to the p-n junction, and then, in the case of silicon based cells, laterally through the top layer until it is collected at a top surface contact. For thin film technology, once the carriers get out the junction they travel vertically through layers, which will conduct the charge carriers to the electrodes. Typically, it can be defined for a layer or for a cell, a *bulk resistance* (R_b), as in Eq 2.6:

Eq 2.6

$$R_b = \frac{\rho \cdot l}{A} = \rho_b \frac{w}{A}$$

where, l is the length of the conducting (resistive) path, ρ_b is the *bulk resistivity* of the bulk cell material (typically 0.5–5.0 Ωcm for a silicon solar cell), A is the cell area, and w is the width of the bulk region of cell -see Figure 2.7b). Since the bulk resistivity is the inverse of conductivity, in the case of solar cells with active layers made of conjugated polymers, their conductivity can spread values ranging from insulators to metals.

Similarly, for the top layer or contacts in which there is a lateral conduction, a *sheet resistivity* ($\rho_\square$) is defined as following:

Eq 2.7

$$\rho_\square = \frac{\rho}{t}$$

where, ρ is the resistivity of this layer. The sheet resistivity is normally expressed as ohms/square or Ω/□, and it is important because determines the spacing between grid lines of the top contact, as shown in Figure 2.8. It is easy to measure experimentally this parameter by using a 'four point probe', as it will be shown in Chapter3.

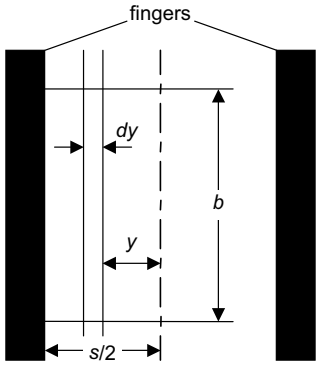

Figure 2.8. Dimensions needed to calculate the minimum spacing for the electrode grid and the power losses due to lateral resistance of the top layer.

2.2. Photovoltaic technologies

Silicon has been, since the growth of silicon crystal ingots and the development of dopant diffusion technology by early 1950s, the foremost semiconductor in photovoltaics in its two crystalline versions: monocrystalline, and polycrystalline. The first device, useful for power generation, was built in 1954 by Chapin et al. (Chapin et al., 1954), and had 4.5% efficiency. Single-junction devices based on silicon wafers account for a theoretical efficiency limit of 32%, the Shockley-Queisser limit, due to thermodynamic limit at 1 Sun and AM 1.5 spectral distribution (Shockley et al., 1961).

Thin-film devices, dubbed by M. Green (Green, 2001) as "second generation" (2G) following the "first generation" (1G) silicon-based, make use of extremely little amount of active materials, thanks to the breakthroughs in sputtering and vapour deposition techniques for amorphous cells. This had a major impact in the preparation of a-Si:H and other semiconductors, mainly chalcogenides - sulphides, tellurides, sellenides-, such as CIS and CdTe. Regardless of the semiconductor involved, thin-film technology offers prospects for a large reduction in material costs by eliminating the costs of the silicon wafer. However, as 2G technologies mature, the price of the constituent materials will again progressively dominate the device final cost.

Other strategy for cost-reduction of the generated electricity is the development of high-efficiency materials. This "third generation" (3G) of solar cells includes high-efficiency III-V multiple-junction or tandem cells, with record efficiencies (over 43% at 418 Suns).

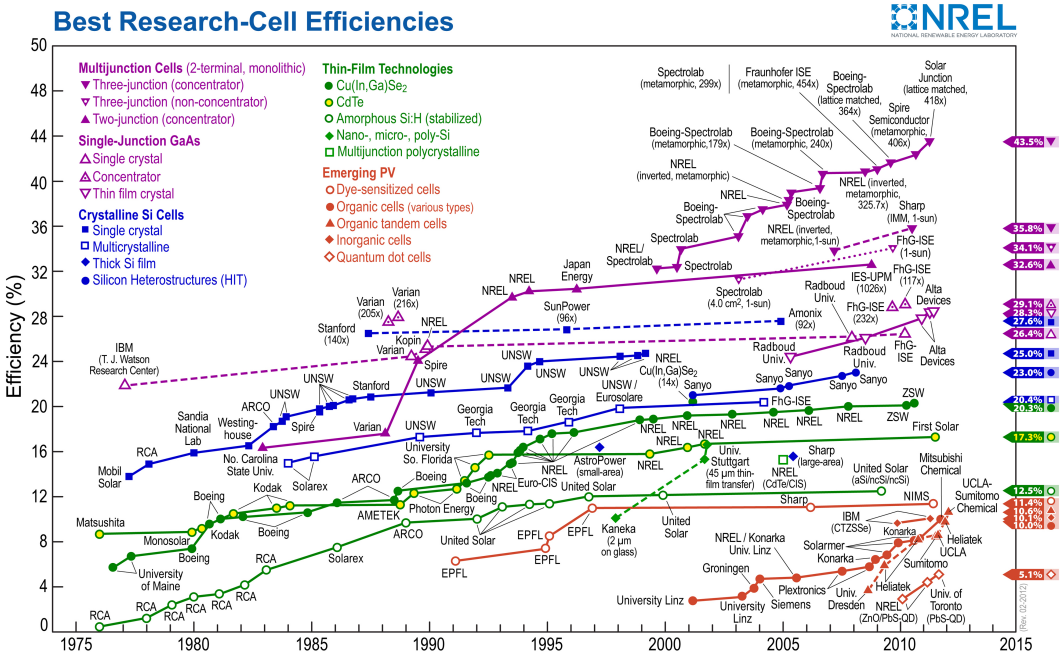

Figure 2.9. Research-cell efficiency plot for various PV technologies, 1976-2011. Data compiled by Lawrence Kazmerski, National Renewable Energy Laboratory (NREL) of United States Department of Energy.

Finally, completely new concepts in terms of device architectures and materials can be included in 3G. The concept of organic solar cells covers two main approaches: Dye-Sensitized Solar Cells (DSSCs) and Full Organic Solar Cells (OSCs). The Dye sensitized cells, also called Hybrid or Grätzel cells, are based on electrochemical processes for light-harvesting in a liquid electrolyte, while charge transfer occurs in an organic-inorganic interface where the organic molecules improve the electron dissociation. DSSCs are based on combination of dyes with metal oxides and an electrolyte (Gratzel, 2001). The efficiencies of DSSC are in the range of 12 % for small lab scale devices, while the lifetime of the devices is rather low compared to inorganic solar cells. DSSC in contrast to the conventional semiconductors separate the function of light absorption from charge carrier transport. Light is absorbed by a sensitizer -complexes made of ruthenium and osmium-, which is anchored to the surface of a wide band gap semiconductor (commonly a mesoporous crystalline TiO_2 film). Charge separation takes place at the interface via photo-induced electron injection from the dye into the conduction band of the solid. Carriers are transported in the conduction band of the semiconductor to the charge collector, a transparent conductor oxide (TCO) (O'Regan et al., 1991).

Regarding full organic solar cells, the active layer consists of small molecule or polymers, and so far the most successful of them are the polymer-fullerene cell, that comprise a mixture of polymer, as donor material, and a fullerene derivative, as acceptor material in the active layer. The first organic PV cell with this semiconductor came as early as 1959, exhibiting poor photovoltage (~ 200 mV) and extremely low efficiency (Kallmann et al., 1959). Shirakawa, MacDiarmid, and Heeger demonstrated in 1977 that doping can control the conductivity of conjugated polymers, and they were rewarded for that contribution with the Nobel Prize in Chemistry in 2000. These results together with the possibility of tailoring the organic molecular structure to improve the photocurrent, and with the property of being solution processable -i.e. massively produced-, have led researchers to look at polymeric solar cells. A major breakthrough in the cell performance came in the late 1970's when Tang, bringing an electron donor and an electron acceptor together in one cell, discovered that much higher efficiencies (about 1%) are attainable (Tang, 1986). But especially, in the last decade, the field of organic photovoltaics (OPVs) has emerged in an exponential way (Nielsen et al., 2010) and has turn into an alternative for a low-cost technology. Semiconducting polymer performance has been since then studied in solar cells (Brabec et al., 2001; Shaheen et al., 2001) and these polymer-based cells are the type of devices that the present thesis is devoted to. Best research-cell efficiency of this technology has recently reached 9.8% (see the chart in Figure 2.9) for polymer-based single-junction OSC, by a consortium of IMEC Solvay and Polyera ("imec Belgium vzw," 2011).

There also exists a second family of OSC based on small molecules, which are usually evaporated; a process that makes its industrial production at low-cost more challenging. Nevertheless, solution-processable small molecules recently proposed have attractive features for application in photovoltaic cells (Lloyd et al., 2007; Roncali, 2009). They can potentially offer the facile processing associated with polymers; are easier to synthesize and purify, and typically show

higher charge carrier mobilities. Recent progress in solution-processable small molecule blends has yielded photovoltaic cells with efficiencies ~6% (Sun et al., 2012), and when preparing cells by vacuum deposition of the molecules the world record is set today -April 2012- in 10.1%; by Heliatek company ("Heliatek, GmbH," 2011), not reflected in Figure 2.9.

2.3. The physics of organic solar cells

Energy transfer processes for amorphous materials differ from crystalline lattices, In a molecular semiconductor light generates excitons, which are long lived compared to the excitons generated in typical inorganic cells, because the electron-hole pairs are tightly bound in polymers. In such cases the electrostatic field (from the difference in work functions of the junction materials) is not usually sufficient to split the exciton. Instead, the excitons drift and only split when they approach the junction at the two blended materials with a different work function. To prevent recombination a distributed junction is necessary to reduce the path that the exciton must travel. Typical distances should be in the order of the exciton diffusion length, a few nanometres (5-15 usually). The photocurrent generation, charge separation and current extraction steps, as well as the configuration of the OSC are described below.

Semiconducting Polymers: a special family

What makes polymers conductive is, on one hand, related to anisotropy and on the other, to the conjugation of the molecular structure (Aasmundtveit et al., 2000; Heeger, 2010). The conditions that favour an increase in molecular anisotropy also favour an increase in electrical conductivity, suggesting that the anisotropy is due to molecular orientation's favouring an increase in conjugation length. With regard to this latter, the electronic structure of all organic semiconductors is based on conjugated π-electrons. A conjugated organic system is made of an alternation between single and double carbon-carbon bonds for an sp^2 hybridisation of the carbon orbitals. Single bonds, known as σ-bonds, are associated with localized electrons, and double bonds contain a σ-bond and a π-bond. The π-electrons are much more mobile than the σ-electrons; they can jump from site to site between carbon atoms thanks to the mutual overlap of π-orbitals along the conjugation path, which causes the wave functions to delocalize over the conjugated backbone. The π-bands are either empty called LUMO (*Lowest Unoccupied Molecular Orbital*) or filled with electrons, named in that case HOMO (*Highest Occupied Molecular Orbital*). The band gap, or the electron jump between these molecular orbitals, ranges for these materials from 1 to 4 eV, and their conductivities from insulator to metal conductivity. They were also named *synthetic metals*.

Extracting the generated photocurrent in polymer solar cells

Four main processes in an OSC occur when OSC are exposed to light (Figure 2.10). They are different to processes in inorganic semiconductors. The primary process in the photocurrent generation are (i) the generation of excitons after absorption of light, either by the donor or by the acceptor; then (ii) the excitons in

either domain diffuse to an interface, where (iii) rapid charge separation into independent holes and electrons will occur; (iv) they will finally move to an electrode before competing processes take place, such as (v) geminate recombination and non geminate recombination, or (vi) electron back transfer from the acceptor to the donor.

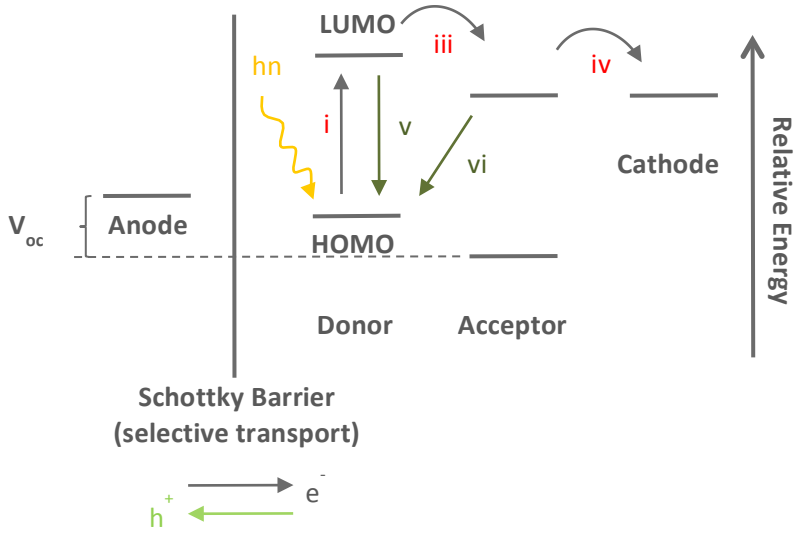

Figure 2.10. Simplified photocurrent generation mechanism: (i) absorption, (ii) exciton diffusion (not shown), (iii) charge separation, and (iv) conduction. Competing processes include (v) recombination and (vi) electron back transfer.

In OPV, as well as in inorganic or traditional cells, a p-n junction design is required for separating the electron-hole pair, in organic compounds this distributed p-n junction is better described as an interface between donor (D) and acceptor (A) materials[3]. Firstly, the junction was a planar heterojunction in a bilayer (Tang, 1986). Efficient charge separation occurs only at the D-A materials interface; thus to achieve a high quantum efficiency it is compulsory what has been so-called *bulk heterojunction* (BHJ) of the donor and the acceptor (Figure 2.11). The range of this BHJ has been indicated to be from a few to hundreds of nanometres length by experiments such as photoluminescence quenching and extracted from photocurrent modelling (Stübinger et al., 2001; Peumans et al., 2003) showing that only photogenerated excitons in proximity to the D-A interface within less than the exciton diffusion length (~10 nm) can be dissociated. But too intimate mixing may result in the impossibility of creating percolating paths for the photogenerated carriers once the exciton has been split. Thus, the critical issue will not only be the relationship between molecular composition and device properties but also between nanomorphology and device properties (Hoppe et al., 2004).

However, it must also be mentioned that slight asymmetries in the charge transport become less relevant in the thin film devices, in which the carrier drift length under short circuit conditions is larger than the active layer thickness.

[3] The concept of donor and acceptor material is relative to each other on the comparison between their HOMO-LUMO level, the electron affinity or the ionization potential of both materials.

It is as well essential in OPV that the device not only possesses many D-A interfaces, but also has a thick layer for sufficient photon absorption. But increasing the thickness of the absorption layer makes very high demands of material quality: in amorphous lattices as polymeric ones, the thicker the layer the higher the probability of defects. Although typical thicknesses are about few hundreds of nm, much less than typical thin fim inorganic cells (≈1μm) or conventional crystalline silicon cells (the thinner are around 120μm).

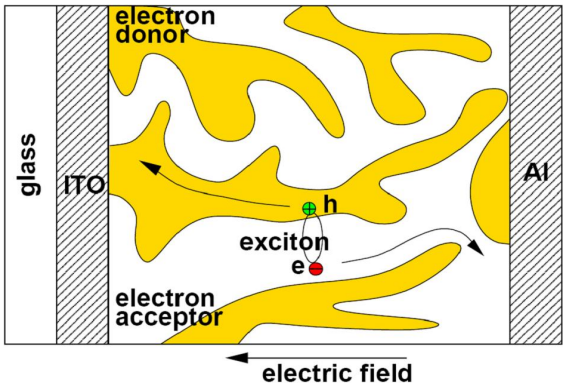

Figure 2.11. Photogeneration in the simplest polymer solar cell structure, type metallic/ semiconducting/ insulating.

The OPV stack

Typical structure for an OSC comprises a pile of functional layers between two electrodes, being designed for allowing the pass of the light and efficient photogenerated carriers collection. As active layer, in the past decades the required internal asymmetry had been provided by the use of organic bilayers (Simon, 1985; Tang, 1986; Hadziioannou et al., 2000, chap. 15). But some other approaches have been proposed more recently in optoelectronic devices as active layers; summing up, bulk heterojunctions made from mixing: polymer/polymer, polymer/fullerene, polymer/perylene and polymer/quantum dot. With regard to full organic solar cells, once asymmetry was achieved by a distributed junction, it was found that those cells based on mixtures of fullerenes and polymers were among the most promising ones. This was obtained by the discovery of fast efficient photo-induced electron transfer [4], from electron-rich conjugated polymers to fullerenes (Wöhrle et al., 1991; Sariciftci et al., 1992), which encouraged the field of OSCs. More recently D-A block copolymers have been investigated (W.-L. Yu et al., 1998; Segura et al., 2000; Svensson et al., 2003). The majority of the initially developed polymers have band gaps higher than 2eV(620nm), which limits their maximum efficiency, and intensive research of low band gap polymers has been done (Bundgaard et al., 2007; Helgesen et al., 2011; Chu et al., 2012; Biniek et al., 2012).

Adjacent layers in between top and bottom contacts must be placed, in order to guide the appropriate charge carriers to the respective electrodes. These intermediate layers are thus hole injector (HIL) or electron transfer (ETL) layers.

[4] Electron transfer reactions, which are also redox reactions, are one the most common and simple chemical reactions in which the electron donor is oxidised and the acceptor reduced. The free energy that drives the reaction is the difference in reduction potentials between donor and acceptor.

PEDOT:PSS is a hole conducting coating that additionally soften the roughness of the substrate and improves the electrical contact between the transparent electrode and the active layer in a standard geometry. Conversely to standard geometries where it is an electron transport material, in inverted ones it acts as a HIL between the back electrode and the active layer.

To complete the device, a transparent electrode in the illuminated side and a bottom electrode are required (Figure 2.12). A transparent oxide of indium and tin (ITO) is generally used since the 1970s as electrode in organic electronics. Although recently due to the scarcity and the high cost of indium, a number of alternatives have been essayed in small laboratory devices as the firstly processed electrode including: carbon nanotubes, graphene, silver nanowires (AgNW), highly conducting polymers and metal grid electrodes. A second approach would involve a non-transparent layer as the firstly processed layer, and then evaporated metals or graphite can be employed. This will be treated in depth in Chapter 3.

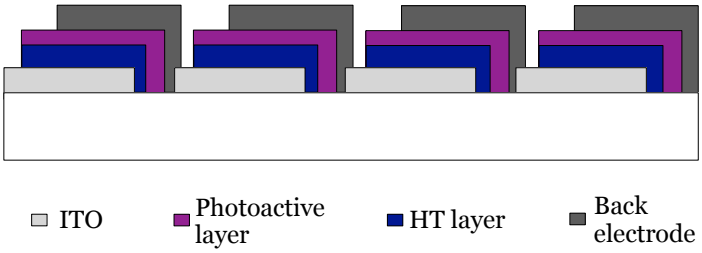

Figure 2.12. OSC stack of layers for a standard configuration of four serially-connected cells.

Successful use of the above mentioned materials has also taken place on different optoelectronic applications, apart from organic solar cells (Tang, 1986; G. Yu et al., 1995; Hide et al., 1997), such as field-effect transistors –FETs-, and photodiodes (Garnier et al., 1994; Sirringhaus et al., 1999), and specially in organic light-emitting diodes –OLEDs- (Baldo et al., 1999; Tang et al., 1987; Burroughes et al., 1990; G. Yu et al., 1994; Yim et al., 2010; Wu et al., 2010).

Their continuous processing, since the deposition can be performed from solution using printing techniques (Krebs et al., 2009), enables to reduce the cost of the cells, both in energy balance and in monetary costs (Espinosa et al., 2011; Azzopardi et al., 2011). The choice of materials to be used as functional layers in a device, the geometries of OSC, and their manufacturing at laboratory scale and medium scale, will be thoroughly discussed in Chapter 3.

2.4. Conclusions

A suitable photovoltaic material, either this is organic or inorganic semiconductor, must have the following properties: it should absorb visible light, possess a band gap between the occupied states and the unoccupied ones -involved in photon absorption-, which matches de solar spectrum and be able to transport charges effectively.

Among the existing PV technologies, organic photovoltaics (OPVs) has evolved in an exponential way in the last five years. There is an active research in this subject; a large number of groups worldwide are working from materials science to engineering and electronics. The progress has been gained by their developments and steps forward, such as the discovery of the semiconductive polymers, the use of bulk heterojunction in the active layer, the inverted geometry structure, the introduction of interfacial layers, and the continuous fabrication; all of which lead to expect fast, cheap and low environmental impact production methods. Therefore, the promises of this emerging technology are likely to occur in the foreseeable future.

Nevertheless, there are still important challenges to overcome in terms of stability and power conversion efficiency, although the latter has increased by a factor of 10 in the last decade.

References

Aasmundtveit, K. E., Samuelsen, E. J., Guldstein, M., Steinsland, C., Flornes, O., Fagermo, C., Seeberg, T. M., et al. (2000). Structural Anisotropy of Poly(alkylthiophene) Films. *Macromolecules*, *33*(8), 3120–3127.

Azzopardi, B., Emmott, C. J. M., Urbina, A., Krebs, F. C., Mutale, J., & Nelson, J. (2011). Economic assessment of solar electricity production from organic-based photovoltaic modules in a domestic environment. *Energy & Environmental Science*, *4*(10), 3741–3753.

Baldo, M. A., Lamansky, S., Burrows, P. E., Thompson, M. E., & Forrest, S. R. (1999). Very high-efficiency green organic light-emitting devices based on electrophosphorescence. *Applied Physics Letters*, *75*(1), 4–6.

Biniek, L., Fall, S., Chochos, C. L., Leclerc, N., Lévêque, P., & Heiser, T. (2012). Optimization of the side-chain density to improve the charge transport and photovoltaic performances of a low band gap copolymer. *Organic Electronics*, *13*(1), 114–120.

Brabec, C. J., Sariciftci, N. S., & Hummelen, J. C. (2001). Plastic Solar Cells. *Advanced Functional Materials*, *11*(1), 15–26.

Bundgaard, E., & Krebs, F. C. (2007). Low band gap polymers for organic photovoltaics. *Solar Energy Materials and Solar Cells*, *91*(11), 954–985.

Burroughes, J. H., Bradley, D. D. C., Brown, A. R., Marks, R. N., Mackay, K., Friend, R. H., Burns, P. L., et al. (1990). Light-emitting diodes based on conjugated polymers. *Nature*, *347*(6293), 539–541.

Chapin, D. M., Fuller, C. S., & Pearson, G. L. (1954). A New Silicon p-n Junction Photocell for Converting Solar Radiation into Electrical Power. *Journal of Applied Physics*, *25*, 676.

Chu, T.-Y., Tsang, S.-W., Zhou, J., Verly, P. G., Lu, J., Beaupré, S., Leclerc, M., et al. (2012). High-efficiency inverted solar cells based on a low bandgap polymer with excellent air stability. *Solar Energy Materials and Solar Cells*, *96*(0), 155–159.

Espinosa, N., García-Valverde, R., Urbina, A., & Krebs, F. C. (2011). A life cycle analysis of polymer solar cell modules prepared using roll-to-roll methods under ambient conditions. *Solar Energy Materials and Solar Cells*, *95*(5), 1293–1302.

Garnier, F., Hajlaoui, R., Yassar, A., & Srivastava, P. (1994). All-Polymer Field-Effect Transistor Realized by Printing Techniques. *Science*, *265*(5179), 1684 –1686.

Gratzel, M. (2001). Photoelectrochemical cells. *Nature*, *414*(6861), 338–344.

Green, M. A. (2001). Third generation photovoltaics: Ultra-high conversion efficiency at low cost. *Progress in Photovoltaics: Research and Applications*, *9*(2), 123–135.

Hadziioannou, G., & Hutten, P. F. van. (2000). *Semiconducting Polymers: Chemistry, Physics, and Engineering* (1st ed.). Wiley-VCH.

Heeger, A. J. (2010). Semiconducting polymers: the Third Generation. *Chem. Soc. Rev.*, *39*(7), 2354–2371.

Hegedus, S. S. (1997). Current–Voltage Analysis of a-Si and a-SiGe Solar Cells Including Voltage-dependent Photocurrent Collection. *Progress in Photovoltaics*

Research and Applications, *5*(3), 151–168.

Helgesen, M., Sørensen, T. J., Manceau, M., & Krebs, F. C. (2011). Photochemical stability and photovoltaic performance of low-band gap polymers based on dithiophene with different bridging atoms. *Polymer Chemistry*, *2*(6), 1355–1361.

Heliatek, GmbH. (2011, December). *Press Release, http://www.heliatek.com/*

Hide, J. G. F., & Wang, H. (1997). Efficient photodetectors and photovoltaic cells from composites of fullerenes and conjugated polymers: photoinduced electron transfer. *Synthetic Metals*, *84*(1-3), 979–980.

Hoppe, H., & Sariciftci, N. S. (2004). Organic Solar Cells: An Overview. *Journal of Materials Research*, *19*(07), 1924–1945.

Kallmann, H., & Pope, M. (1959). Photovoltaic Effect in Organic Crystals. *The Journal of Chemical Physics*, *30*(2), 585.

Krebs, F. C., Gevorgyan, S. A., & Alstrup, J. (2009). A roll-to-roll process to flexible polymer solar cells: model studies, manufacture and operational stability studies. *Journal of Materials Chemistry*, *19*(30), 5442–5451.

Lloyd, M. T., Anthony, J. E., & Malliaras, G. G. (2007). Photovoltaics from soluble small molecules. *Materials Today*, *10*(11), 34–41.

Lynn, P. A. (2010). *Electricity from Sunlight: An Introduction to Photovoltaics*. John Wiley and Sons.

Markvart, T., & Castaner, L. (2005). *Solar Cells: Materials, Manufacture and Operation* (1st ed.). Elsevier Science.

Nelson, J. (2003). *The Physics of Solar Cells* (1st ed.). Imperial College Press.

Nielsen, T. D., Cruickshank, C., Foged, S., Thorsen, J., & Krebs, F. C. (2010). Business, market and intellectual property analysis of polymer solar cells. *Solar Energy Materials and Solar Cells*, *94*(10), 1553–1571.

Overstraeten, R. J. V., & Mertens, R. P. (1986). *Physics, Technology and Use of Photovoltaics,* (1st ed.). Taylor & Francis.

O'Regan, B., & Gratzel, M. (1991). A low-cost, high-efficiency solar cell based on dye-sensitized colloidal TiO2 films. *Nature*, *353*(6346), 737–740.

Peumans, P., Yakimov, A., & Forrest, S. R. (2003). Small molecular weight organic thin-film photodetectors and solar cells. *Journal of Applied Physics*, *93*(7), 3693–3723.

Roncali, J. (2009). Molecular Bulk Heterojunctions: An Emerging Approach to Organic Solar Cells. *Acc. Chem. Res.*, *42*(11), 1719–1730.

Sariciftci, N. S., Smilowitz, L., Heeger, A. J., & Wudl, F. (1992). Photoinduced Electron Transfer from a Conducting Polymer to Buckminsterfullerene. *Science*, *258*(5087), 1474 –1476.

Segura, J. L., & Martín, N. (2000). Functionalized oligoarylenes as building blocks for new organic materials. *J. Mater. Chem.*, *10*(11), 2403–2435.

Shaheen, S. E., Brabec, C. J., Sariciftci, N. S., Padinger, F., Fromherz, T., & Hummelen, J. C. (2001). 2.5% efficient organic plastic solar cells. *Applied Physics Letters*, *78*, 841.

Shockley, W., & Queisser, H. J. (1961). Detailed Balance Limit of Efficiency of p-n Junction Solar Cells. *Journal of Applied Physics*, *32*, 510.

Simon, J. (1985). *Molecular Semiconductors: Photoelectrical Properties and Solar Cells*. Springer-Verlag.

Sirringhaus, Brown, P. J., Friend, R. H., Nielsen, M. M., Bechgaard, K., Langeveld-Voss, B. M. W., Spiering, A. J. H., et al. (1999). Two-dimensional charge transport in self-organized, high-mobility conjugated polymers. *Nature*, *401*(6754), 685–688.

Stübinger, T., & Brütting, W. (2001). Exciton diffusion and optical interference in organic donor–acceptor photovoltaic cells. *Journal of Applied Physics*, *90*(7), 3632–3641.

Sun, Y., Welch, G. C., Leong, W. L., Takacs, C. J., Bazan, G. C., & Heeger, A. J. (2012). Solution-processed small-molecule solar cells with 6.7% efficiency. *Nat Mater*, *11*(1), 44–48.

Svensson, M., Zhang, F., Veenstra, S. C., Verhees, W. J. ., Hummelen, J. C., Kroon, J. M., Inganäs, O., et al. (2003). High‐Performance Polymer Solar Cells of an Alternating Polyfluorene Copolymer and a Fullerene Derivative. *Advanced Materials*, *15*(12), 988–991.

Tang, C. W. (1986). Two‐layer organic photovoltaic cell. *Applied Physics Letters*, *48*(2), 183–185.

Tang, C. W., & VanSlyke, S. A. (1987). Organic electroluminescent diodes. *Applied Physics Letters*, *51*(12), 913.

Wenham, S. R., Green, M. A., & Watt, M. E. (2007). *Applied Photovoltaics*. Earthscan.

Wu, J., Agrawal, M., Becerril, H. A., Bao, Z., Liu, Z., Chen, Y., & Peumans, P. (2010). Organic Light-Emitting Diodes on Solution-Processed Graphene Transparent Electrodes. *ACS Nano*, *4*(1), 43–48.

Wöhrle, D., & Meissner, D. (1991). Organic Solar Cells. *Advanced Materials*, *3*(3), 129–138.

Yim, Y., Park, J., & Park, B. (2010). Solution-Processed Flexible ITO-Free Organic Light-Emitting Diodes Using Patterned Polymeric Anodes. *Journal of Display Technology*, *6*(7), 252–256.

Yu, G., Gao, J., Hummelen, J. C., Wudl, F., & Heeger, A. J. (1995). Polymer Photovoltaic Cells: Enhanced Efficiencies via a Network of Internal Donor-Acceptor Heterojunctions. *Science*, *270*(5243), 1789 –1791.

Yu, G., Zhang, C., & Heeger, A. J. (1994). Dual-function semiconducting polymer devices: Light-emitting and photodetecting diodes. *Applied Physics Letters*, *64*(12), 1540.

Yu, W.-L., Meng, H., Pei, J., Huang, W., Li, Y., & Heeger, A. J. (1998). Synthesis and Characterization of a New p–n Diblock Light-Emitting Copolymer. *Macromolecules*, *31*(15), 4838–4844.

imec Belgium vzw. (2011, December). *Press Release, http://www2.imec.be/be_en/press/imec-news/imecpolyerasolvayopv.html*

CHAPTER 3
Polymer solar cells: Materials, processing and device characterization

Few technologies have attracted so much attention and funding as polymer solar cells, which proves this is a booming field. There exists active research in the materials field synthetizing new polymers, in the printing and coating field, and in the process conditions. The scope of the present Chapter is to discuss the ingredients used for fabricating organic solar cells, and which is the performance of devices fabricated with the most successful combination of them at a laboratory scale. The different methods of laboratory processing followed to prepare these devices, both at a lab-scale, and in a semi-industrial scale will be explained. Therefore, continuous processing techniques towards a continuous manufacturing of organic solar cells will be herein reviewed. Finally, the techniques that have been used to characterize both layers and devices will be presented.

3.1. Organic solar cell geometry

Polymer solar cells have typical sandwiched structures comprising a series of layers, one on top of another. Depending on the order of these layers and the side of illumination, one can have regular or standard structure -the most used at small-scale processing-, or inverted geometry.

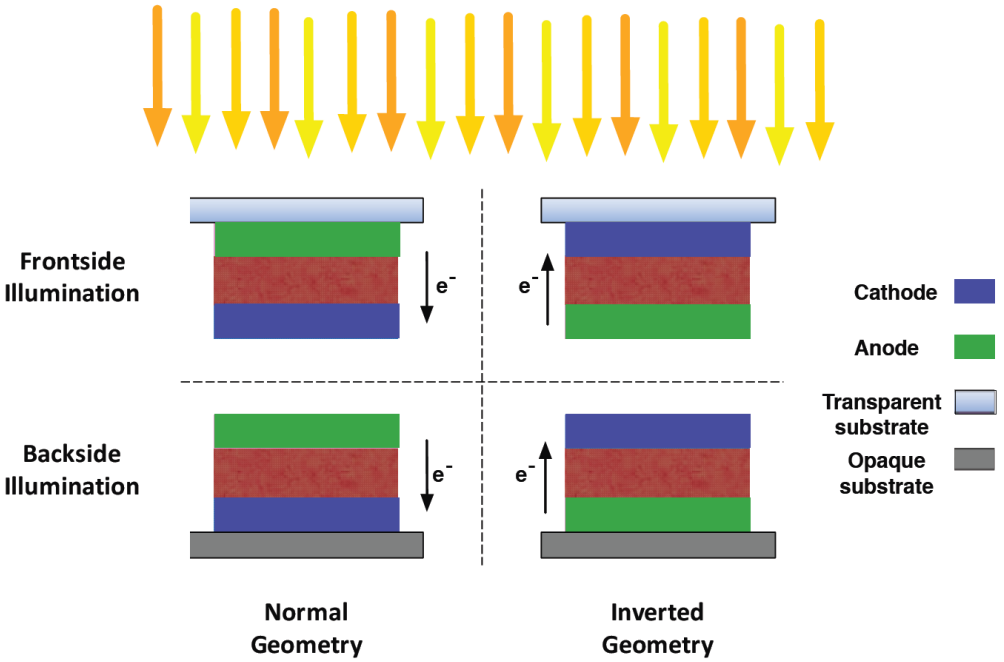

Figure 3.1. Normal and inverted geometry of OSC depending on the order of the layers and the side of illumination, where the electrons flux is shown.

Normal device structures (see Figure 3.1 left) use a front transparent electrode acting as anode (commonly indium tin oxide, ITO), and a back non-transparent electrode as cathode –aluminium is the most popular-. After a transparent anode is set down on a transparent base, a selective conductor layer is deposited on top, followed by the active layer, where light harvesting and photovoltaic effect take place. In the simplest configuration the device would just need to be completed with another selective conductor for guiding the electrons to the opposite electrode, the cathode.

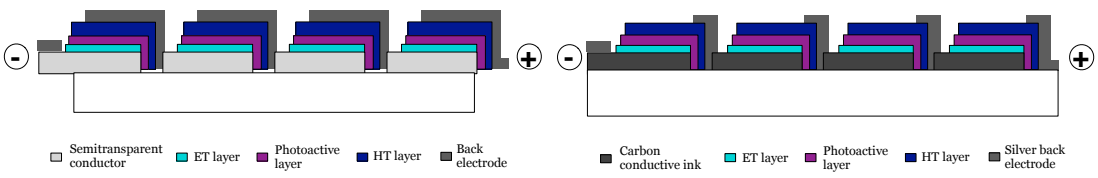

Figure 3.2. Typical organic solar module that comprises four cells serially connected for inverted devices for front (left image) and back illumination (right image) for which the electrode size is reduced in order for the light to enter through the back. ET stands for electron transport, and HT for hole transport.

When a metal with a higher work function than ITO is used as back electrode, and selective layers allow electrons to flow towards the cathode, these devices

receive the name of *inverted*. Figure 3.2, shows both possibilities for inverted geometry. Since the same level of performance can be achieved, many groups working in OPV, especially those devoted to a R2R fabrication have chosen this geometry due to the following advantages (Gevorgyan, 2010):

- First, the inverted devices behave better in the presence of humidity because of the less reactive silver electrode gives stable operation, despite this fact, they show poor stability in the presence of oxygen (Krebs, Gevorgyan, et al., 2009).
- The inverted device geometry gives the possibility to replace the interfacial layer of PEDOT:PSS as a buffer layer between ITO and active layer, which has been shown to introduce chemical and morphological instabilities at the interface with ITO (de Jong et al., 2000). In addition, PEDOT:PSS has non-negligible absorption in the visible region of the light spectrum[21] and substitution of PEDOT with more transparent TiO_x or ZnO can drastically improve the absorption of the active layer.
- The mobility of holes in the blend of P3HT:PCBM is higher than for electrons, as seen in organic FET devices by (Waldauf et al., 2006). Despite such difference might create unbalanced charge transport and space charge build-up in the device; in the case of inverted geometry that might be beneficial. Since illumination occurs through the bottom ITO electrode, holes have to travel through a longer distance compared to the slower-moving electrons (more excited carriers are created at the illuminated side of the layer) in inverted architecture. However, as mentioned in Chapter 2, slight charge transport asymmetries are not relevant this thin films due to the carrier drift length.

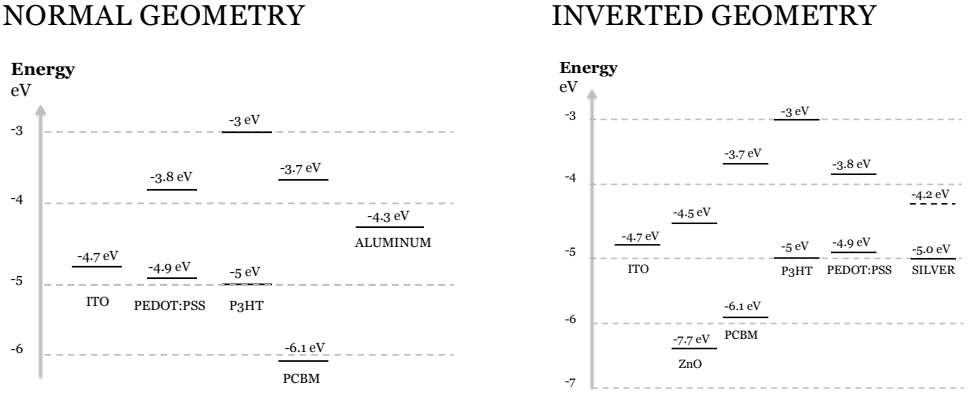

Figure 3.3. Energy levels in normal (left) and inverted (right) devices, for different constituent materials of organic solar cells, for example ITO, buffer layers and metal electrodes.

- The inverted geometry offers the possibility of using different materials less reactive to the surrounding environment than aluminium. It tends to oxidise rapidly in atmospheric conditions; shortening the devices lifetime significantly. Silver with high work function spreading from -4.2eV to -5eV (Figure 3.3) are suitable as anode and can be used under printable formulations, while aluminium needs an evaporated interfacial layer, to improve contact with the active layer. It is not a replacement because

obviously the device configuration changes and other functional layers are required.

- Finally, with inverted geometry, PEDOT:PSS layer which is usually a thick layer, is deposited sandwiched between active layer and silver (usually), therefore preventing the diffusion of silver atoms towards the active layer and this enhances the stability.

3.2. Materials

As seen in Chapter 2, the electronic transport properties of the conjugated polymers are strongly dependant on the structural arrangements of the macromolecules. A palette of these polymers have been intensively studied since the 1950s (Kallmann et al., 1959; Burroughes et al., 1990; Abad et al., 2012) and successfully incorporated in solar cells. To extract the photogenerated current, transport electrons, inject holes, and provide ohmic contact, other layers must be incorporated in the devices. In the following sections, materials will be reviewed with a view towards the continuous processing of polymer solar cells.

Polymers have been so far almost always processed using organic solvents, and the inks are specially formulated for the deposition technique, either for one device a time or for a continuous mode. The continuous processing of these cells, or roll-to-roll (R2R) fabrication will be dealt with in section 3.4.

Solvents for processing

Solvents are a key element of the ink handling since the mixture of solvents can modify the nanomorphology in polymer solar cells, e.g. controlling the phase separation (Dang, Wantz, et al., 2011; Yao et al., 2008). They also allow us for changing the viscosity of the ink and thus changing the wetting and making it more or less suitable for a certain deposition technique. For instance, in a donor/acceptor system as MDMO-PPV:PCBM the use of chlorobenzene lead to a finer phase separation (~50-nm grain size) than toluene (Hoppe et al., 2004). It has been found that a full separation of the two compounds of the active layer, enhances the collection of charge to the electrodes, being the dissociation of exciton diminished as in a bi-layer structure (Dang, Wantz, et al., 2011).

However, solvents may also deteriorate the adjacent layer. It was shown visually with a powerful technique as light beam induced current (LBIC), in section 3.5 further explained, that solvent-based silver degrades the active layer (Krebs et al., 2011).

As proposed in (R. Søndergaard, Hösel, et al., 2012), ink formulations can be divided in emulsions, suspensions and solutions. In Table 3.1, the main solvents that have been used in OPV can be seen at a glance. For PEDOT:PSS aqueous solution is generally used and alcohols and organic solvents are used to process the ETL; while with the active layer, chlorinated solvents are needed, as seen in the majority of reports. However, some trials have been recently done to process everything from water (Andersen et al., 2011; Larsen-Olsen, Andersen, et al., 2012; Larsen-Olsen, Andreasen, et al., 2012; R. Søndergaard et al., 2011) . This can imply an adverse potential of damaging the layers that have been pre-

deposited. Therefore, the orthogonality of the solvents (that a new layer's solvent does not dissolve the previous deposited layer) is a must.

Table 3.1. Choice of solvents as a function of layer, and deposition techniques that can be used for film forming.

Layer	Solvent	Techniques	References
Active (P3HT:PCBM)	Chloroform Chlorobenzene Dichlorobenzene 1,2,3,4-tetrahydro-naphthalene 1,2,4-trichlorobenzene Tetrahidrofurane Toluene Water	Spin coating Slot die coating Screen Printing Spray coating Ink jet printing	(Krebs, Jørgensen, et al., 2009) (Larsen-Olsen, Andreasen, et al., 2012) (Girotto, Rand, Genoe, et al., 2009)
ETL (ZnO)	Acetone Water Methanol	Spin coating Slot die coating	(Espinosa, Dam, et al., 2011) (Andersen et al., 2011) (Alstrup et al., 2010)
HIL (PEDOT:PSS)	Isopropanol Water	Spin coating Slot die coating Ink jet printing Flexographic printing Gravure	(Hübler et al., 2011)
Electrode (Silver paste, Graphite)	Isopropanol Water	Slot die coating Ink jet printing Screen printing Flexographic printing Rotary screen printing Spray coating	(Hübler et al., 2011)

As proven by life-cycle analysis (LCA), which will be treated in depth in Chapter 4, the processing of OPVs does not leave room for the use of solvents different than water and perhaps some alcohols, if they are meant to be produced on a large scale (Espinosa et al., 2012; Espinosa, García-Valverde, et al., 2011).

3.2.1. Substrate

Glass in all existing thicknesses and sizes, ranging from 1 to several hundreds of cm^2, has been used when the scale of production is one device a time. Conversely, if the throughput rises to m^2/h and roll-to-roll machinery is therefore employed, plastic foil is required. Thus, if this is the case, the plastic substrate must have a high transparency in the illumination side, but also a low permeability since it acts as a barrier, and a relatively high melting point above the processing temperature.

From all the available plastic foils, polyethylene (PE), polyethylene naphthalate (PEN), biaxially oriented polypropylene (BOPP), or polyethylene terephthalate (PET) films are widely used in the converting and packaging industry. In fact they are usually laminated films with several layers, that might function as oxygen, light or moisture barriers, or may be release layers to which adhesives will not stick, or conductive antistatic layers to prevent charge building up. But barrier requirements to oxygen and moisture are stricter for OSC (Figure 3.4 a), and not

every barrier film or product can satisfy them. More and more companies are now offering new developed materials specifically for OSC (Figure 3.4 b).

PET is the most used flexible substrate for OSC (Burrows et al., 2001; Zhou et al., 2008; Krebs, 2009a, 2009b; Krebs, Gevorgyan, et al., 2009; Krebs et al., 2010; R. Søndergaard, Hösel, et al., 2012).

Kapton ® is a polyimide film that also fulfils –actually, in excess- permeability criteria. It makes sense to use it for OPV when drying or heating treatment temperature is above the low glass transition temperature of the PET; or when possibly, metallizing a film on top is required (Manceau et al., 2011). It has an exceptional stability and dielectric quality that makes it suitable for being a substrate under special requirements.

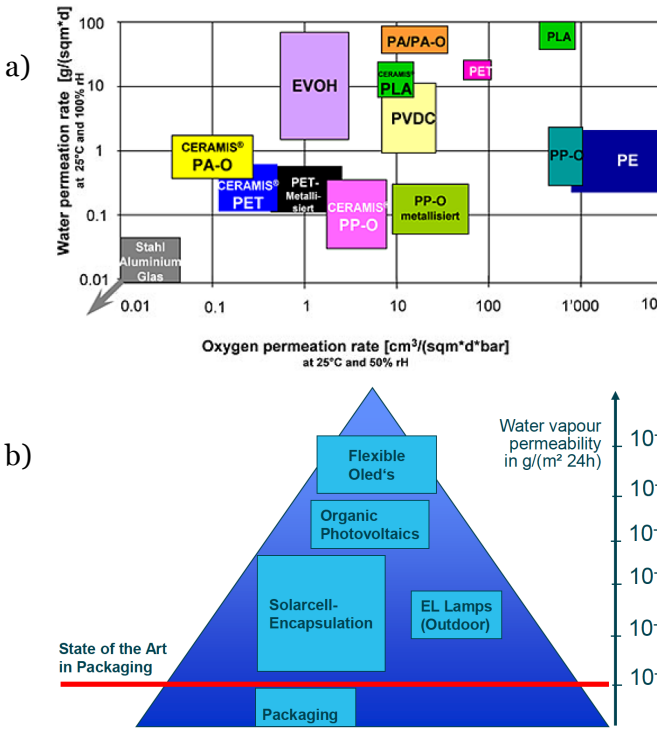

Figure 3.4. Classification of plastic foils as a function of water and oxygen permeation (a) and water permeability range required for technical products (b) by AMCOR ®.

Biopolymers are expected to grow in the mid term, and they could constitute a substitute for fossil fuels plastics if they provide the required levels of permeability. This could be the case for bioplastics as polylactic acid (PLA) or polyethylene furandicarboxylate (PEF). Moreover, the production of bioplastics can reduce the embodied energy in the fabrication to around half compared to PET by itself (Eerhart et al., 2012). In Chapter 4 energy related issues will be further discussed.

3.2.2. Front electrode

High transparency, around 80% on the 400–1100nm spectrum range, and a good conductivity, $\sigma > 10^3$ $(\Omega cm)^{-1}$ are two essential properties required for this layer.

In a device with normal structure this electrode behaves as hole collector -or anode- and in an inverted geometry it is an electron collector -or cathode.

The need for a transparent and highly conductive layer as an electrode in printed electronics started in the mid-1970s. Indium tin oxide (ITO), has both characteristics when deposited by vacuum sputtering tools. It was sputtered first on glass and now on flexible substrates, and it is commercially available in a myriad of qualities, sizes and substrates.

But indium, the main component of ITO, is a rare and scarce element, which has been declared, like many other rare earth metals, as *critical* in a EU report (European Commission, 2010). Rare earths are, as can be guessed by its name, uncommonly encountered in earth under concentrated forms; they are found in Earth as a result of a collision of a meteorite millions of millions of years ago. Since they are dispersed, their extraction must be performed via processing tones and tones of ores in order to extract a few kilograms of the precious metals. They also have geopolitical considerations since these materials are only exploited in China and USA. Moreover, ITO processing has been proven by life-cycle analysis to be the largest contributor to the embedded energy in the cell. These issues will be presented in Chapter 4.

In order to avoid the problem of indium scarcity, other transparent conducting oxides indium-free could substitute ITO. According to (Tadatsugu, 2008), one of the best candidates is aluminium zinc oxide (AZO).

As the firstly processed electrode being transparent or semi-transparent, a number of alternatives have been recently reported at laboratory scale including: carbon nanotubes (Rowell et al., 2006; van de Lagemaat et al., 2006; Tung et al., 2009), or graphene (Wang et al., 2009; Bae et al., 2010; Wu et al., 2010), silver nanowires -AgNW- (Madaria et al., 2011), and highly conducting polymers and metal grid electrodes (Na et al., 2008; Krebs, 2009b, 2009c; Galagan et al., 2011).

A second approach involves a non-transparent layer as the firstly processed layer, being then the front electrode a combination of HTL and a metallic grid. An example of this is the use of evaporated aluminium–chromium as the firstly processed non-transparent electrode, the semitransparent electrode having been processed lastly and being comprised of a doped polythiophene derivative (PEDOT:PSS) in combination with a metallic current collecting grid (Manceau et al., 2011; Zimmermann et al., 2011).

Therefore, the routes towards low cost and low environmental impact OSC, should be ITO-free, use non-scarce materials, and solution- processable inks instead of vacuum processed rare metals.

3.2.3. Active layer

Sandwiched between HIL and ETL, is the active layer. The most used approach is a bulk heterojunction (BHJ). It is a blend of two materials; one acting as donor and the other as acceptor of electrons. These two materials interpenetrate each other creating -ideally- two percolated networks at a scale which ranges rom a few to hundred of nanometres. The aim is to match with the interpenetrated

structure a length scale of the same order of magnitude than the exciton diffusion length (5-20nm). The formation of the exciton and its separation in charge carriers at the interface of the two different materials, takes place in the active layer. Figure 3.5 shows several examples of conjugated organic moieties.

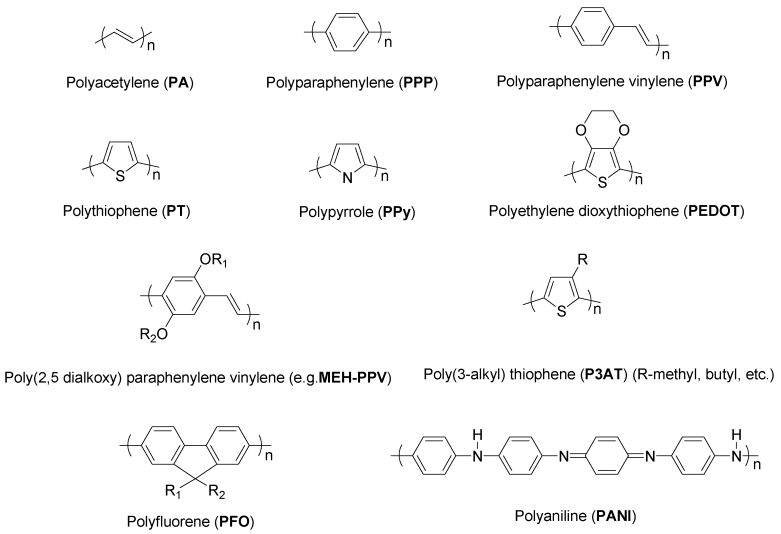

Figure 3.5. Examples of molecular structures of semiconducting polymers used in OSC, named as First and Second Generation (Heeger, 2010). Note the bond-alternated structures needed for enabling conductivity.

Donor materials: electron injectors

For a good donor material in OSC, HOMO levels should range from -4.8 to -5.75 eV. Design rules for donors can be found in (Scharber et al., 2006). First used in bilayer devices (diodes), and after in BHJ concept, (poly((2-methoxy-5-(2-ethylhexoxy)-p-phenylene)vinylene), or MEH-PPV, reached significant improvements in the beginning (Yu et al., 1995).

But an important development came in the 1990s with the discovery of an effective route to synthesise regioregular (HT) poly-3-alkylthiophenes, P3AT. These regioregular polymers (Mn=20,000 to 40,000) possess improved properties over the related regiorandom polymers, enhancing electrical conductivity, nonlinear optical properties and crystallinity[1]. They can be obtained electrochemically (Chen et al., 1995) or chemically following a regiospecific polymerization reported by (McCullough et al., 1992). The latter presents a higher degree of regioregularity, which makes it the method most used commercially. It is a one-pot synthesis consisting of a regioselective lithiation of 2-bromo-3-alkylthiophene and subsequent in situ generation of the Grignard reagent, followed by polymerization in which a catalyst- $NiCl_2$- rises from 98 to 100% HT-HT couplings. In Chapter 4, where an inventory of materials for OSC is gathered, processing route of P3AT will be detailed.

[1] For example, regioregular poly (3-dodecylthiophene) exhibits a conductivity of 1000 Scm compared with 20 Scm for its regiorandom analogue.

One of these P3ATs, poly-3-hexyl-thiophene, P3HT, has become nowadays the win-win option in OPV. At the present, the main suppliers of commercial PATs are e.g. Rieke Metals Inc., Plextronics, Merck, Honeywell.

A new group of more complex molecular structures, that allow for example for self-assembly BHJ, form a third generation of semiconducting polymers. Examples of these repeating units can be seen in Figure 3.6, and include bithiophene and polycarbazole copolymers (Blouin et al., 2008).

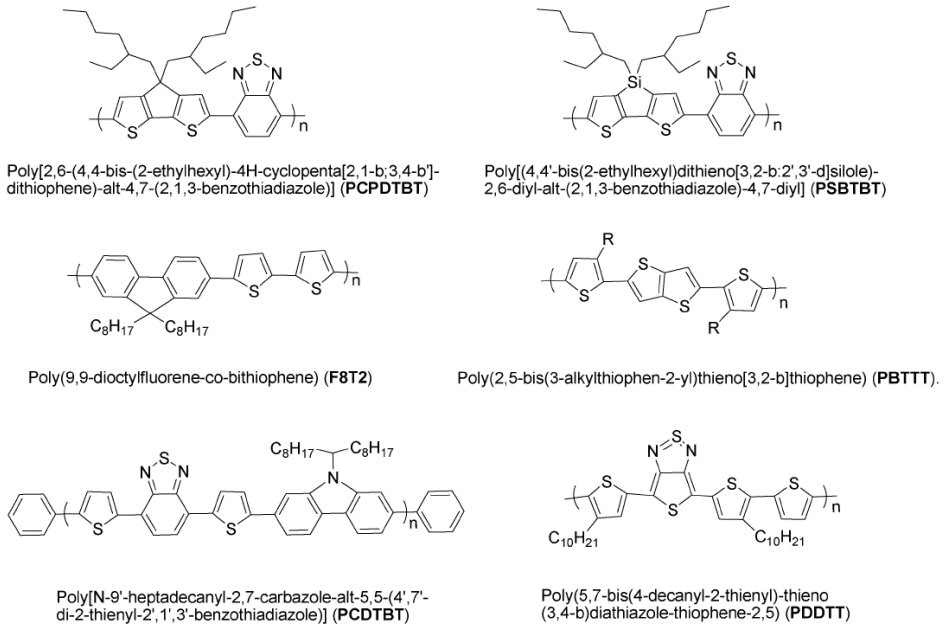

Figure 3.6. Third generation thiophene- and thidaizole- based semiconducting polymers (Heeger, 2010).

Acceptor materials

In theory, to have an optimal solar cell, the acceptor bandgap should be around 1.4eV. And as seen in Chapter 2, having band gaps higher than 2eV limits the, maximum efficiency, that in this case would be 31% under 1 sun AM1.5.

Despite these limitations, the best electron acceptors are ball-shaped carbon molecules called fullerenes. The simplest one is C_{60} consisting of 60 carbon atoms bounded together to form a soccer ball sphere. They were firstly manufactured by carbon arc discharge method, also known by plasma, where individual graphite rods are vaporized with electrical currents in presence of low-pressure inert gas (Krätschmer et al., 1990, p. 60). Other methods more controlled, consist in an initial evaporation of catalyst layers or particles followed by plasma enhanced chemical vapour deposition, PECVD (Kymakis et al., 2002). Fullerenes can be produced too by pyrolysis of hydrocarbon fuel at low pressure, and these methods are more commonly used today to produce soot-containing fullerenes. At the same time they have much lower impact than plasma methods (Anctil et al., 2011). The weight yield of C60 in this soot is very low, about 0.5 per cent (Takehara et al., 2005) at an industrial scale. Therefore subsequent cleaning and purification is used to separate more than 90% of the produced C_{60}.

Fullerenes can not be solved if they do not have an organic side chain as radical. A common functionalization of C60 molecule with this side chain is phenyl-C61-butyric acid methyl ester, or PCBM. Its 3-steps synthesis from C60 requires high amount of energy, and according to (Hummelen et al., 1995), each of these steps demands the same energy as the synthesis of a conjugated polymer. In the same way as for P3AT, fullerene synthesis routes are further described in Chapter 4.

The PCBM content in the active layer is 50 to 80 per cent, generally it is set to 60 per cent, and can be commercially provided by Solenne B.V in Europe, or SES Research, MTR Ltd., Term–USA, American Dye Source Inc., BuckyUSA, in USA.

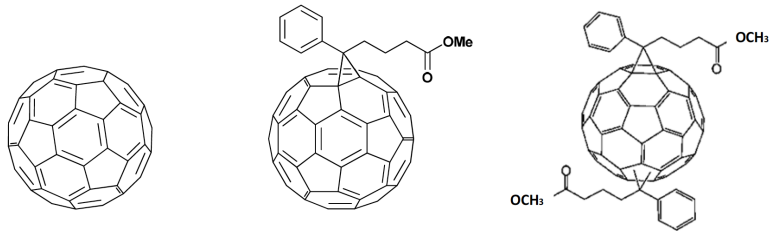

Figure 3.7. Molecular structures of commonly fullerene-based used as electron-acceptor materials.

In hybrid solar cells, where inorganic particles and hydrocarbon chains mix together, many inorganic acceptors have been reported in combination with P3HT or PPV, i.e. TiO_2, ZnO, CdSe, CdS, PbS, PbSe, SnO_2, and Si, as gathered by (Helgesen et al., 2010).

Best seller active layer

Named as *best seller* by (Dang, Hirsch, et al., 2011), the most prominent reported D-A combination for BHJs is the mixture P3HT:PCBM. The same authors made a review and they found that between 2002 and 2010, 1033 publications dealt with the bulk heterojunction based on these two materials. In this survey, 579 of these papers reported operating photovoltaic cells with their respective power-conversion efficiencies (PCEs) ranging from a low 0.5 to a –maybe excessive for a single junction- 6.5%. But this combination has limitations. The highest V_{oc} achieved has been 0.66V and this is to some extent due to the high HOMO of the PCBM and the wide band gap of P3HT that limits the photocurrent. Research must be carried out to find novel electron acceptor, polymers preferably.

3.2.4. Intermediate layers

Functional layers usually surround the active layer, with the ability to be more selective for one of the two species, injecting holes or electrons from the active layer towards the corresponding electrodes. The focus has been directed on solution-processed interface layers over vacuum processes, such as thermal evaporation or sputtering.

Hole injector materials

Although there has been several attempts to use small molecules as hole selective layer, it has been limited almost exclusively to PEDOT:PSS because it serves to

stabilize the work function of ITO and to planarize it, thus enabling formation of nearly defect free thin films on top (Günes et al., 2007). PEDOT:PSS has evolved and now exists in various formulations that provide exceptionally high conductivity and transparency. In addition, PEDOT:PSS is highly stable photochemically and is stable towards oxidative conditions.

But one of the Achilles heels of PEDOT:PSS is its hygroscopic nature. There has been much effort too to replace it, since the spincoating of PEDOT:PSS on top of the active layer is not easy, due to hydrophobicity of the active layer –previous layer in inverted geometries-. This problem is however never encountered under laboratory conditions where experimenters work under relatively dry indoor conditions or in a glove box environment. But this affinity for water represents a problem when deposited by a roll-to-roll method, due to the high surface tension of the PEDOT:PSS solutions. Vanadium oxide has been tried as a replacement for it (J.-S. Huang et al., 2009). In section 3.3.3 preliminary results of the work in this particular issue will be presented.

Electron transport materials

Whilst the performance of hole-transporting conjugated polymers has advanced rapidly over the past years, the number of high-performance electron-transporting polymers has grown less rapidly, since the developments have been driven so far by normal geometry devices. One of the main difficulties in this case is to synthesize conjugated polymers with high electron affinities in order to allow electron withdrawing from donors and to ensure transport stability (Gwinner et al., 2012). Therefore, inorganic metal transparent oxides have been used as electron transport layer (ETL) instead.

Mainly, ZnO and TiO_x can act as an extra electron carrier between active layer and front electrode (P3HT and ITO commonly). Zinc oxide nanoparticles (ZnO np) has been widely reported to be prepared according to (Womelsdorf et al., 2004), being redispersable in organic solvents as seen in Table 3.1, depending on the previous deposited layer, and can be stabilized with methoxyethoxyacetic acid (MEA) as a ligand ass reported by (Krebs et al., 2008).

TiO_x under amorphous phase prepared at low-temperature (150 oC) hydrolysis sol–gel process was shown to be effective for use in OLEDs and OSC. TiO_x also acts as a hole-blocking layer and optical spacer, which enhances absorption inside a thin device by modulating the optical field. It is responsible of a 40% enhancement in photocurrent and EQE a P3HT:PCBM system (Kim et al., 2006).

ZnO possesses higher electron mobility than TiO_x and it constitutes a widely used ETL since 2007 (Takanezawa et al., 2007; Steven K Hau et al., 2008; Krebs, 2008; Krebs et al., 2010; Zimmermann et al., 2009).

3.2.5. Back electrode

Vacuum deposited metals have been used so far for small-scale devices, such as aluminium or silver. Underneath, sometimes a protective layer of a few nanometres of calcium or lithium fluoride is pre-evaporated to prevent the migration of aluminium into the layer beneath. Thermal metal evaporation is an

energy intensive process, as it requires powerful vacuum pumps that can represent a large share of the embodied energy in a device. Some groups have reported the substitution of ITO as front electrode by the use of extremely thin layers of silver, so the layer is semitransparent (O'Connor et al., 2008; Ajuria et al., 2011).

With respect to electrodes compatible with R2R, metal nanoparticle solutions have been used, but in this case the electrodes are non transparent. Solution based titanium oxide has served as electron selective contact in highly efficient inverted cells (Waldauf et al., 2006). But silver is at present the only real candidate. It can be easily deposited by screen printing under the form of highly viscous inks, although many other techniques have been tried to deposit electrodes, as spray (Girotto, Rand, Steudel, et al., 2009), flexography, rotoscreen printing (Espinosa et al., 2012). Several types of silver paste are commercially available, sintered thermally or UV cured.

Printable metal back electrodes have been investigated in this context, by LBIC mapping of a final solar cell device (Krebs et al., 2011), in order to identify the causes of poor performance. These pastes are composed of relatively large silver particles, which ensure good conductivity, but with an unknown amount of binders, resins and rheology modifiers, which can deteriorate rapidly the layer beneath as mentioned in the Solvents section 3.2. Screen printable water based silver pastes have been prepared *just* using an aqueous binder, silver flakes, and water (R. Søndergaard et al., 2011).

3.2.6. Encapsulant and sealing

Whilst in inorganic technologies ethyl vinyl acetate (EVA) and poly vinyl butyral (PVB) are the most used encapsulants in PV, in organic PV, encapsulation and substrate permeability to oxygen and water are key aspects for the life time, due to degradation of the active layer and oxidation of the cathode.

The initial encapsulation of organic electronic devices has benefited from the number of barrier films used for food, medicine and electronics; usually ordinary polyethylene terephthalate (PET). But the permeation to oxygen and water must be lower for OSC than for food packaging (see Figure 3.4). Therefore, materials engineered specifically to flexible electronics purpose have been developed (Burrows et al., 2001). Such barrier films consist of multiple layers, where at least one layer is silicon or aluminium oxides (SiO_x or Al_2O_3) and the others are polymer materials such as PET. These oxides are impermeable to oxygen and water, but defects after deposition can interfere the barrier properties. A thicker layer is generally better, even though a too thick layer will crack when the device is bended (Grüniger et al., 2004). Barrier films can have Al_2O_3 sputtered on the polymer with thicknesses of between 10nm to 60nm, while polymer film thickness varies from a dozen of μm to one hundred μm. At Risø DTU, back encapsulation material is a PET thin film about 130 μm, although more recently, polyurethane has been tried there as encapsulant (R. R. Søndergaard, Makris, et al., 2012).

3.3. Laboratory fabrication of polymer solar cells

During the realization of the present PhD work, the setting up for the laboratory was performed, and a procedure for preparing OSC at a lab scale has been adapted for the conditions of our laboratory at UPCT, as explained in the following sections. The replacement of PEDOT:PSS by a vanadium oxide from solution will be as well presented.

3.3.1. Preliminary work. Setting up the lab facilities

First of all the designing job was done in the group at UPCT. This was a planning to determine the equipment and material required for the fabrication of OPV cells of several cm^2. It consisted in the steps shown in left part of Figure 3.8. A) substrate preparation, B) spin-coating of HTL and active layer, C) electrode evaporation, D) external contacts and encapsulation. A side-view of a complete device (out of scale) is shown in E).

Regarding the deposition of layers, a custom spin coater was used. The back electrode could be deposited by vacuum, as well as by screen printer, although this latter has not been used in preparation of functional solar cells yet. Contacts masks were prepared in stainless steel, laser patterned with the geometry shown in Figure 3.8 bottom right. Then, a vacuum chamber was customized and set up to be used as thermal evaporator, as shown in Figure 3.8 top right.

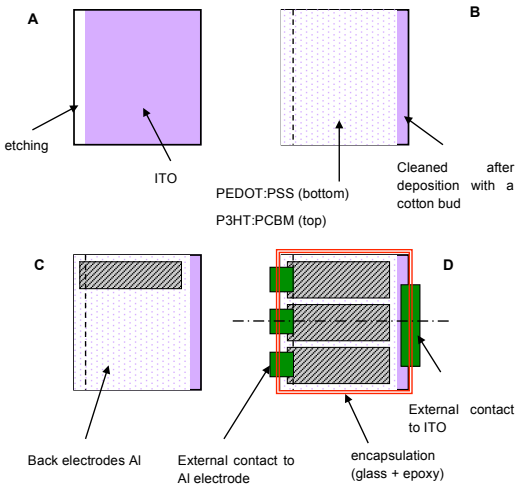

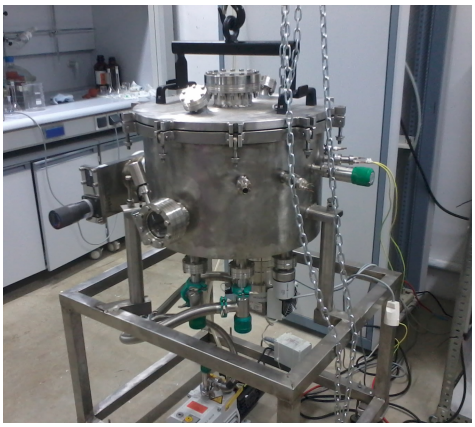

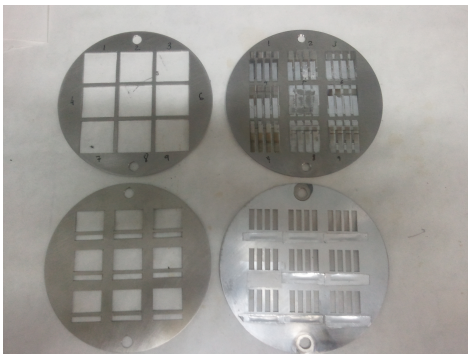

Figure 3.8. Top left, detailed scheme of several steps involved in the fabrication of a OSC. Right top, vacuum chamber for evaporating, and right bottom contact masks and cell holder fabricated at Universidad Politécnica de Cartagena.

3.3.2. Procedure for fabricating cells

For preparing OSC, the recipe detailed in Figure 3.9 was followed, which is grounded on relevant literature. Initially, a cleaning step is always performed. A glass substrate covered with indium tin oxide (ITO) is carefully cleaned with acetone, isopropanol and oxygen plasma. Previous to deposition of the PEDOT:PSS, water solution is heated at 50ºC and stirred for 30 min. Then it is filtered and is deposited by spin coating on the cleaned substrate at 1800rpm, a thin film PEDOT:PSS that will work as hole injector layer. After that, the device is transferred to a nitrogen glove box, and annealed at 70 ºC for 2 hours. Then, the blend for the active layer is prepared: a blend of P3HT and PCBM. The polymer and the functionalized fullerene are deposited by spin coating from a toluene/dichlorobenzene solution, in this case at 900 rpm. Finally, two metals layers are deposited as back electrode. First, a 60nm Calcium layer, and second a 150nm Aluminium layer. Both are usually thermally evaporated in vacuum.

The cell can be prepared either inside or outside a Nitrogen atmosphere, but in the later case the efficiency has been demonstrated to be lower. It can be encapsulated to prevent air contact.

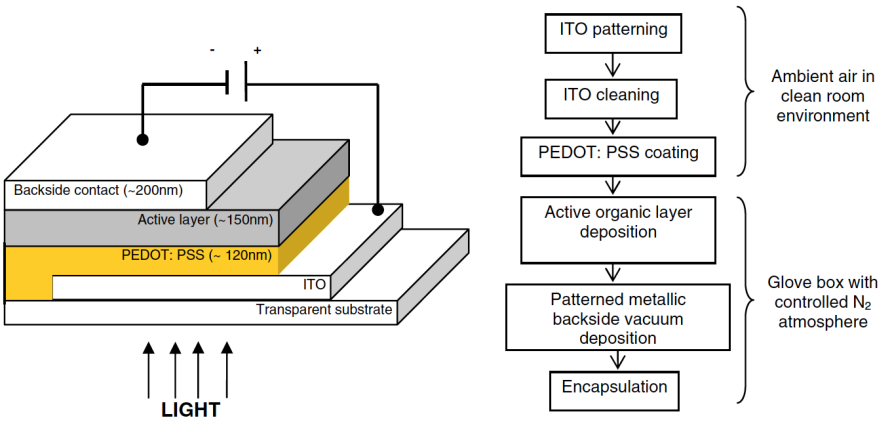

Figure 3.9. Steps in the manufacturing of OSC devices with a normal configuration in the laboratory at UPCT.

A set of 9 sample cells can be fabricated at once by using the masks, shown in Figure 3.10.

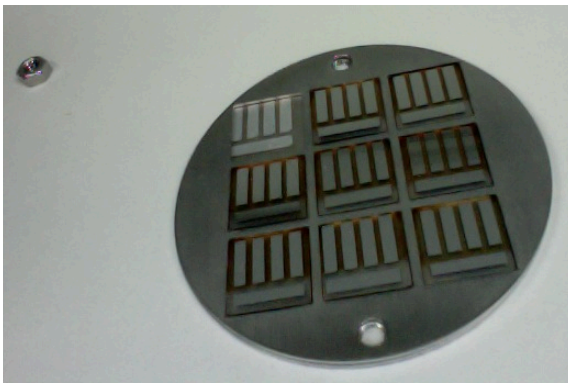

Figure 3.10. Organic solar cells on glass substrates of 4 cm² with the layers: ITO/PEDOT:PSS/P3HT:PCBM/Al, as manufactured at Universidad Politécnica de Cartagena.

3.3.3. Replacement of materials

Due to the issues mentioned in section 3.2.4 with PEDOT:PSS, a vanadium isopropoxide diluted in isopropanol was used as a replacement. Vanadium seemed to be a good candidate to replace PEDOT:PSS, since it is the 13th most-abundant element in the Earth's crust -global resources are estimated to exceed 63 million tons, and could be deposited from solution. For that purpose, two different types of polymer solar cell modules were constructed at Risø during my stay in 2010: one type was a standard device with PEDOT:PSS and another type where PEDOT:PSS had been replaced with hydrated vanadium(V) isopropoxide. We fabricated small devices on glass, and complete modules on PET with the structure displayed in Figure 3.11, and that work has been reported in (Espinosa, Dam, et al., 2011).

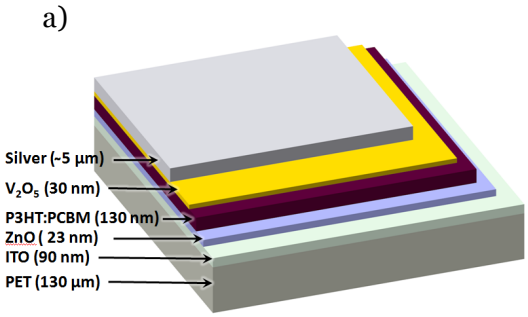

Figure 3.11. Schematic of inverted cell fabricated using V_2O_5 instead of PEDOT:PSS, with typical layer thicknesses shown.

To certificate the structure and the packaging of vanadium oxide layer, X-Ray diffraction and SEM images were used, as it will be explained in section 3.5.1. The power conversion efficiency (PCE) was limited by the resistance of the vanadium(V)oxide and interface layers which reduces the current density in comparison with optimized cells manufactured with PEDOT:PSS; being for completed modules up to 0.18 %, in contrast to single cells on glass substrates where efficiencies of 0.4% were achieved. This is shown further in section 3.5.2.

3.4. Towards a continuous processing of OSCs

To take advantage of the flexibility of the polymer solar cells and join together with the packaging (or converting) industry capabilities was something very straightforward when working OPV devices with laboratory efficiencies above 3% were achieved. One of the first reported R2R fabrications of functional polymer solar cells was just 3 years ago (Krebs, 2009a). As a part of my PhD, I spent almost 4 months at Risø DTU in Denmark, in 2010. I had the opportunity to work at the experimental semi industrial scale set up that was running there, and know with large detail how this fabrication line works and which are the key conditions for this manufacturing process, all of that served as a foundation for carrying out detailed life-cycle assessments afterwards. There is roll-to-roll machinery specially designed and adjusted for depositing from solution flexible polymer solar cells and some of the most used techniques and the steps of manufacturing have been depicted in Figure 3.12 and Figure 3.13.

Based on the techniques used at Risø and literature in the field, film-forming methods most appropriated for fabricating polymer solar cells, thus being R2R compatible as shown in Figure 3.20, where a group of optimized and alternative deposition techniques is presented and it will be described in the following sections.

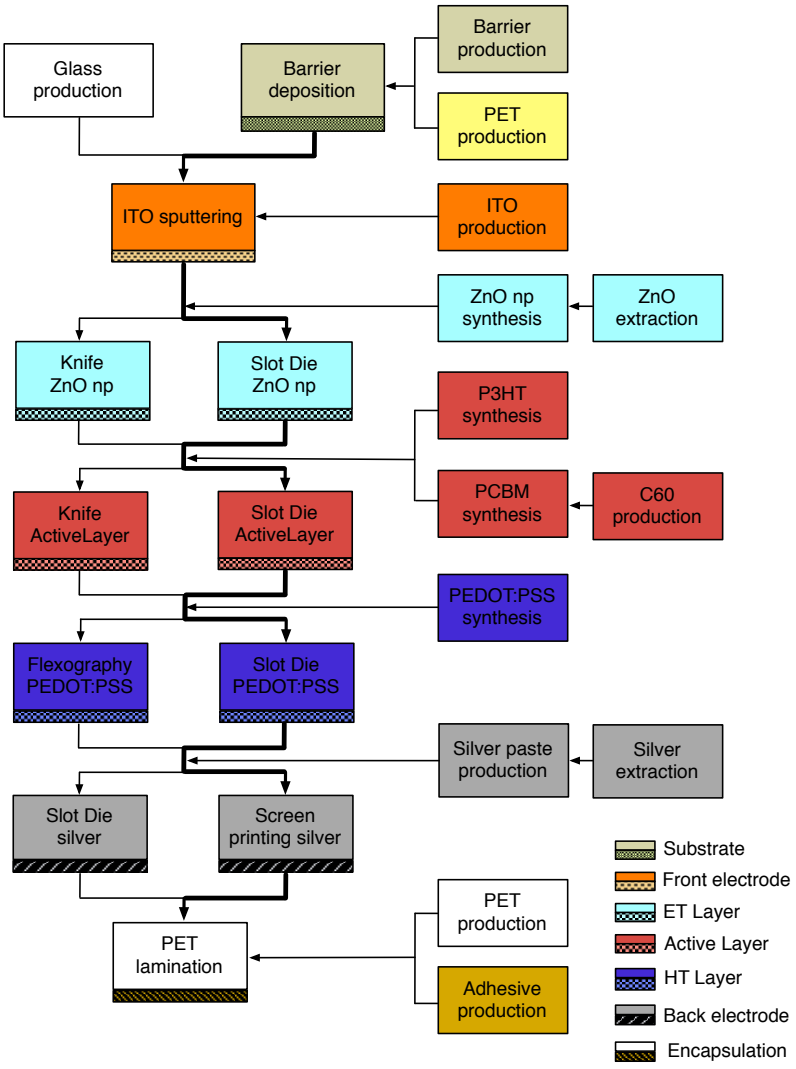

Figure 3.12. Alternative deposition techniques, the optimized routes are shown in bold, for the different OSC manufacturing steps, showing the production of materials involved in the fabrication.

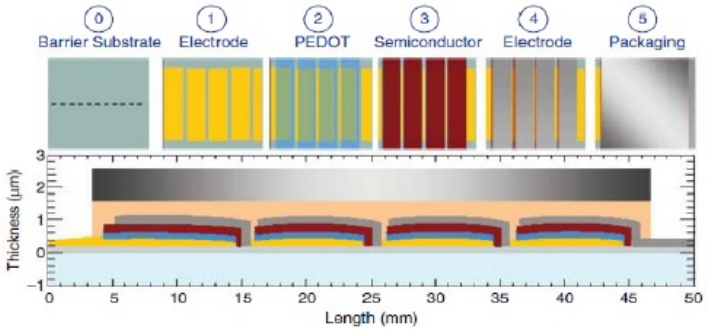

Figure 3.13. Side and front view of the main 5 steps involved in the manufacturing of a 4-stripes polymer solar cells in: (1) electrode deposition, (2) hole transport layer PEDOT-based, (3) semiconductor layer, (4) back electrode, and (5) packaging.

Techniques classification

Thin-film processing can be primarily classified as a function of the physical state of the material, as shown in Figure 3.14. Film-forming process can provide patterning or not. If we consider a patterned liquid-state deposition, printing and coating are two of these solution deposition methods. It is no clear sometimes why a technique is a printing or a coating one. For historical reasons, they have been named printing when for reproducing text and images, and coating when the solution was somehow poured trough a slot with a simple patterning. From now on, in this work, I will follow the old criteria of the name.

Printing as a massive technique started in Europe in 1439, with Gutenberg's printing press. A printing machine serves for applying pressure to an ink and it passes therefore to a substrate trough a pattern, transferring this way a motif to a that substrate. Coating machinery had to wait 500 years to be developed by the hand of a Swiss textile engineer, Jacques E. Branderberger. By 1908, he developed the first machine for the manufacturing of transparent sheets of regenerated cellulose and patented in (Brandenberger, 1918). Coating and printing technologies have since then evolved empirically, by trial and error, even without links to the scientific understanding of the applicable principles. The complexities of the field are such that the formulator's craft is still essential in developing and using these techniques. The need to reduce pollution and energy budget while maintaining and, preferably, improving coating performance of the industrial processes requires radically new formulations on a short time scale. There is a fine line between R& D and innovation at industrial level, but an increased understanding of the underlying science can help the field of OSC to work more effectively. Being independent of a formulator's craft is essential for scientists working in this field.

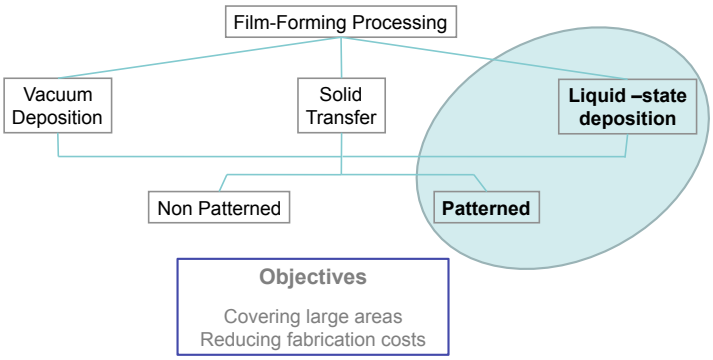

Figure 3.14. Film-forming processing classification attending to the physical state of the material to be deposited and to the capability of the technique to pattern thin films.

3.4.1. Printing techniques

Printing is a relatively simple method for creating patterned films. However most of the printing techniques require high-density inks. Apart from other distinctions, the most used printing techniques can be distinguished by the principles to transfer ink to the substrate, and ink separation between printed and non printed areas (see Figure 3.15). These two principles determine the overall setup of the respective machinery, ink supply, as well as processable

materials and achievable properties of the deposited polymer. Techniques as offset, gravure and flexography, known as *mass printing*, have non permeable ink transfer and no ink separation. They are typical rotary printing methods and high-speed processes.

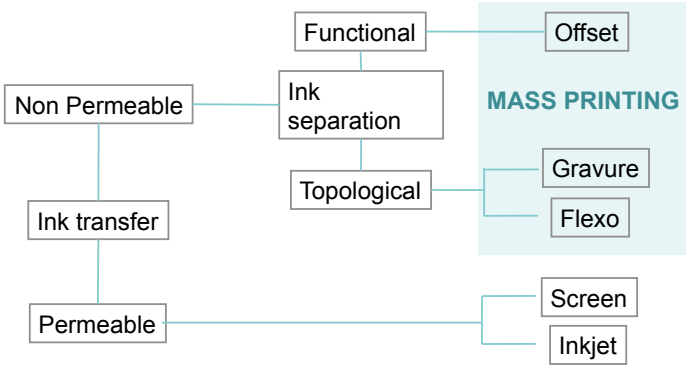

Figure 3.15. Classification of printing processes by ink transfer and ink separation principles.

Flexography & Gravure

Ink separation for these both techniques is due to topological differentiation, i.e. the printing parts are situated below or above nonprinting parts. Flexographic printing, often abbreviated to flexo, is a R2R technology in which the transfer of the ink is made from a relief plate (see Figure 3.16 left). The final pattern stands out from the printing plate, which is typically made from rubber or a photopolymer. Conversely, in gravure technique the ink is transferred by surface tension from the indentations on a cylinder, forming the pattern, to the web (see Figure 3.16 right).

The flexo system consists of an ink roll, partially immersed in a tank, where ink is continuously transferred to a ceramic cylinder, named as *anilox* roll, which has the pattern engraved into the exterior as cells or micro wells. This allows the collection of ink, which is then transferred to the 3D mirrored image on a second cylinder, the *printing* cylinder. It performs the final transfer to the web, as shown in Figure 3.16. Roll-to-roll flexographic printing has not been yet reported to be used for processing the active layer in polymer solar cells, but there is a case of processing a modified PEDOT:PSS (Hübler et al., 2011) and a patterning of conductive grids (width below 50 μ m), which could potentially be used as electrode structures (R. Søndergaard, Hösel, et al., 2012).

Gravure, or rotogravure, widely used in high-volume print runs like magazines, postcards and packaging, is always rivalling with offset printing, albeit rotogravure presses are the fastest and the widest presses. The dizzying figures are speeds up to 15 m/s, and web widths above 4 meters. The depth of the cavities or indentations in the so-called *gravure cylinder*, defines the thickness of the final imprint. The engraved cells on the gravure cylinder are continuously filled from the ink bath and a doctor blade removes the excess of ink, ensuring that the ink is only present in the cavities. Gravure printing is suitable for printing low viscous inks; appropriated therefore for OPV typical inks, and has been used with that purposes by (Ding et al., 2009; Kopola et al., 2010; Voigt et al., 2011).

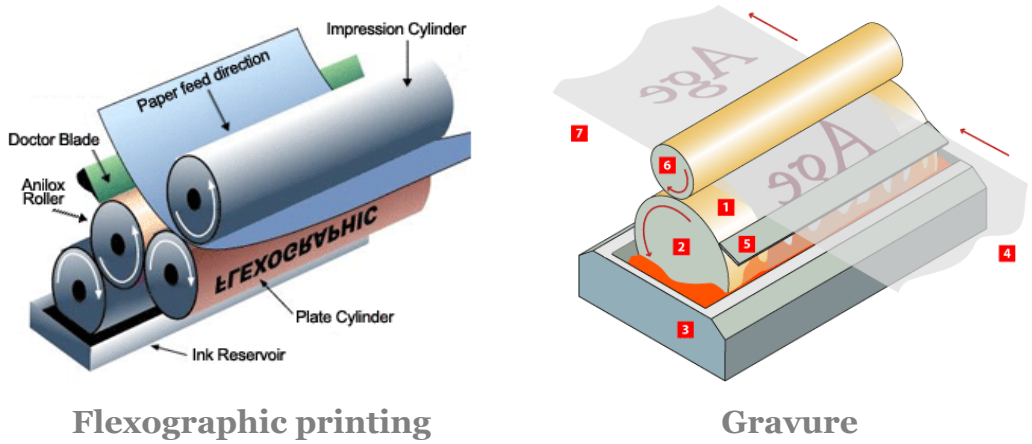

Figure 3.16. Flexographic scheme (left image) and gravure where inking unit, anilox roll, and substrate is shown.

Screen printing

It is also known as serigraphy, a combination of words *seri* (*silk* in latin) and *graphein* (*writing* in greek), hence the other designation: silkscreen printing. The process involves a screen of woven material (i.e. synthetic fibre or steel mesh) that has been glued to a frame under tension, and a squeegee to extend the paste and push it, through the open areas of the screen, onto the substrate.

The wet thickness of the coated film is in principle given by the theoretical paste volume of the screen, V_{screen}, i.e. the volume between the threads of the mask and the thickness of the emulsion. V_{screen} measured in the volume of ink per area of open screen (cm^3/m^2). Typical wet layer thicknesses are in the range of 10 to 500 micron. Final dry film thickness, d, depends then on V_{screen}, and the pick-out ratio, K_p, and also on the concentration of the solid material in the ink in g/cm^3, *c*, and ρ is the density of the material in the final film in g/cm^3.

Limiting factors or challenges to overcome are the large wet film thickness and the relatively high viscosity, that difficult the ink handling. The low volatility of the coating solution implies as well a larger energy budget to dry or cure the ink.

Since it allows for the formation of very thick layers, with a high viscosity, is very suitable for printing electrodes in an OSC, as seen in section 3.2.5. But also screen printing of active layers have been reported (Krebs, Jørgensen, et al., 2009).

Flat-bed screen printing is the most used form so far, but there also exists a rotating version. In rotary screen printing, the ink is contained inside the rotating cylinder with a fixed internal squeegee. Both techniques have significant differences although the principles of functioning are very similar. These differences are well explained in (R. Søndergaard, Hösel, et al., 2012). Summing up, flat-bed screen printing is operated at a lower cost than rotary version, and it is possible to make adjustments between prints if needed, which is an important aspect. In terms of production it is also possible to print on very large areas with rotary screens (on the scale of $10m^2$). But in terms of speed, edge definition/resolution, and achievable wet thickness, rotary screen printing is far superior to flat-bed screen printing by at least one order of magnitude. Besides,

the ink is less exposed to the surroundings due to geometric issues and it is a two-dimensional printing technique that allows for the largest wet thickness achievable (> 300 μm). However, rotary screen printing is not as well suited for laboratory work as the flat-bed technique because of the cost of the mask, the more delicate operation, the difficult adjustment and the relatively time-consuming cleaning procedures.

Ink jet printing

In-jet printing is a technique in which a printing moving head delivers tiny droplets of ink at a well-defined location of the surface to be printed. Two basic approaches exist for drop creation and acceleration in inkjet printing (IJP) systems: continuous and drop on demand systems. In continuous mode the ink is pumped through a nozzle to form a continuous liquid jet, which is broken into drops by means of an acoustic wave generated by a piezoelectric device. Uniformly spaced and sized droplets are obtained by imposing a periodic perturbation, leading to surface tension driven jet break-up. Ejected droplets are then electrically charged and deflected according to the desired design. Continuous-mode inkjet is mainly used for high-speed applications such as textile printing and labelling.

In drop-on-demand (DOD) systems, droplets are discontinuously created by acoustic pulses generated, either piezo-electrically (mainly for non-water based inks) or thermally (when having water-based inks). The main features of IJP are smaller drop size and higher accuracy. In a thermal DOD inkjet printer (or bubble-jet) ink is heated locally to form a rapidly expanding vapour bubble that ejects an ink droplet. Thermal DOD usually uses water as solvent, which can represent a problem with some organic-soluble polymers, to use this technique. Piezoelectric DOD inkjet printing relies on the deformation of some piezoelectric material to cause a sudden volume change and hence generate an acoustic pulse for ejecting the droplets.

Several limiting factors to droplet formation may be present. The achieved resolution so far is the transistor channel length of 50μm (Doggart et al., 2009). The viscosity should be suitable low, typically below 20mPa (20cPoise); otherwise too much kinetic energy is dissipated by viscous forces and no droplet is ejected. However, the lower the viscosity the greater the velocity and amount of fluid propelled forwards, which usually lead to the formation of long tails behind the head of the drop.

The restrictions on ink formulations have had a negative impact on the use of this technology for organic solar cells. IJP has so far been reported to be used in small devices (0.03 – 1 cm^2, up to 3.7 % PCE), processing either the PEDOT:PSS layer, the P3HT:PCBM, layer, or both (Hoth et al., 2007, 2009). Nevertheless, the possibility for complex pattern formation and high resolution makes the ink-jet technique an interesting future candidate for OPV processing.

3.4.2. Coating techniques

Coating methods are in principle more compatible with low viscosity solutions, than printing ones, since it is not necessary that the design stays on top of the

substrate while it dries. Classification of these methods can be done regarding the number of layers, but this limits the underlying principles of coating. If the mechanism that controls the thickness -or weight- of the wet film is considered, then three basic groups appear:

- Self-metered: The thickness of the film is adjusted by the method itself. Examples are dip coating, kiss coating and meniscus or bead roll coating.
- Doctored: here a two-part applicator is used. The continuous liquid film is applied by any method, and a doctoring device is then used to remove excess coating. It thus controls the final coating weight. This method can give good coating quality and stability with many different coatings. The disadvantage is that the coating solution is either wasted or if it recirculates back, can pollute the fresh solution. Examples are air knife coaters, blade and knife coaters, Mayer rod coaters, and dip and scrape coaters.
- Pre-metered: the thickness here is controlled by the mass flow circulating. The coating thickness is just the flow rate per unit width divided by the substrate speed, so coverage is not dependent on viscosity. Examples are slide coaters, slot die coaters, extrusion coaters and precision curtain coaters.

Knife and slot die coating

Knife coating is very similar to small-scale doctor blade technique, and laboratory results can be transferred quite easily to roll-to-roll knife coating. This comprises an ink reservoir, placed before a blade that serves to supply ink to the meniscus, as it is gradually deposited behind the knife, passing the web by at the same time.

In the case of slot-die coating, a simple pattern like stripes of a well-defined width along the web direction is possible. The ink is pumped throughout a die, which contains slots, to form meniscus. Wet thickness can be adjusted by controlling the speed of the web or the ink supply (or both). The natural limits to the achievable wet thicknesses depend on the coating window, which is defined mostly by the ink properties and the web surface properties, but also by the coating geometry. Web speeds are in the range of a few meters per minute.

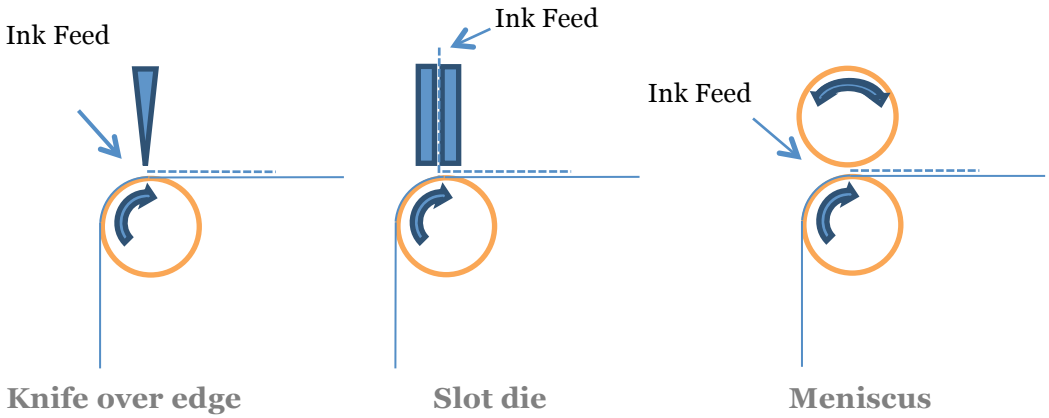

Figure 3.17. Scheme of three coating methods: Knife over edge, Slot die and Meniscus coating.

The easiness of controlling coverage and the excellent coating uniformity and quality, joined together with the multilayer coating capability, make these methods very suited to be applied with low viscosity solutions in OPV. For the

intermediate layers of polymer solar cells, these techniques have been the most used so far (Blankenburg et al., 2009; Krebs, 2009a; L. Wengeler et al., 2011; Zimmermann et al., 2011).

Spray coating

Another widely used film-forming technique is spray coating. The film is formed through droplets and without physical contact between the coating head and the web. Despite it is called coating; no continuous wet film is formed. Similar to inkjet printing the ink is applied through droplets but where ink-jet printing achieves high graphical resolution through control of the droplets, spray coating does not allow for control of the pattern since it is *per se* a zero-dimensional coating technique. It is possible to pattern through a shadow mask but it is likely impractical outside of the laboratory. Spray coating has been employed in several literature reports for the laboratory preparation of many of the layers in the OPV stack as the active area (Susanna et al., 2011), for depositing a silver back electrode (Girotto, Rand, Steudel, et al., 2009; S.K. Hau et al., 2009; Girotto, Rand, Genoe, et al., 2009; Na et al., 2010), and in one case for the three stack layers; i.e. electron transport, active, and hole transport layers (Vak et al., 2007; X. Huang et al., 2010; Lukas Wengeler et al., 2012)

Curtain, Slide and Multilayer slot die coating

These techniques allow for the simultaneous formation of many layers (> 10), and could ideally allow for the formation of the entire solar cell stack in one or two single coating steps. This would imply less energy involved in its fabrication (for machinery, web handling and drying) without having to increase the web speed. But those techniques have to be run at a high web speed, typically 5 – 20 m/s.

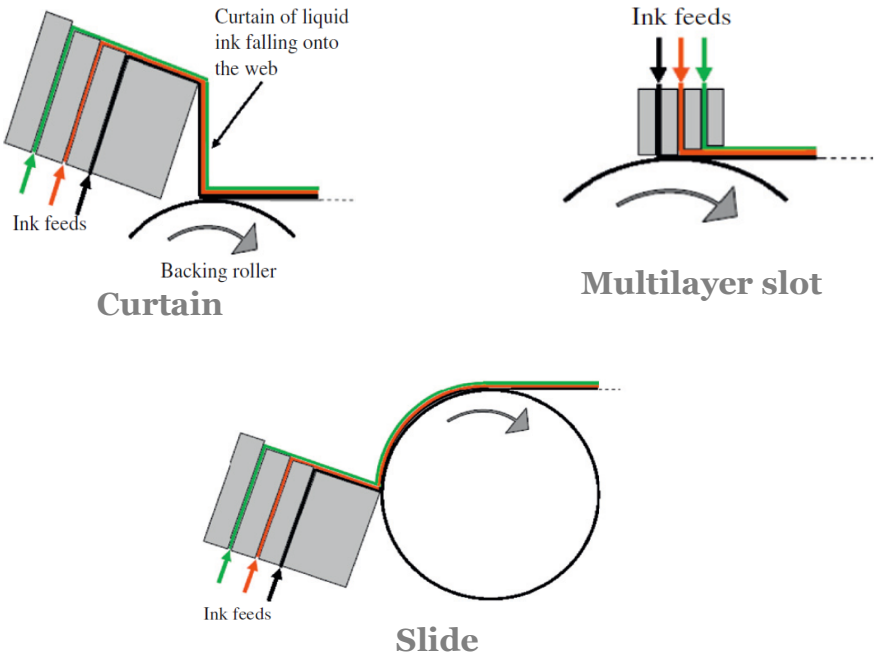

Figure 3.18. Pre-metered coating methods, where the thickness is controlled by the mass flow circulating.

Though, double slot-die coating is possible to work at much lower web speeds and on a much smaller scale than curtain and slide coating, and also allows for a much simpler control of the ink flow. Its potential is therefore large and it is the only multilayer coating technique that has been employed for organic solar cells in a full R2R process. It has been possible to simultaneously coat an aqueous nanoparticle dispersion of P3HT:PCBM and an aqueous dispersion of PEDOT:PSS on top of doped zinc oxide in (Larsen-Olsen, Andreasen, et al., 2012).

3.4.3. Ancillary processing: Lamination and Drying

There are several manufacturing steps further the coating and printing ones in a R2R process. As for example it can ben necessary changing the surface tension of the raw substrate for printing jobs. Corona treatment is a widely applied solution in the converting industry for that purpose. The utilization of a RF plasma pre-treatment, of an organic substrate surface leads to improvements in the optoelectronic properties of unheated films without damaging the polymers (Herrero, 2002).

After the drying and before the rewind steps there might be a post-treatment section, e.g screen printed silver ink of back electrodes -in inverted type OPVs-, may be crosslinked with ultraviolet light, or an electron beam or another sheet may be laminated onto the coated substrate. However, drying is the most used post-film formation. By heating the wet film, the solvents can be removed leaving a dry film of the desired thickness.

Thermal annealing shows significant improvement in the performance of OPV devices, generally being a slightly better post-production annealing method, and a large number of research has been conducted to study the effects of annealing temperature and time on the device performance (Campoy-Quiles et al., 2008; Lilliedal et al., 2010). The reasons of the improvement rely on the ability of heat for efficiently forming percolation paths in a BHJ, minimizing therefore bulk recombination and increasing crystallization of polymer lattices which improves the charge carrier. Nanodomains sizes increase up to optimize values corresponding to the exciton diffusion lengths in each material, which have been determined for P3HT:PCBM to be from 10 to 100nm. Corresponding images by atomic force microscopy are later shown in section 3.5.1.

Another post film formation treatment can be a patterning step. OPV manufacturing, as seen in Chapter 2, requires a serial connection to boost carrier mobility of the polymer. This can be performed by forming stripes directly or by a subtracting method as laser patterning. Lasers are a good tool to do this since they do not damage the layer beneath when removing the top one: well-controlled small amounts of heat are released. They are also compatible with a R2R processing.

Lamination

After the solar cell stack has been printed, it needs to be encapsulated on the printed side to provide the modules operational stability and mechanical protection of the delicate printed layer stack. The process of lamination is in

principle realized with very simple equipment, with the same basic principle of joining two lines of web and applying pressure as they are fed between two rollers. The use of cold lamination typically employs a pressure sensitive adhesive that is lined and applied to the laminate by a lamination process followed by removal of the liner and lamination onto the solar cell stack. This is very easy to control at the laboratory level at high speeds (> 20 m/min is easily accessible). Hot melt lamination uses the same principle, but here the film has usually an adhesive material on it, which becomes adhesive when heated. UV lamination requires that an uncured adhesive or glue is applied by printing or coating immediately prior to bringing the two foils together. In the laminator, the glue is cured by application of UV-light. In terms of operation, hot-melt is by far the easiest method in comparison with cold lamination; this last is slightly more complicated because the handling of the sticky adhesive -this implies that only one side of the foil can be handled-. UV-lamination is by far the most complicated since it also involves a printing or coating step, where the UV-curing adhesive has to be previously printed (R. Søndergaard, Hösel, et al., 2012).

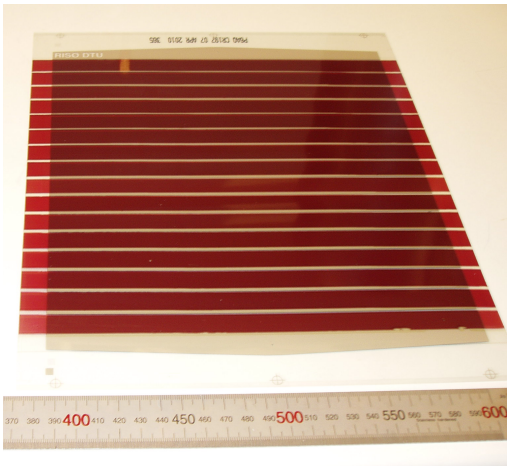

Figure 3.19. Typical 16-stripe flexible module produced at Risø DTU.

3.4.4. Choosing the optimum method

Given that the deposition of these organic materials could be entirely from solution, each layer could be deposited by an individual film-forming technique. Figure 3.12 shows different methods for depositing different layers by R2R that have been tested at Risø DTU. Nevertheless, an ideal process should involve multilayer solution processing, reducing coating and printing steps, but as seen in section 3.4, this is still a challenge.

Coating or printing methods have different capabilities and operation data, and therefore advantages and drawbacks, and the number of different coating methods can rise up to 1000. This work presents an assessment of the most suited film-forming technologies (presented in section 3.4), but not massively explored in the context of polymer solar cells (Espinosa et al., 2010).

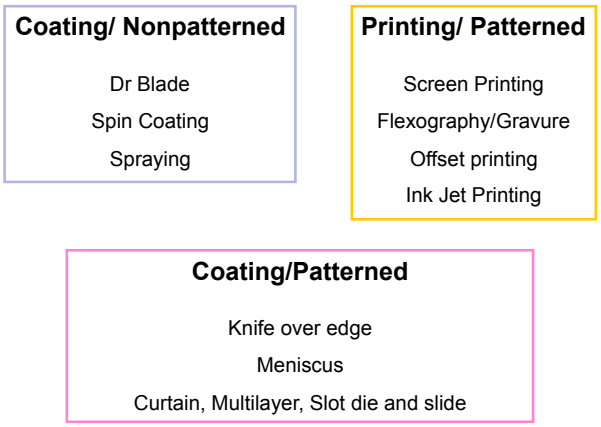

Figure 3.20. Film forming techniques compatible with R2R evaluated.

This analysis have been grounded on a multi-criteria decision making methodology (MCDM), to provide support to the decision-maker in the process of identifying the ideal coating technique/s for polymer solar cells.

To find a right combination of techniques for a multilayer product, whatever it is, the first stage consists of establishing the window of coatability or product requirements range. A summary with the more suitable properties for each deposition technique can be seen in Table 3.2. These properties have been extracted from literature (Krebs, 2009d; Wagner, 2009) expert questionnaires, and personal experience in the facilities at Risø DTU. They have been grouped in criteria and subcriteria and have been weighed, according to Eq 3.1 and the decision-maker preferences, with linguistic labels.

Eq 3.1

$$\omega_i = \frac{\left(\prod_{j=1}^{n}\left(a_{ij}, b_{ij}, c_{ij}\right)\right)^{1/n}}{\sum_{i=1}^{m}\left(\prod_{j=1}^{n}\left(a_{ij}, b_{ij}, c_{ij}\right)\right)^{1/n}}$$

In order to deal with unstructured and multi criteria problems, the analytic hierarchy process (AHP), which was developed by Saaty (1980), has been employed. As a result three groups seemed to appear in which the technologies have similar score:

- First group, formed by Gravure, Flexography, Offset, Inkjet, Curtain and Screen, showed a short distance to positive ideal solution, because their operation values are inside the window of coatability. Furthermore, this first group reveals a certain predominance of printing techniques over coating ones.
- Second score group, formed by Slot die, Doctor Blade, Knife over edge. The cited technologies have a farther distance to ideal solution, but could be acceptable methods.
- Third group is Slide coating scored as the worst technique for the purpose of organic layers deposition, mainly due to the low score in criteria such as Thickness control, Reproducibility and Maximum throughput, which are parameters with high weights in the criteria selection process.

Table 3.2. Classification of techniques as a function of their characteristics in four criteria: Design Control, Ink properties, Reproducibility and Energy input.

	DESIGN CONTROL					INK PROPERTIES		REPRODUCIBILITY	ENERGY INPUT		
	Thickness Control			Dimensional Control	Number of layers	Viscosity (Pa·s)	Ink preparation		Ink waste	Max. Throughput (m^2/h)	Embedded energy
	Wet thickness (µm)	Volatility	Speed (m/min)								
A1. DOCTOR BLADE	10-100	medium	0.001-0.1	0	1	0.01-40	simple	very low	low	low	high
A2. KNIFE OVER EDGE	10-750	low	1-100	0	1	0.05-100	moderate	very low	very low	5000	medium
A3. SLOT DIE	10-500	medium	1-1000	1	3	0.01-300	moderate	high	very low	50000	low
A4. SLIDE	25-250	medium	1-1000	pseudo/quasi 2/3	17	0.01-300	critical	high	very low	100000	low
A5. CURTAIN	5-500	high	10-1000	pseudo/quasi 2/3	17	0.015-2	critical	high	very low	100000	low
A6. SCREEN	3-500	low	0.01-100	2	1	0.1-100	demanding	low	very low	100	high
A7. INKJET	0.3-500	high	0-1	digital master	1	0.001-0.01	moderate	medium	very low	50	high
A8. FLEXOGRAPHY	0.8-200	very high	1-1000	2	1	0.01-1	demanding	high	very low	50000	very low
A9. GRAVURE	0.8-80	very high	1-1000	2	1	0.01-2.5	difficult	high	very low	100000	very low
A10. OFFSET	3-210	very low	3-300	2	1	2-100	demanding-difficult	medium	very low	50000	medium

3.5. Characterization techniques

An important part in the research of OPVs is the proper understanding and characterization of the devices in terms of chemical and morphological properties but also in terms of photovoltaic performance. There are numerous techniques for characterization, which can be divided into two categories: (i) techniques that provide either morphological and/or chemical information from specific spatial locations in the device, and (ii) techniques that provide information from the performance of the device. This section presents results obtained measuring the devices fabricated at UPCT and Risø DTU; following the routes presented in sections 3.3 for small scale devices and 3.4 for R2R modules. Characterization results of the analysis of some materials that compose these devices are herein presented.

3.5.1. Materials and film characterization

UV-vis

The absorption of UV light corresponds to the excitation of outer electrons. Measuring the spectral absorption distribution of films, in the wavelength range from near ultraviolet to near infrared, can serve to give an idea of morphology changes (such as crystallinity of the polymer) in the materials or blends during device processing (for example after thermal annealing) as it was shown in section 3.4.3. It can be done with a spectroscopy, by shining monochromatic light on the sample film and recording the transmitted light. The sample can be a pure glass substrate with coated film to be tested. The absorption for given wavelength can be calculated from the value of the transmitted light. From the absorption measurements one can roughly estimate the optical bandgap of the absorbing semiconductor. The absorption spectrum measurements can UV-Vis spectra presented in Figure 3.21 correspond to spincoated films of P3HT:PCBM and PEDOT:PSS, both onto ITO/glass plates. Since absorption depends on the thickness and PEDOT:PSS layer was very thin (hundreds of nanometer), it can be seen that PEDOT PSS transmission is high, although it can absorb a large amount of visible light when the layer is thick. ITO spectra are a constant of 80% transmission (for the hole range 350-850nm).

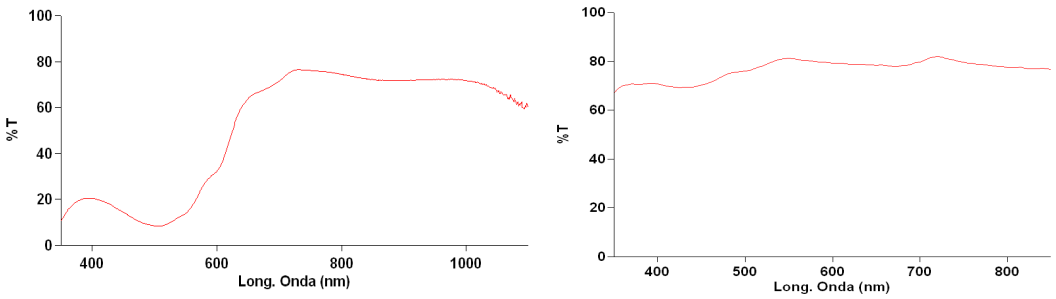

Figure 3.21. UV-Vis spectra of spincoated films in air of P3HT:PCBM (left) and PEDOT:PSS (right), deposited over ITO-glass plates.

Atomic Force Microscopy

Atomic Force Microscopy (AFM), also known as Scanning Force Microscopy (SFM), is an imaging technique that typically maps the surface with respect to surface topography (Binnig et al., 1986). AFM covers a limited analysis area (from atomic resolution to hundreds of micrometers), has an excellent lateral resolution (nm range) and an excellent height resolution (that can be sub nanometre, <0.1nm, range), which makes it an ideal tool for study the film morphology. The operating principle of AFM is as follows: A cantilever with a sharp tip (probe) is used to scan the specimen surface. When the tip is brought into proximity of a sample surface, forces between the tip and the sample lead to a deflection of the cantilever. The deflection of the cantilever is recorded by the reflection of a laser beam from the cantilever surface, the laser signal is detected by a photodiode connected to a feedback system which controls the piezo-scanner, in order to maintain the tip-sample interaction constant, in this way the piezo-scanner follows the topography of the sample and a 3D image of the surface can be plotted.

The typical application for AFM with regard to OPVs has been to monitor and thus optimize the nanostructure of bulk heterojunction (BHJ) blend films in order to understand how the nanostructure of BHJ affects the OPV efficiency.

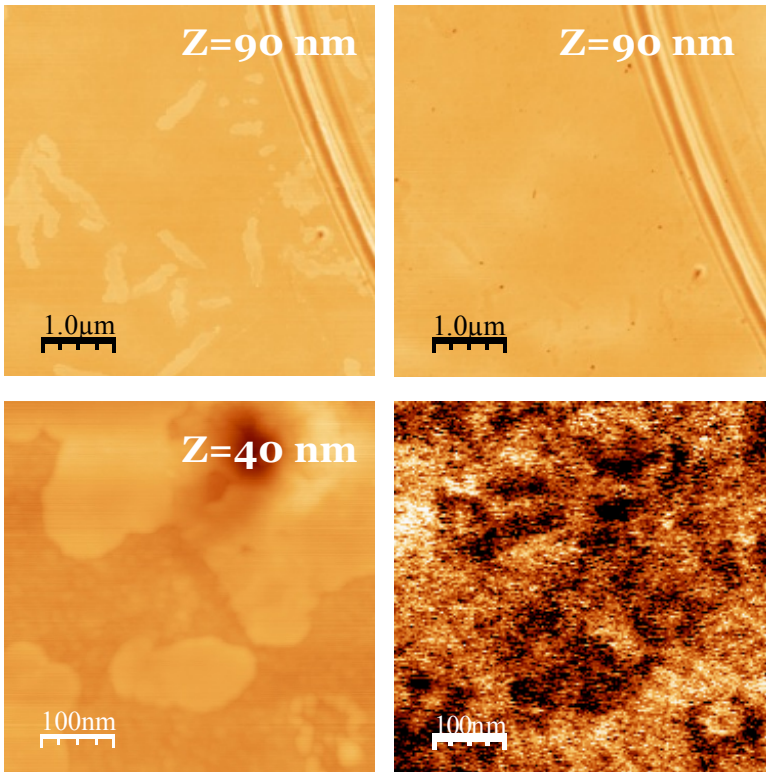

Figure 3.22. Images of pristine P3HT:PCBM blend (top left) and after 20 min Ar ion bombardment under UHV conditions (top right). Layered structures (top images) disappear at 30min. Layered structures (bottom images) have a contact potential difference with respect to blend background of 170 mV measures by KPM technique (bottom right).

AFM setup at our University allows performing AFM nanoscale studies of the same region, even if the sample is taken out of the AFM system for different processes. This experimental set up was used to measure segregation phase in

P3HT:PCBM films (with concentrations of 21 and 18.5 mg/ml in chlorobenzene) before and after Ar ion bombardment. It is well known that polymer blends most often tend to cleave into separate phases rather than form a uniform medium. In this case, P3HT segregated towards the surface, as seen in Figure 3.22, where arranged structures of this polymer appear with a height of 3.2 nm, in agreement with observed X-Ray studies (Abad et al., 2012)

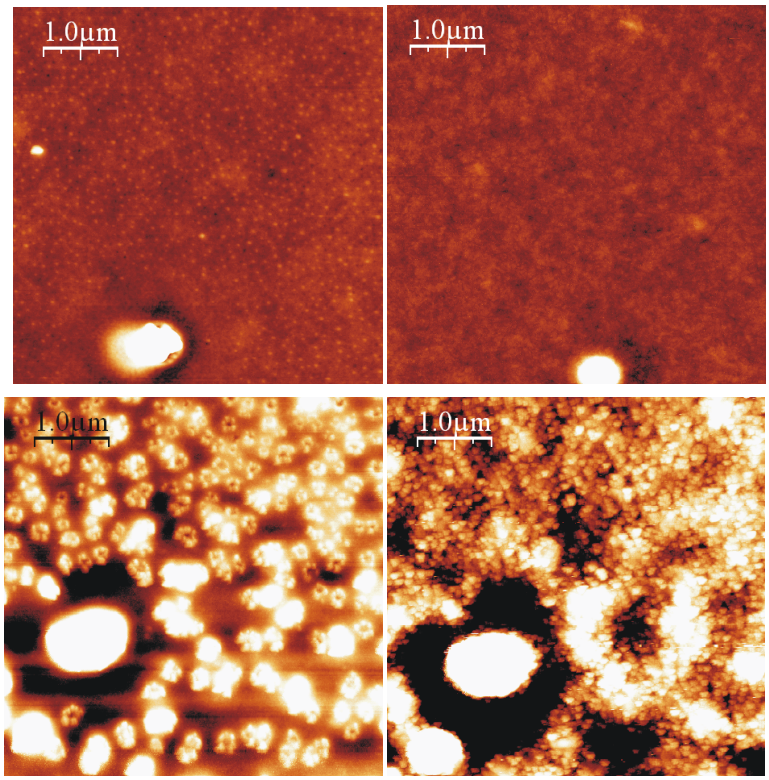

Figure 3.23. Images of pristine P3OT thin films (top left), after 7 min UV and O_3 exposure (top right), 15 min UV and O_3 exposure (bottom left), 30 min UV and O_3 exposure (bottom right). The observed changes are due to the real effect of radiation and O_3 since the same region is observe each time.

AFM has proven to be a powerful tool to investigate the degradation of the devices due to morphology changes. Therefore, films of 100 nm thickness of other common polythiophene, P3OT, prepared by spin coating on conducting and insulating substrates, were exposed to UV irradiation and O_3. As shown in Figure 3.23, for short time exposures (7-10 minutes) the roughness and the thickness of the films do not change, conversely the colour of the sample is lost. After 10 minutes of UV irradiation the roughness increases, small grain like structures appear and the film thickness decreases, while the light attenuation is almost constant. These grains become denser after 10 minutes of irradiation (in Figure 3.23 bottom left) and finally, the grains have merged into clusters (in Figure 3.23 bottom right). We conclude that degradation of P3OT thin films when irradiated by UV light occurs in two steps. Firstly, it occurs an initial chemical reaction with ozone generated by the UV irradiation that varies the optical absorption of the films. We attribute these changes to the breaking of the conjugated bonds of the polymer chain; additionally, local conductivity is reduced. In a second step, the films are etched away by further chemical reaction with ozone (Abad et al., 2011).

Differential Scanning Calorimetry

Subsequent heating and cooling cycles of an specimen, allows extracting relevant parameters of the material phase transitions. This is known as differential scanning calorimetry (DSC) and from calorimetric temperature diagrams at different scan rates, melting and crystallization temperatures can be obtained. A calorimetric glass transition can be also identified.

DSC of bulk P3HT and P3OT samples was performed at different temperature scan rates using a Mettler-Toledo DSC822e calorimeter. Nitrogen was used as purge gas, and samples were scanned at 1, 6, 10, 15, 20, 25 and 30°C/min, in a temperature range spanning from minus 145°C to positive 250°C. The heat flow needed to conduct the experiments was kept in the range of 0.5–15 mJ/s, matching the optimum range of the instrument. For all the solutions a total mass of 12.4 mg was used. Besides crystallization and melting temperatures, a low temperature calorimetric glass transition was identified. This transition was somehow expected because of the coexistence of amorphous and crystalline phases, which had been further supported by scanning force microscopy images (Figure 3.22).

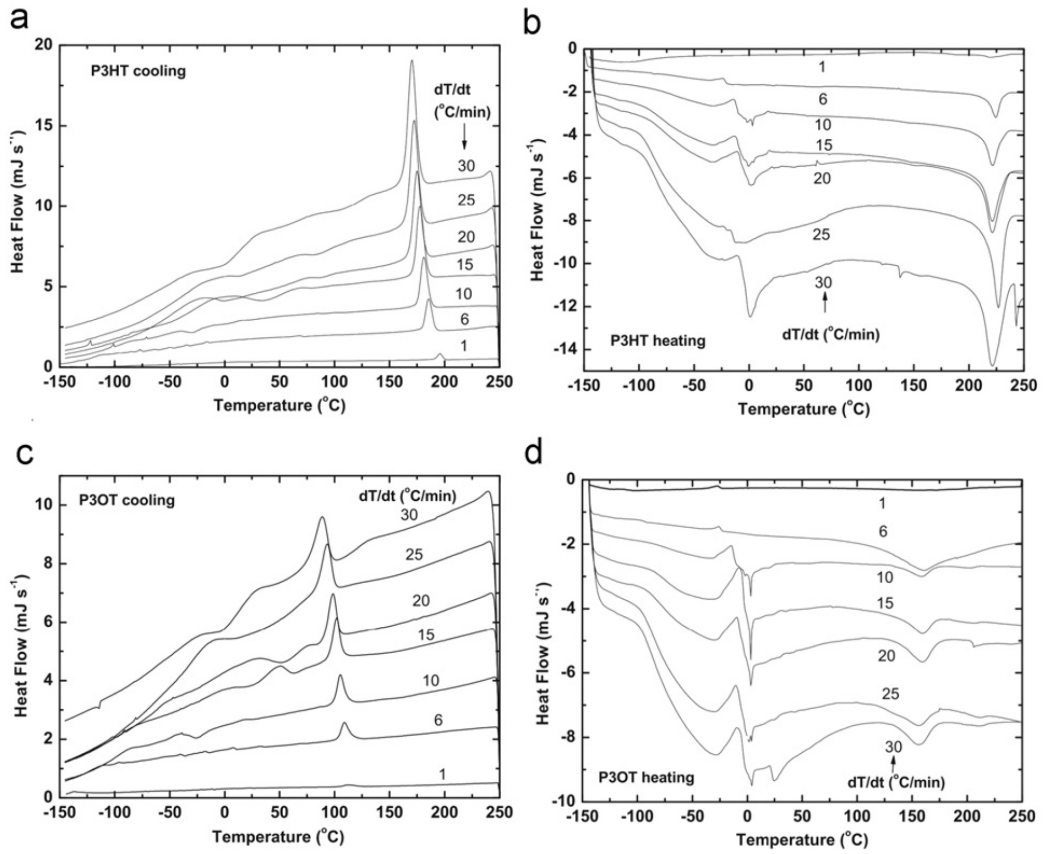

Figure 3.24. (a) Cooling and (b) heating DSC temperature scans at different scan rates for a bulk sample of P3HT. (c) Cooling and (d) heating DSC temperature scans at different scan rates for a bulk sample of P3OT.

The (a) cooling and (b) heating DSC temperature scans at different scan rates for a bulk sample of P3HT can be seen in Figure 3.24. The crystallization peak is observed at the right hand side of the plots (a). The melting peak is observed at

the right hand side of the plots (b). Also, (c) cooling and (d) heating DSC temperature scans at different scan rates for a bulk sample of P3OT ae shown. The crystallization peak is observed at the right hand side of the plots (c). The signature of a glass transition at low temperature is evident from the slope change in the left hand side of the plots (d). The different scan rates (dT/dt) are indicated by the numbers of each plot (Abad et al., 2012).

These mass values were also used to obtain an estimated heat capacity at constant pressure from our heat flow measurements for both materials. The obtained melting and crystallization temperatures at different scan rates are shown in Figure 3.25.

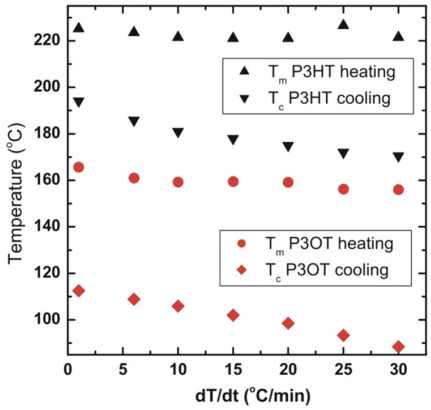

Figure 3.25. Melting (T_m) and crystallization (T_c) temperatures for P3HT and P3OT obtained from the peak temperatures of the heating and cooling calorimetric scans as a function of the temperature change rate (dT/dt).

Grazing incidence X-ray diffraction

To track the eventual structural changes with an information depth selected at will, grazing incidence X-ray diffraction (GIXRD) is a very suitable technique; from a few nm to several hundreds of μm, just by changing the incidence angle. Polymer layer orientations were characterized by GIXRD experiments carried out at fixed wavelength of 8.26 nm on a six-circle diffractometer at SpLine beam line (BM25B), European Synchrotron Radiation Facility (ESRF), Grenoble, France, as reported in (Abad et al., 2012). A point scintillation detector, which allows performing high-resolution diffraction experiments was used. The sample was placed on a heating stage covered with an air-tight Kapton housing filled with 1 bar of nitrogen in order to avoid the degradation of the sample. Two incidence angles, α = 0.15° and 2.00°, were used and the temperature range was from 21°C to 120°C, as shown in Figure 3.26.

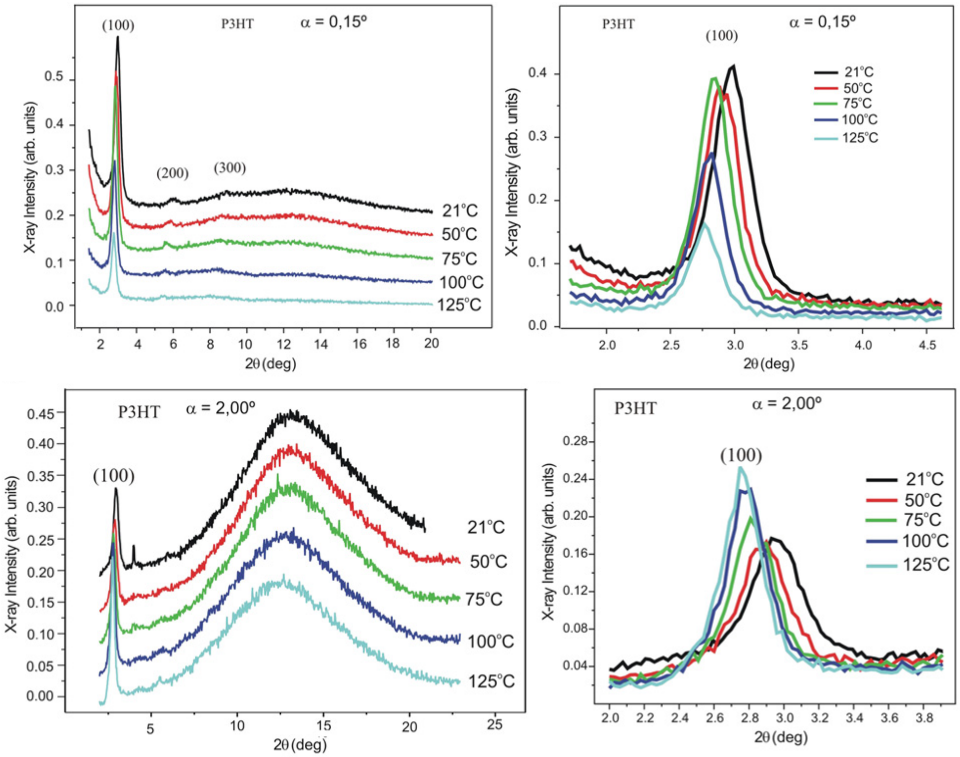

Figure 3.26. X-ray diffraction profiles of P3HT taken at 0.15° (top images) and 2.00° (bottom images) beam incidence angle, at different annealing temperatures. A zoom of the 2–4° region can be seen top and bottom at the right.

Grazing incidence wide angle X-ray scattering (GIWAXS) was also used to determine the packaging of vanadium and certificate its crystalline structure, as published in (Espinosa, Dam, et al., 2011). It was done by simulating the GIWAXS pattern according to published $V_2O_5 \cdot (H_2O)_n$ structures. The strongest scattering feature near the centre of the image in Figure 3.27 left, corresponds to the 001 reflection, whereas the weaker scattering at the edges of the image, correspond to the 110 and 111 reflections, showing that the crystallites are preferentially oriented with the ab-plane parallel to the substrate surface.

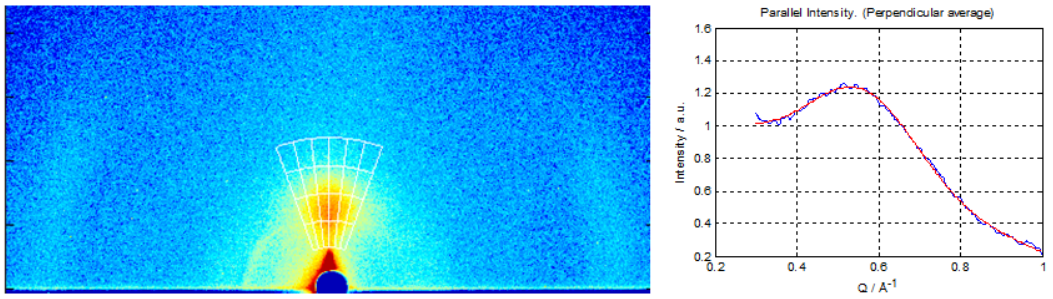

Figure 3.27. Left: The GIWAXS data as measured, with intensities represented on a color log scale. Right: Integration over 001 peak, assuming sample to detector distance of 121 mm, yields a d-spacing of 11.1 Å

3.5.2. Device measurement

IV Curve Measurements

One of the primary techniques for evaluating the performance of a PV device is based on simple measurements of the diode characteristics of the solar cell. The devices produced at UPCT along this thesis were characterized under a Sun simulator AM1.5 Class AAB. The method also requires as a voltage source, to make a voltage sweep, and an electrometer for measuring and recording the corresponding current generated by the device. With these recorded data, the IV curves can be plotted. Parameters such as V_{oc}, I_{sc}, *FF*, *PCE*, R_{sh}, R_s can be then extracted from the measured IV curves, which are the most important values that define the device performance (as detailed in Chapter 2). Dark IV characteristics are usually performed as well since they can be useful for extracting information about: series resistance, shunt resistance, saturation currents and ideality factor of the equivalent one-diode circuit model

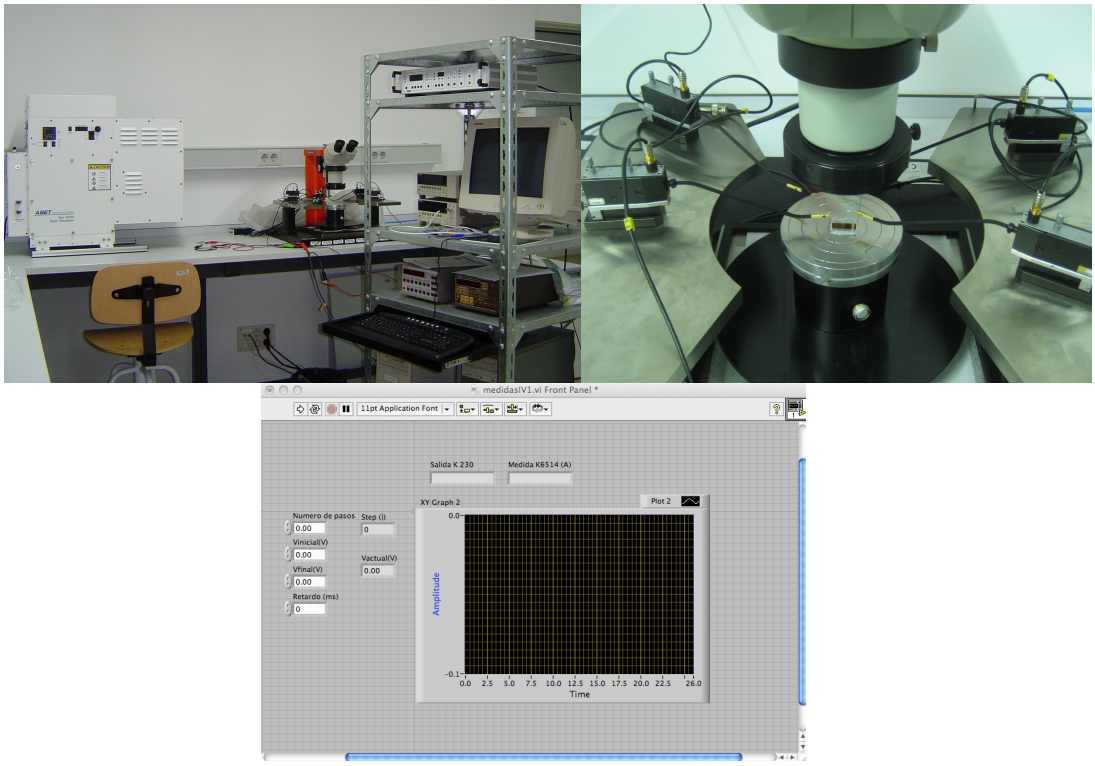

Figure 3.28. Sun simulator (top left) and four point probe (top right) set up at UPCT, showing homemade Labview interface (bottom) for automated measurements.

This characterization technique has been the most used in the laboratory experiments at UPCT. With the equipment and software in Figure 3.28, an example of IV curve, is shown in Figure 3.29, which was generated measuring one of the large amount of devices fabricated along this PhD period.

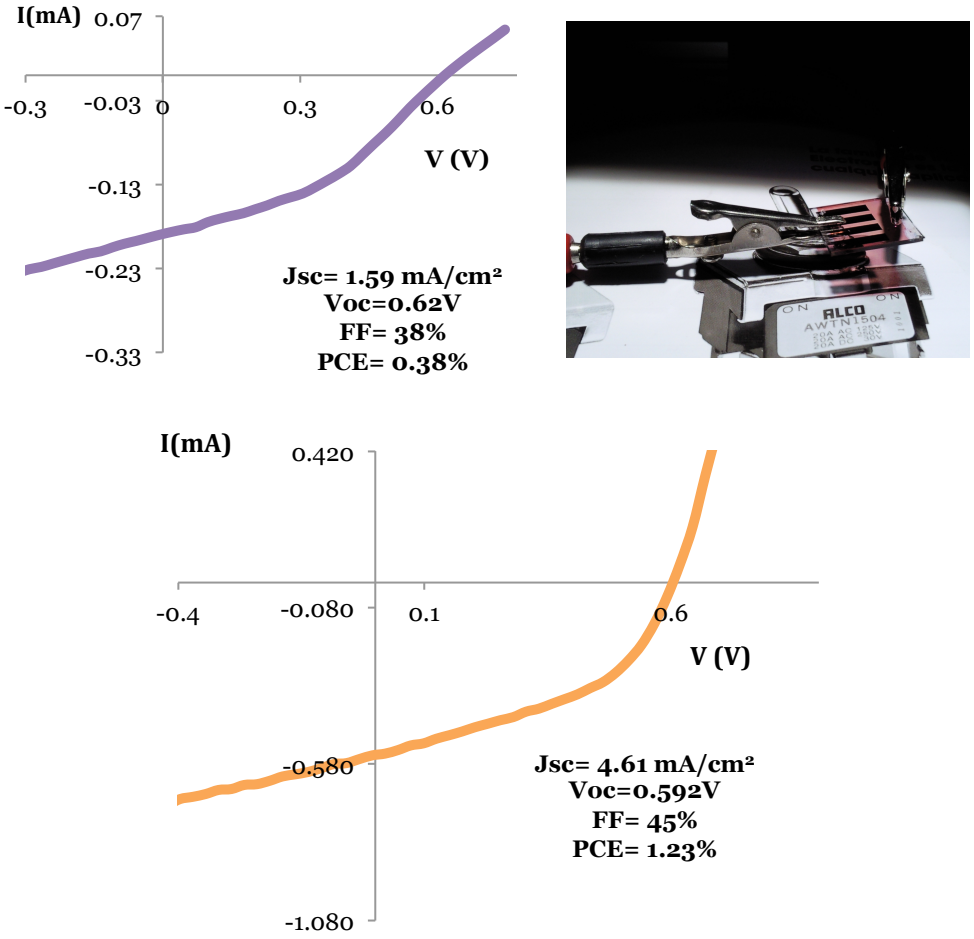

Figure 3.29. IV curves plotted (top left and bottom) of laboratory solar cells samples, under 1000 W/m² sun AM1.5 (right) at UPCT. Each stripe has 1.2 10^{-5} m² and have the structure Glass/ITO/PEDOT:PSS/P3HT:PCBM/Al.

While studying the degradation of devices, it is essential to measure all the diode characteristics periodically, since depending on the type of material and measuring conditions each photovoltaic parameter might behave differently. Often the decay of device efficiency is a consequence of the decay of photocurrent. Small devices, were fabricated Risø DTU, where substitution of PEDOT:PSS by a Vanadium oxide solution, as previously explained in section 3.3.3. To gather typical PV parameters, an special software for making time studies, while exposing a device under the Sun simulator was used. These results are plotted in the same graph, as shown in Figure 3.30. It is also observed that in some cases the decay of FF and even V_{oc}, can result in decrease of PCE as well.

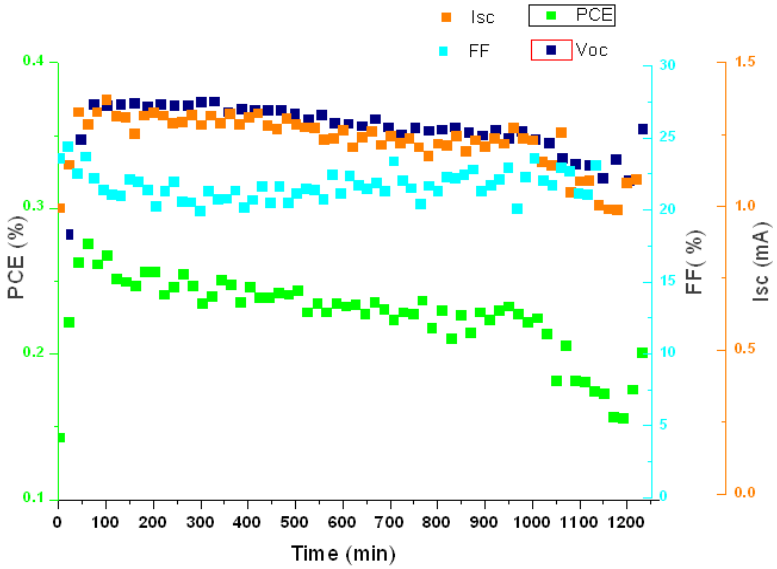

Figure 3.30. Time study showing PCE, I_{sc}, V_{oc} and FF during 20h under a solar simulator at Risø DTU of devices fabricated with the structure: Glass/ITO/ZnO/P3HT:PCBM/V_2O_5/Ag.

Different silver pastes were tried -as a back electrode-as well; such as UV cured, water based -fabricated at Risø DTU- and PV410 Dupont®, that have been screen printed in small devices with structure: Glass/ITO/ZnO/P3HT:PCBM/VO_2/Ag, where the VO_2 concentration was varied from 12.5 mg/ml to 25 mg/ml . The performances are very low for UV cured and water based inks as seen in Figure 3.31.

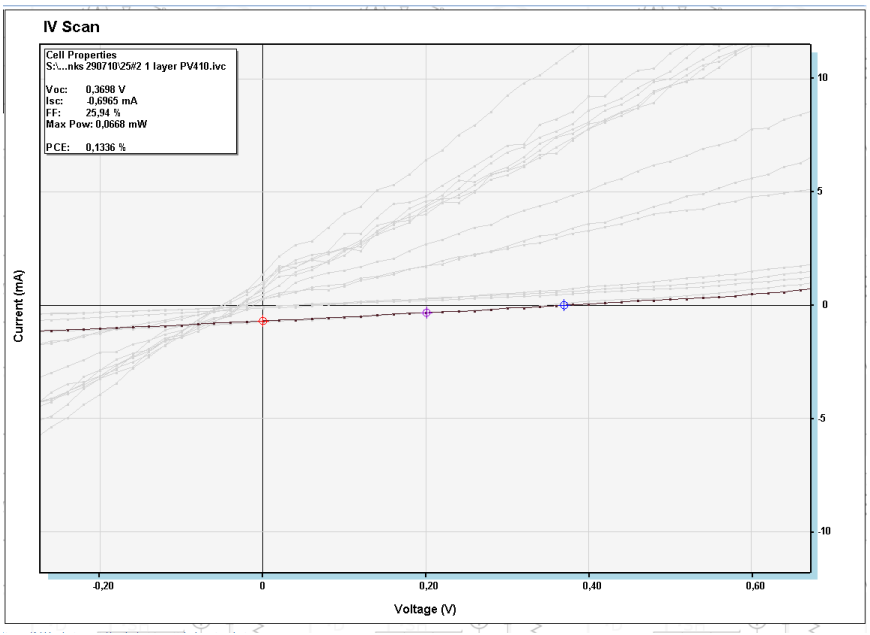

Figure 3.31. PV parameters and IV curves of OPV devices, where different silver inks UV cured, water based and Dupont have been applied by screen printing.

A number of A4-size 16-cell modules with vanadium oxide were produced with on PET substrates in a full R2R process, with an active area of 360 cm². These 50 modules showed a reasonable yield, as seen in Figure 3.32, with a few modules

around module number 360, which did not function. For the remaining modules the performance varied slightly.

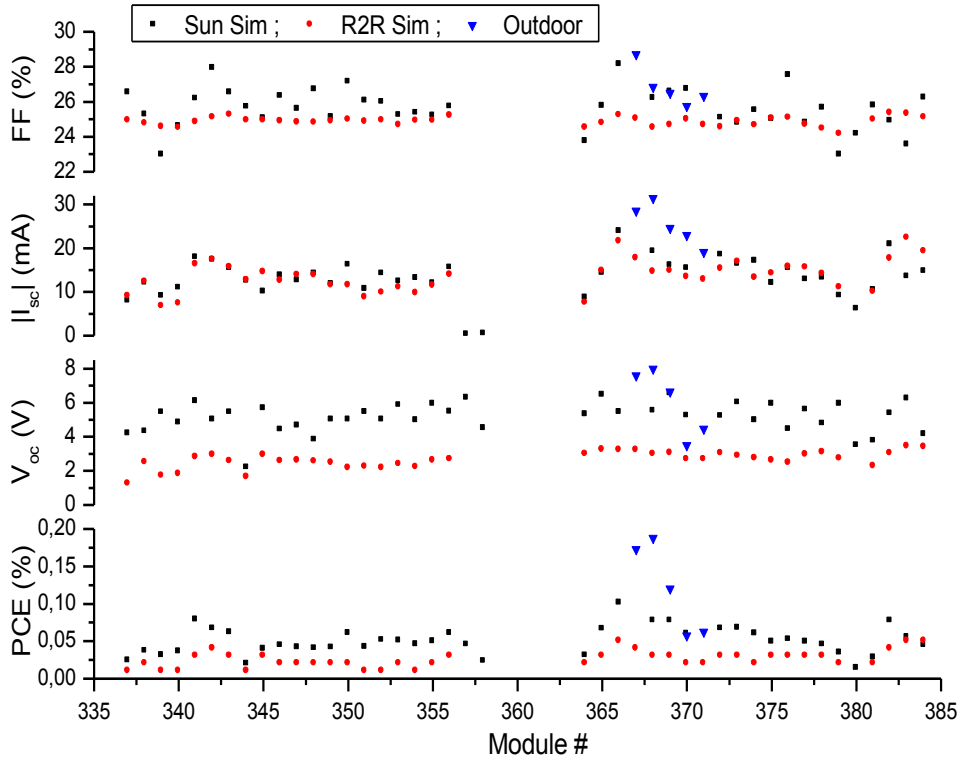

Figure 3.32. Comparison of the open-circuit voltage, V_{oc}, the short-circuit current, I_{sc}, the fill-factor, FF and the photon conversion efficiency, PCE for R2R modules made with a vanadium oxide layer. They were measured under two different sun simulators, and 5 modules were measured in outdoor conditions as well.

3.6. Conclusions

The materials and geometries commonly used in organic solar cells have been reviewed in this Chapter, and first idea that can be draft is that the geometry must encompass the processing choice.

Moreover, routes towards low cost and low environmental impact OSC, should not include non-scarce materials, but the use of solution processable inks instead of vacuum processed rare metals. With regard to solvents for processing OSC, the challenge for the near future, goes through avoiding environmentally harmful products, as chlorinated or aromatic. Moreover, if these OSC are meant to be produced on a large scale, they should simply use water.

Small devices with normal and inverted geometries, both at a lab scale and a larger scale, have been produced along this PhD work with the above aims –low cost and low environmental impact. On the one hand looking for the use of abundant materials, a vanadium isopropoxide solution was used as a replacement of PEDOT: PSS, due as well to the fact that PEDOT deposition is difficult and embeds a large amount of energy.

On the other hand, production of OSC should be as well increased on a larger scale, both in terms of processed area and processing time. A number of different coating and printing techniques suitable for their use in OSC processing has been herein presented. This number can rise up to 1000, and in this sense, analysis grounded on a multi-criteria decision making methodology has been used to the assessment of the most suited film-forming technologies. In terms of going towards an environmentally friendly R2R processing of polymer solar cells, there is a semi industrial scale pilot plant at Risø DTU, where these manufacturing techniques have been already tested with good results in functional devices.

There are challenges still with the understanding of the links between the nanoscale behaviour and the performance at a device scale. AFM experiments conducted, as well as DSC or GIWAXS, can provide this useful information, e.g. they are key to investigate the degradation of the devices due to morphology changes.

References

Abad, J., Espinosa, N., Ferrer, P., García-Valverde, R., Miguel, C., Padilla, J., Alcolea, A., et al. (2012). Molecular structure of poly(3-alkyl-thiophenes) investigated by calorimetry and grazing incidence X-ray scattering. *Solar Energy Materials and Solar Cells*, *97*(0), 109–118.

Abad, J., Urbina, A., & Colchero, J. (2011). Influence of UV radiation and ozone exposure on the electro-optical properties and nanoscale structure of P3OT films. *Organic Electronics*, *12*(8), 1389–1398.

Ajuria, J., Etxebarria, I., Cambarau, W., Muñecas, U., Tena-Zaera, R., Jimeno, J. C., & Pacios, R. (2011). Inverted ITO-free organic solar cells based on p and n semiconducting oxides. New designs for integration in tandem cells, top or bottom detecting devices, and photovoltaic windows. *Energy & Environmental Science*, *4*(2), 453.

Alstrup, J., Jørgensen, M., Medford, A. J., & Krebs, F. C. (2010). Ultra Fast and Parsimonious Materials Screening for Polymer Solar Cells Using Differentially Pumped Slot-Die Coating. *ACS Applied Materials & Interfaces*, *2*(10), 2819–2827.

Anctil, A., Babbitt, C. W., Raffaelle, R. P., & Landi, B. J. (2011). Material and Energy Intensity of Fullerene Production. *Environmental Science & Technology*, *45*(6), 2353–2359.

Andersen, T. R., Larsen-Olsen, T. T., Andreasen, B., Böttiger, A. P. L., Carlé, J. E., Helgesen, M., Bundgaard, E., et al. (2011). Aqueous Processing of Low-Band-Gap Polymer Solar Cells Using Roll-to-Roll Methods. *ACS Nano*, *5*(5), 4188–4196.

Bae, S., Kim, H., Lee, Y., Xu, X., Park, J.-S., Zheng, Y., Balakrishnan, J., et al. (2010). Roll-to-roll production of 30-inch graphene films for transparent electrodes. *Nat Nano*, *5*(8), 574–578.

Binnig, G., Quate, C. F., & Gerber, C. (1986). Atomic Force Microscope. *Physical Review Letters*, *56*(9), 930–933.

Blankenburg, L., Schultheis, K., Schache, H., Sensfuss, S., & Schrödner, M. (2009). Reel-to-reel wet coating as an efficient up-scaling technique for the production of bulk-heterojunction polymer solar cells. *Solar Energy Materials and Solar Cells*, *93*(4), 476–483.

Blouin, N., Michaud, A., Gendron, D., Wakim, S., Blair, E., Neagu-Plesu, R., Belletête, M., et al. (2008). Toward a Rational Design of Poly(2,7-Carbazole) Derivatives for Solar Cells. *J. Am. Chem. Soc.*, *130*(2), 732–742.

Brandenberger, J. E. (1918). Composite cellulose film.

Burroughes, J. H., Bradley, D. D. C., Brown, A. R., Marks, R. N., Mackay, K., Friend, R. H., Burns, P. L., et al. (1990). Light-emitting diodes based on conjugated polymers. *Nature*, *347*(6293), 539–541.

Burrows, P. ., Graff, G. ., Gross, M. ., Martin, P. ., Shi, M. ., Hall, M., Mast, E., et al. (2001). Ultra barrier flexible substrates for flat panel displays. *Displays*, *22*(2), 65–69.

Campoy-Quiles, M., Ferenczi, T., Agostinelli, T., Etchegoin, P. G., Kim, Y., Anthopoulos, T. D., Stavrinou, P. N., et al. (2008). Morphology evolution via self-organization and lateral and vertical diffusion in polymer:fullerene solar cell blends. *Nature Materials*, *7*(2), 158–164.

Chen, T. A., Wu, X., & Rieke, R. D. (1995). Regiocontrolled synthesis of poly (3-alkylthiophenes) mediated by Rieke zinc: their characterization and solid-state properties. *Journal of the American Chemical Society*, *117*(1), 233–244.

Dang, M. T., Hirsch, L., & Wantz, G. (2011). P3HT:PCBM, Best Seller in Polymer Photovoltaic Research. *Advanced Materials*, *23*(31), 3597–3602.

Dang, M. T., Wantz, G., Bejbouji, H., Urien, M., Dautel, O. J., Vignau, L., & Hirsch, L. (2011). Polymeric solar cells based on P3HT:PCBM: Role of the casting solvent. *Solar Energy Materials and Solar Cells*, *95*(12), 3408–3418.

Ding, J. M., De La Fuente Vornbrock, A., Ting, C., & Subramanian, V. (2009). Patternable polymer bulk heterojunction photovoltaic cells on plastic by rotogravure printing. *Solar Energy Materials and Solar Cells*, *93*(4), 459–464.

Doggart, J., Wu, Y., & Zhu, S. (2009). Inkjet printing narrow electrodes with <50 μm line width and channel length for organic thin-film transistors. *Applied Physics Letters*, *94*(16), 163503–163503–3.

Eerhart, A. J. J. E., Faaij, A. P. C., & Patel, M. K. (2012). Replacing fossil based PET with biobased PEF; process analysis, energy and GHG balance. *Energy Environ. Sci.*, *5*(4), 6047–6422.

Espinosa, N., Dam, H. F., Tanenbaum, D. M., Andreasen, J. W., Jørgensen, M., & Krebs, F. C. (2011). Roll-to-Roll Processing of Inverted Polymer Solar Cells using Hydrated Vanadium(V)Oxide as a PEDOT:PSS Replacement. *Materials*, *4*(1), 169–182.

Espinosa, N., García-Valverde, R., García-Cascales, M. S., & Urbina, A. (2010). Towards low-cost manufacturing of organic solar cells: multi-criteria assessment of fabrication technologies. Presented at the International Conference on Renewable Energies and Power Quality, Granada.

Espinosa, N., García-Valverde, R., Urbina, A., & Krebs, F. C. (2011). A life cycle analysis of polymer solar cell modules prepared using roll-to-roll methods under ambient conditions. *Solar Energy Materials and Solar Cells*, *95*(5), 1293–1302.

Espinosa, N., Hösel, M., Angmo, D., & Krebs, F. C. (2012). Solar cells with one-day energy payback for the factories of the future. *Energy Environ. Sci.*, *5*(1), 5117–5132.

European Commission. (2010). *Critical raw materials for the EU: Report of the Ad-hoc Working Group on defining critical raw materials*.

Galagan, Y., J.M. Rubingh, J.-E., Andriessen, R., Fan, C.-C., W.M. Blom, P., C. Veenstra, S., & M. Kroon, J. (2011). ITO-free flexible organic solar cells with printed current collecting grids. *Solar Energy Materials and Solar Cells*, *95*(5), 1339–1343.

Gevorgyan, S. A. (2010). *Production, Characterization and Stability of Organic Solar Cell Devices*. Risø DTU National Laboratory for Sustainable Energy, Denmark.

Girotto, C., Rand, B. P., Genoe, J., & Heremans, P. (2009). Exploring spray coating as a deposition technique for the fabrication of solution-processed solar cells. *Solar Energy Materials and Solar Cells*, *93*(4), 454–458.

Girotto, C., Rand, B. P., Steudel, S., Genoe, J., & Heremans, P. (2009). Nanoparticle-based, spray-coated silver top contacts for efficient polymer solar cells. *Organic electronics*, *10*(4), 735–740.

Grüniger, A., & Rudolf von Rohr, P. (2004). Influence of defects in SiOx thin films on their barrier properties. *Thin Solid Films*, *459*(1–2), 308–312.

Gwinner, M. C., Brenner, T. J. K., Lee, J.-K., Newby, C., Ober, C. K., McNeill, C. R., & Sirringhaus, H. (2012). Organic field-effect transistors and solar cells using novel high electron-affinity conjugated copolymers based on alkylbenzotriazole and benzothiadiazole. *Journal of Materials Chemistry*, *22*(10), 4436–4439.

Günes, S., Neugebauer, H., & Sariciftci, N. S. (2007). Conjugated Polymer-Based Organic

Solar Cells. *Chem. Rev.*, *107*(4), 1324–1338.

Hau, Steven K, Yip, H.-L., Baek, N. S., Zou, J., O'Malley, K., & Jen, A. K.-Y. (2008). Air-stable inverted flexible polymer solar cells using zinc oxide nanoparticles as an electron selective layer. *Applied Physics Letters*, *92*(25), 253301–253301–3.

Hau, S.K., Yip, H. L., Leong, K., & Jen, A. K. Y. (2009). Spraycoating of silver nanoparticle electrodes for inverted polymer solar cells. *Organic electronics*, *10*(4), 719–723.

Heeger, A. J. (2010). Semiconducting polymers: the Third Generation. *Chem. Soc. Rev.*, *39*(7), 2354–2371.

Helgesen, M., Søndergaard, R., & Krebs, F. C. (2010). Advanced materials and processes for polymer solar cell devices. *Journal of Materials Chemistry*, *20*(1),36.

Herrero. (2002). Transparent films on polymers for photovoltaic applications. *Vacuum*, *67*(3-4), 611–616.

Hoppe, H., & Sariciftci, N. S. (2004). Organic Solar Cells: An Overview. *Journal of Materials Research*, *19*(07), 1924–1945.

Hoth, C. N., Choulis, S. A., Schilinsky, P., & Brabec, C. J. (2007). High Photovoltaic Performance of Inkjet Printed Polymer:Fullerene Blends. *Advanced Materials*, *19*(22), 3973–3978.

Hoth, C. N., Choulis, S. A., Schilinsky, P., & Brabec, C. J. (2009). On the effect of poly (3-hexylthiophene) regioregularity on inkjet printed organic solar cells. *J. Mater. Chem.*, *19*(30), 5398–5404.

Huang, J.-S., Chou, C.-Y., Liu, M.-Y., Tsai, K.-H., Lin, W.-H., & Lin, C.-F. (2009). Solution-processed vanadium oxide as an anode interlayer for inverted polymer solar cells hybridized with ZnO nanorods. *Organic Electronics*, *10*(6), 1060–1065.

Huang, X., Yu, Z., Huang, S., Zhang, Q., Li, D., Luo, Y., & Meng, Q. (2010). Preparation of fluorine-doped tin oxide (SnO2:F) film on polyethylene terephthalate (PET) substrate. *Materials Letters*, *64*(15), 1701–1703.

Hummelen, J. C., Knight, B. W., LePeq, F., Wudl, F., Yao, J., & Wilkins, C. L. (1995). Preparation and Characterization of Fulleroid and Methanofullerene Derivatives. *The Journal of Organic Chemistry*, *60*(3), 532–538.

Hübler, A., Trnovec, B., Zillger, T., Ali, M., Wetzold, N., Mingebach, M., Wagenpfahl, A., et al. (2011). Printed Paper Photovoltaic Cells. *Advanced Energy Materials*, *1*(6), 1018–1022.

Kallmann, H., & Pope, M. (1959). Photovoltaic Effect in Organic Crystals. *The Journal of Chemical Physics*, *30*(2), 585.

Kim, J. Y., Kim, S. H., Lee, H. H., Lee, K., Ma, W., Gong, X., & Heeger, A. J. (2006). New Architecture for High-Efficiency Polymer Photovoltaic Cells Using Solution-Based Titanium Oxide as an Optical Spacer. *Advanced Materials*, *18*(5), 572–576.

Kopola, P., Aernouts, T., Guillerez, S., Jin, H., Tuomikoski, M., Maaninen, A., & Hast, J. (2010). High efficient plastic solar cells fabricated with a high-throughput gravure printing method. *Solar Energy Materials and Solar Cells*, *94*(10), 1673–1680.

Krebs, F. C. (2008). Air stable polymer photovoltaics based on a process free from vacuum steps and fullerenes. *Solar Energy Materials and Solar Cells*, *92*(7), 715–726.

Krebs, F. C. (2009a). Polymer solar cell modules prepared using roll-to-roll methods: Knife-over-edge coating, slot-die coating and screen printing. *Solar Energy Materials and Solar Cells*, *93*(4), 465–475.

Krebs, F. C. (2009b). All solution roll-to-roll processed polymer solar cells free from indium-tin-oxide and vacuum coating steps. *Organic Electronics*, *10*(5), 761–768.

Krebs, F. C. (2009c). Roll-to-roll fabrication of monolithic large-area polymer solar cells free from indium-tin-oxide. *Solar Energy Materials and Solar Cells*, *93*(9), 1636–1641.

Krebs, F. C. (2009d). Fabrication and processing of polymer solar cells: A review of printing and coating techniques. *Solar Energy Materials and Solar Cells*, *93*(4), 394–412.

Krebs, F. C., Gevorgyan, S. A., & Alstrup, J. (2009). A roll-to-roll process to flexible polymer solar cells: model studies, manufacture and operational stability studies. *Journal of Materials Chemistry*, *19*(30), 5442–5451.

Krebs, F. C., Jørgensen, M., Norrman, K., Hagemann, O., Alstrup, J., Nielsen, T. D., Fyenbo, J., et al. (2009). A complete process for production of flexible large area polymer solar cells entirely using screen printing--First public demonstration. *Solar Energy Materials and Solar Cells*, *93*(4), 422–441.

Krebs, F. C., Søndergaard, R., & Jørgensen, M. (2011). Printed metal back electrodes for R2R fabricated polymer solar cells studied using the LBIC technique. *Solar Energy Materials and Solar Cells*, *95*(5), 1348–1353.

Krebs, F. C., Thomann, Y., Thomann, R., & Andreasen, J. W. (2008). A simple nanostructured polymer/ZnO hybrid solar cell—preparation and operation in air. *Nanotechnology*, *19*, 424013.

Krebs, F. C., Tromholt, T., & Jørgensen, M. (2010). Upscaling of polymer solar cell fabrication using full roll-to-roll processing. *Nanoscale*, *2*(6), 873–886.

Krätschmer, W., Lamb, L. D., Fostiropoulos, K., & Huffman, D. R. (1990). Solid C60: a new form of carbon. *Nature*, *347*(6291), 354–358.

Kymakis, E., & Amaratunga, G. A. J. (2002). Single-wall carbon nanotube/conjugated polymer photovoltaic devices. *Applied Physics Letters*, *80*(1), 112–114.

Larsen-Olsen, T. T., Andersen, T. R., Andreasen, B., Böttiger, A. P. L., Bundgaard, E., Norrman, K., Andreasen, J. W., et al. (2012). Roll-to-roll processed polymer tandem solar cells partially processed from water. *Solar Energy Materials and Solar Cells*, *97*(0), 43–49.

Larsen-Olsen, T. T., Andreasen, B., Andersen, T. R., Böttiger, A. P. L., Bundgaard, E., Norrman, K., Andreasen, J. W., et al. (2012). Simultaneous multilayer formation of the polymer solar cell stack using roll-to-roll double slot-die coating from water. *Solar Energy Materials and Solar Cells*, *97*(0), 22–27.

Lilliedal, M. R., Medford, A. J., Madsen, M. V., Norrman, K., & Krebs, F. C. (2010). The effect of post-processing treatments on inflection points in current-voltage curves of roll-to-roll processed polymer photovoltaics. *Solar Energy Materials and Solar Cells*, *94*(12), 2018–2031.

Madaria, A. R., Kumar, A., & Zhou, C. (2011). Large scale, highly conductive and patterned transparent films of silver nanowires on arbitrary substrates and their application in touch screens. *Nanotechnology*, *22*, 245201.

Manceau, M., Angmo, D., Jørgensen, M., & Krebs, F. C. (2011). ITO-free flexible polymer solar cells: From small model devices to roll-to-roll processed large modules. *Organic Electronics*, *12*(4), 566–574.

McCullough, R. D., & Lowe, R. D. (1992). Enhanced electrical conductivity in regioselectively synthesized poly(3-alkylthiophenes). *J. Chem. Soc., Chem. Commun.*, (1),

70–72.

Na, S.-I., Kim, S.-S., Jo, J., & Kim, D.-Y. (2008). Efficient and Flexible ITO-Free Organic Solar Cells Using Highly Conductive Polymer Anodes. *Advanced Materials*, *20*(21), 4061–4067.

Na, S.-I., Yu, B.-K., Kim, S.-S., Vak, D., Kim, T.-S., Yeo, J.-S., & Kim, D.-Y. (2010). Fully spray-coated ITO-free organic solar cells for low-cost power generation. *Solar Energy Materials and Solar Cells*, *94*(8), 1333–1337.

O'Connor, B., Haughn, C., An, K.-H., Pipe, K. P., & Shtein, M. (2008). Transparent and conductive electrodes based on unpatterned, thin metal films. *Applied Physics Letters*, *93*(22), 223304–223304–3.

Rowell, M. W., Topinka, M. A., McGehee, M. D., Prall, H.-J., Dennler, G., Sariciftci, N. S., Hu, L., et al. (2006). Organic solar cells with carbon nanotube network electrodes. *Applied Physics Letters*, *88*(23), 233506–233506–3.

Scharber, M. C., Mühlbacher, D., Koppe, M., Denk, P., Waldauf, C., Heeger, A. J., & Brabec, C. J. (2006). Design rules for donors in bulk-heterojunction solar cells - Towards 10 % energy-conversion efficiency. *Advanced Materials*, *18*(6), 789–794.

Susanna, G., Salamandra, L., Brown, T. M., Di Carlo, A., Brunetti, F., & Reale, A. (2011). Airbrush spray-coating of polymer bulk-heterojunction solar cells. *Solar Energy Materials and Solar Cells*, *95*(7), 1775–1778.

Søndergaard, R., Helgesen, M., Jørgensen, M., & Krebs, F. C. (2011). Fabrication of Polymer Solar Cells Using Aqueous Processing for All Layers Including the Metal Back Electrode. *Advanced Energy Materials*, *1*(1), 68–71.

Søndergaard, R., Hösel, M., Angmo, D., Larsen-Olsen, T. T., & Krebs, F. C. (2012). Roll-to-roll fabrication of polymer solar cells. *Materials Today*, *15*(1–2), 36–49.

Søndergaard, R. R., Makris, T., Lianos, P., Manor, A., Katz, E. A., Gong, W., Tuladhar, S. M., et al. (2012). The use of polyurethane as encapsulating method for polymer solar cells—An inter laboratory study on outdoor stability in 8 countries. *Solar Energy Materials and Solar Cells*, *99*(0), 292–300.

Tadatsugu, M. (2008). Present status of transparent conducting oxide thin-film development for Indium-Tin-Oxide (ITO) substitutes. *Thin Solid Films*, *516*(17), 5822–5828.

Takanezawa, K., Hirota, K., Wei, Q.-S., Tajima, K., & Hashimoto, K. (2007). Efficient Charge Collection with ZnO Nanorod Array in Hybrid Photovoltaic Devices. *J. Phys. Chem. C*, *111*(19), 7218–7223.

Takehara, H., Fujiwara, M., Arikawa, M., Diener, M. D., & Alford, J. M. (2005). Experimental study of industrial scale fullerene production by combustion synthesis. *Carbon*, *43*(2), 311–319.

Tung, V. C., Chen, L.-M., Allen, M. J., Wassei, J. K., Nelson, K., Kaner, R. B., & Yang, Y. (2009). Low-Temperature Solution Processing of Graphene–Carbon Nanotube Hybrid Materials for High-Performance Transparent Conductors. *Nano Letters*, *9*(5), 1949–1955.

Vak, D., Kim, S. S., Jo, J., Oh, S. H., Na, S. I., Kim, J., & Kim, D. Y. (2007). Fabrication of organic bulk heterojunction solar cells by a spray deposition method for low-cost power generation. *Applied Physics Letters*, *91*, 081102.

Voigt, M. M., Mackenzie, R. C. I., Yau, C. P., Atienzar, P., Dane, J., Keivanidis, P. E., Bradley, D. D. C., et al. (2011). Gravure printing for three subsequent solar cell layers of inverted structures on flexible substrates. *Solar Energy Materials and Solar Cells*, *95*(2),

731–734.

Wagner, J. R. (2009). *Multilayer flexible packaging*. Rochester, USA.

Waldauf, C., Morana, M., Denk, P., Schilinsky, P., Coakley, K., Choulis, S. A., & Brabec, C. J. (2006). Highly efficient inverted organic photovoltaics using solution based titanium oxide as electron selective contact. *Applied Physics Letters*, *89*(23), 233517–233517–3.

Wang, Y., Chen, X., Zhong, Y., Zhu, F., & Loh, K. P. (2009). Large area, continuous, few-layered graphene as anodes in organic photovoltaic devices. *Applied Physics Letters*, *95*, 063302.

Wengeler, L., Schmidt-Hansberg, B., Peters, K., Scharfer, P., & Schabel, W. (2011). Investigations on knife and slot die coating and processing of polymer nanoparticle films for hybrid polymer solar cells. *Chemical Engineering and Processing: Process Intensification*, *50*(5–6), 478–482.

Wengeler, Lukas, Schmitt, M., Peters, K., Scharfer, P., & Schabel, W. (2012). Comparison of large scale coating techniques for organic and hybrid films in polymer based solar cells. *Chemical Engineering and Processing: Process Intensification*, *in press*(0).

Womelsdorf, H., Hoheisel, W., & Passing, G. (2004, March 23). Nanoparticulate, redispersible zinc oxide gels. Patent.

Wu, J., Agrawal, M., Becerril, H. A., Bao, Z., Liu, Z., Chen, Y., & Peumans, P. (2010). Organic Light-Emitting Diodes on Solution-Processed Graphene Transparent Electrodes. *ACS Nano*, *4*(1), 43–48.

Yao, Y., Hou, J., Xu, Z., Li, G., & Yang, Y. (2008). Effects of Solvent Mixtures on the Nanoscale Phase Separation in Polymer Solar Cells. *Advanced Functional Materials*, *18*(12), 1783–1789.

Yu, G., Gao, J., Hummelen, J. C., Wudl, F., & Heeger, A. J. (1995). Polymer Photovoltaic Cells: Enhanced Efficiencies via a Network of Internal Donor-Acceptor Heterojunctions. *Science*, *270*(5243), 1789 –1791.

Zhou, Y., Zhang, F., Tvingstedt, K., Barrau, S., Li, F., Tian, W., & Inganäs, O. (2008). Investigation on polymer anode design for flexible polymer solar cells. *Applied Physics Letters*, *92*(23), 233308–233308–3.

Zimmermann, B., Schleiermacher, H.-F., Niggemann, M., & Würfel, U. (2011). ITO-free flexible inverted organic solar cell modules with high fill factor prepared by slot die coating. *Solar Energy Materials and Solar Cells*, *95*(7), 1587–1589.

Zimmermann, B., Würfel, U., & Niggemann, M. (2009). Longterm stability of efficient inverted P3HT:PCBM solar cells. *Solar Energy Materials and Solar Cells*, *93*(4), 491–496.

de Jong, M. P., van IJzendoorn, L. J., & De Voigt, M. J. A. (2000). Stability of the interface between indium-tin-oxide and poly(3,4-ethylenedioxythiophene)/poly(styrenesulfonate) in polymer light-emitting diodes. *Applied Physics Letters*, *77*(14), 2255.

van de Lagemaat, J., Barnes, T. M., Rumbles, G., Shaheen, S. E., Coutts, T. J., Weeks, C., Levitsky, I., et al. (2006). Organic solar cells with carbon nanotubes replacing In_2O_3:Sn as the transparent electrode. *Applied Physics Letters*, *88*, 233503.

CHAPTER 4
Life Cycle Assessment as a research directing tool

There are key elements with regard to the production processes and materials typically employed in organic photovoltaics, like thermal budgets, better barrier materials, thinner adhesives, the development of new semitransparent electrode materials that can be printed or coated –and therefore, vacuum steps are avoided-, and other issues that need a tool to be analysed and prioritized. Life-cycle assessment can do it and it can provide as well a better understanding of the way the technology is produced and is impacting the environment. This Chapter gathers the work I have been doing during my PhD in life-cycle assessment applied to several OPV systems: to OPV modules manufactured at a semi industrial scale, to a product integrating polymer solar modules, and finally to a new set of alternative routes to fabricate low-environmental impact OPV modules. This effort sought to establish the parameters that are critical for the beneficial use of polymer solar cells in society and to firmly demonstrate where the potential of the organic photovoltaic technology is.

4.1. Life Cycle Thinking

A comprehensively supported basis of decision-making is required for a more sustainable world to address critical developments, e.g. resource scarcity, climate change, but also rapid evolutions and social changes, by means of innovative and sustainable solutions. Life Cycle Thinking provides an assisted base that fulfils these requirements. The major strength of this way of thinking is that it can be applied to almost everything.

In this dissertation, a particular energy system such as organic solar cells has been studied under this view. Energetic systems are meant to be sustainable, in the sense that it is not reasonable to spend more energy to produce a system that the energy delivered by the system throughout its lifetime. Even so, the use of energy needs to be carefully considered; it can have different impacts during different stages, which will be discussed in section 4.2. Life cycle assessments/analyses (LCA) are an unbeatable tool to point out weaknesses and strengths providing a useful feedback for development. A LCA characterizes and quantifies the total environmental burdens of a product system, from raw materials extraction to end-of-life management.

The Society of Environmental Toxicology and Chemistry (SETAC) was the first international organisation to work for the development of LCA by 1980's (Guinée, 2002), although LCA guidelines and methodologies were later established by (International Organisation for Standardisation (ISO), 1997) in ISO 14040 series (14040 to 14049). The latter have been an excellent foundation during my PhD period for conducting several life-cycle analysis, which will be presented in section 4.3.

4.1.1. Phases of a life cycle assessment

A LCA is carried out in four main phases as illustrated in Figure 4.1, in accordance with ISO 14040 and 14044.

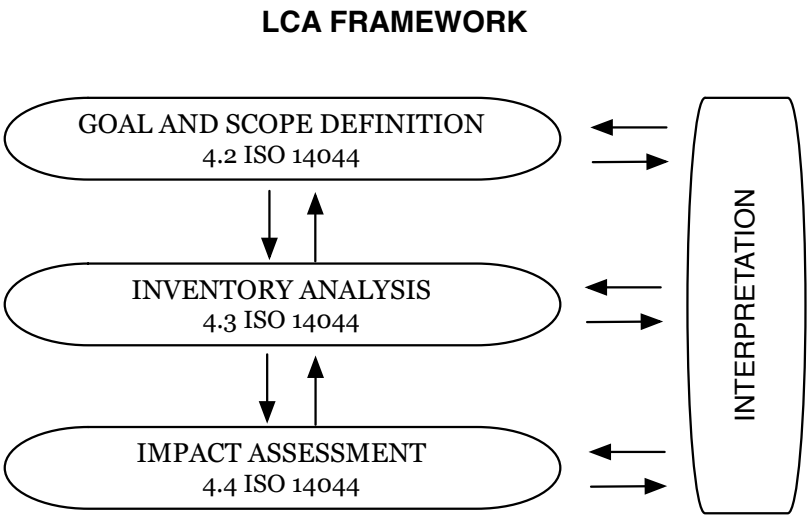

Figure 4.1. Four major phases to perform a life cycle analysis according to ISO 14040 series.

Goal and Scope definition

First of all, the main objectives have to be unambiguously established: that is, what calculation will be accomplished (e.g. analysing an OPV manufacturing by a cradle-to-gate or cradle to-grave analysis, or for hot-spot identification, etc.). The reasons of the study must be specified as well. The product or service under study must be characterized, and all the assumptions must be herein detailed. So, product function and functional unit should be chosen and clearly presented.

The functional unit describes the primary function(s) fulfilled by a product system, and indicates how much of this function is to be considered in the intended LCA study. It will be used as a basis for selecting one or more alternative product systems that might provide these function(s). The functional unit enables different systems to be treated as functionally equivalent and allows reference flows to be determined for each of them (Guinée, 2002). For instance, possible functional units for a PV production can be defined in terms of the module power (in W_p), the module area (m^2) or cell area (m^2), or the energy output (kWh_{el}), as it will be further discussed in section 4.2.1. Even, all of them could be chosen at once: " a m^2 of processed substrate, where 560 cm^2 are OPV module with 360 cm^2 of active area, delivering an output of 18 kWh_{el}.

On the basis of the functional unit, a number of alternative product or services can be declared functionally equivalent and reference flows will be determined for these systems. The reference flow is a measure of the outputs from processes in a given product system which are required to fulfil the function expressed by the functional unit.

The system boundary demarcates which processes are considered in the analysis. So that it must be specified whether the analysis incorporates also direct energy to process and direct energy to produce materials used in the manufacturing -primary and ancillary-, whether the energy used for manufacturing the capital equipment is left outside, or whether recycling and end of life stages are taken into account or not.

Life cycle inventory

The inventory analysis is the LCA phase that involves the compilation and quantification of inputs and outputs of a given product or service, throughout its life cycle.

Material inventory is a collection of all the material flows in the manufacturing process of the product, expressed per functional unit. This inventory is the basis for calculating the embedded energy.

Life cycle inventory (LCI) is also a compilation of all the energy flows for materials production and manufacturing, expressed per functional unit:

- The energy required for the material production or *embodied energy in materials*, i.e. the specific energy for raw material extraction and production activities.
- The energy involved in the manufacturing, or *direct process energy,* is the electricity or heat consumption in the different processing steps.

By compilation of material and energy inventories, the energy input for processing materials and the energy input during product manufacturing can be estimated. This enables a careful determination of the overall embedded energy in the modules, widely called Cumulative Energy Demand (CED). All the energy results are usually converted to Equivalent Primary Energy (EPE), in units of MJ_{EPE}/kg. The actual conversion factors between EPE and heat or electricity depend on the corresponding energy mix of the country under consideration.

According to the LCA standard 14044, all the releases to soil, water and air generated during the entire life cycle are included in this inventory as well. However, this requires more information than is typically available, so often emissions inventory is simplified to emissions of CO_2 equivalents related to the energy consumption during the entire life cycle.

Life cycle Impact Assessment

The Life cycle Impact Assessment (LCIA) is the process by which the amount and significance of the potential environmental effects arising from the LCI are identified and evaluated. Inputs and outputs obtained from the LCI, are classified and allocated to some environmental indicators, e.g. *Global warming potential* (GWP), *Ozone layer depletion, etc.*

An additional important environmental quality indicator for renewable energy technologies will be calculated as well, the *equivalent CO_2 emission factor*. It is defined as all the emissions contributing to global warming expressed in kg "CO_2 equivalents" per generated kWh electricity.

Interpretation

This is the phase in which the results of the analysis and all choices and assumptions made during the course of the analysis are discussed. The main elements of the interpretation phase are collected in ISO 14043: an evaluation of results (in terms of consistency and completeness), an analysis of results (for instance, in terms of robustness), and the formulation of the conclusions and recommendations of the study.

4.1.2. Limitations and uncertainties of LCA methodology

Despite the holistic nature is the major strength of an LCA as said before, it can be at the same time a limitation; since this broad approach can only be done at the expense of simplifying other aspects.

A further limitation can be the availability of data. There is a large number of databases that collect information about life cycle of materials and products. But in practice, data are frequently obsolete, incomparable, or of unknown quality. This leads to uncertainties that can be however taken into account by uncertainty analysis.

Information on the uncertainty of the model outcomes provides useful knowledge to assess the reliability of LCA-based decisions and to guide future research towards more accurate life cycle assessments. In order to accommodate this, throughout the LCA studies performed during my PhD, we have tried to give a

qualitative indication of the energy requirements that we have estimated, by introducing the following qualifications: ++ very good, + good, 0 fair, - low, -- very low; as will be shown below.

When a new process or material is analysed, it is usual that databases lack the information needed for the study. In this case, the CA of a particular product can be extremely complicated because every step of the material process has to be carefully analysed. On the other hand, when this analysis includes a detailed explanation of methodology and scope, and is published in scientific journals or included in databases, it becomes available to other researchers and can be the building block of a broader study. LCA is therefore a collective work for which every step is built by different researchers; it is a global holistic study of a full process that can be considered a collective creation.

4.2. LCA in photovoltaic technologies

4.2.1. Environmental aspects of photovoltaics

Energy requirements for photovoltaic technologies were firstly strongly criticised because it was considered that the energy embodied in the system manufacture was larger than the energy delivered by the system throughout its lifetime. Therefore large effort was devoted to LCA studies which were detailed in a large number of publications. Literature in LCA for PV systems[1] dates back to 1991 when Novem, the Netherlands Agency for Energy and Environment launched a project lead by E. Alsema and E. Nieuwlaar, called “Environmental aspects of solar cell technology”.

In energy systems such as PV systems, conversion efficiency is often used as the metric to evaluate the performance and potential usefulness of a technology or system. But it does not take into account the scale of the problem at hand and the potential unavailability of elements or components, nor does it take into account if it is possible to create the required energy producing unit in a given amount of time and whether the energy producing unit is capable of delivering back the energy spent creating it in a reasonable time. Considerable literature address life-cycle assessments of energy systems, since it is a very useful tool and ideally reveals whether a given system pays back the energy spent making it quickly and whether it needs to operate for significantly longer times.

In particular, for renewable energy technologies, the Energy Pay-Back Time (EPBT) and the Energy Return Factor (ERF)[2], are two key environmental quality parameters. They can be determined from the total embodied energy and the electricity output of the device produced, as defined in Eq 4.1 and Eq 4.2.

The EPBT is the time required for the solar PV system to generate the equivalent amount of energy consumed in the construction and decommissioning phases. The ERF expresses the total amount of energy generated per unit of invested energy.

[1] Hagedorn and Hellriegel in late 1980s produced several studies in German.
[2] Also known by Energy Return of Investment (EROI)

Eq 4.1

$$EPBT = \frac{E_{EMB}}{E_{GEN}}$$

Eq 4.2

$$ERF = \frac{E_{GEN} \cdot L}{E_{EMB}} = \frac{L}{EPBT}$$

where, E_{EMB} is the total primary energy input during the PV module life cycle, E_{GEN} is the primary energy generated per year of operation by the PV module, and L is the lifetime of the PV module.

In order to calculate both parameters, assumptions have to be undertaken about a functional unit, life-time system, efficiency of the system and geographical considerations to account for irradiance levels and ambient temperature.

Functional unit and other assumptions

With regard to the functional units that can be chosen in a PV context, Erik Alsema has an interesting discussion in his paper (Alsema, 1998) and the possibilities are:

- kWh of electricity produced by the PV system
- W_p of module power
- m^2 of module area
- m^2 of cell area
- module

The *kWh* and -to a lesser extent- the W_p are the most used functional of units because they are directly related to the end user service. But kWh or W_p units present disadvantages since extra parameters, which have little relation to the energy consumption during module production -namely irradiation, PV system performance, module efficiency and lifetime- have to be introduced.

Energy requirements for module production like energy for material consumption and for processing, are “area dependent”. The *module* is neither a convenient functional unit because modules do not have a standard size or power rating.

So, given the objective of producing OPV modules, in our work and throughout this thesis an *area* unit will be the most convenient functional unit. Afterwards it can be converted into a PV parameter such as W_p or kWh. A more detailed discussion will be given below in the case of the LCA work performed during my PhD, since different approaches have been accomplished for the calculation of environmental impact and costs, for laboratory fabrication procedures (Garcia-Valverde et al., 2009), and for larger scale module manufacturing (Espinosa et al., 2011; Espinosa, García-Valverde, et al., 2012; Espinosa, Hösel, et al., 2012).

For calculating the energy yield, the efficiency must be detailed for PV modules, as well as the geographical site of installation that determines the irradiance levels, and the lifetime for calculating ERF.

Energy mix

An additional important environmental quality indicator for renewable energy technologies is the equivalent CO_2 emission factor, defined as all the emissions contributing to global warming expressed in kg "CO_2 equivalents" per generated kWh electricity. A further assumption has to be taken into account the energy mix for the geographical location of the manufacturing process should be selected in order to know CO_{2eq} produced per kWh_{el}. This site for the cases presented in section 4.3 has been Denmark.

Energy Payback times in PV

Once functional unit has been stated and the efficiency and lifetime of the PV modules are clear, EPBT calculations can be performed. It has been thoroughly investigated for all PV technologies already on the market, and ranges between 4.12 and 0.73 years. The most significant values are the following: mono-Si: 4.12 to 2.68 years, depending on a range of power conversion efficiencies (11.8 -14%) given for commercial modules (Alsema, 1998; Knapp et al., 2001; Alsema et al., 2005; Jungbluth, 2005); poly-Si, 2 years for 13 % efficiency (Alsema et al., 2005; Jungbluth, 2005); amorphous-Si, 1.13 years for 7% efficiency (Alsema et al., 2000); CIS, 2.26 to 2.2 years for 8.9 - 11% efficiency (Knapp et al., 2001; Raugei et al., 2007), and CdTe, 1.61 to 0.73 years for 11-13% (Kato et al., 2001; Raugei et al., 2007). Other hybrid and organic technologies have also been studied, delivering a broad set of EPBT figures ranging between 5 to 0.6 years (Greijer et al., 2001; Azzopardi et al., 2010; Roes et al., 2009; García-Valverde et al., 2010; Espinosa et al., 2011; Espinosa, García-Valverde, et al., 2012; Espinosa, Hösel, et al., 2012). Table 4.1 lists a selection of renewable energy technologies and their energy pay back times.

In some LCA studies for PV technologies, the balance of system (BOS) has been included for the calculation of EPBT and ERF. This will have higher impacts in the future calculations since optimized PV manufacturing process will have less share in the total embodied energy compared to BOS components whose learning curves are evolving more slowly than those for solar cell technology. Although much effort is being devoted to reduce the BOS embedded energy. For example SMA Germany won a price for their energy efficient factory in 2010[3], when they run at full capacity this would be 5,200,000 kWh/year per 4 GW maximum capacity = 3.25 kWh per 2.5 W inverter. In addition to this they also use biogas for production of heat and electricity. Inverters are nowadays being designed for delivering smaller power, as well even being matched with the energy produced by one module, i.e. microinverters, which can have the advantages in comparison with kW and MW-scale inverters such as: compactness or modularity of the PV facility (1 module is *per se* one installation), the extraction of the maximum power per module, and reducing mean time between fails. Microinverters for OPV are very promising.

[3] See http://www.sma.de/fileadmin/fm-dam/documents/de/1._Preis__SMA_Solar_Technology_AG.pdf

Table 4.1. A listing of different renewable energy technologies and their EPBT (in years). MJ/kWh$_{el}$.

Energy source/Technology		EPBT (years)	Source
Wind			
	On land	0.26	(Schleisner, 2000)
	Offshore	0.39	
PV technologies	Silicon Mono and polycrystalline	1.65-4.12	(Alsema et al., 2005; Knapp et al., 2001)
	Amorphous silicon	1.13	(Alsema, 1998)
	GaAs PV	2.36-5	(Kato et al., 2001; Raugei et al., 2007)
	GaInP/GaAs	2.14-4.6	
	CdTe	0.73-1.61	(Kato et al., 2001; Raugei et al., 2007)
	CIS	2.02-2.26	(Knapp et al., 2001; Raugei et al., 2007)
	Dye sensitized	0.74-2.1	(Greijer et al., 2001)
	OPV	0.2-4	(Espinosa et al., 2011; García-Valverde et al., 2010; Roes et al., 2009)
	Hybrid		(Azzopardi et al., 2010)
Hydropower		0.5	(Gagnon et al., 2002; Pehnt, 2006)
Geothermal		0.54	(Pehnt, 2006)
Biomass	Gassification	< 5	(Leung et al., 2004)
	Biomass combustion	5-10	(Hohenstein et al., 1994)

4.2.2. Economy and markets for OPV

Economical analysis concerns of organic solar cells are attracting attention in view of the recent publications (Azzopardi et al., 2008, 2011; Emmott et al., 2012; Kalowekamo et al., 2009; Powell et al., 2009). Moreover, the market share for OPV, estimated in around $2 million during 2011, and it is projected to increase from $56 million last year (2011) to reach $387 million in revenues by 2016 (Nanomarkets, 2011).

So far, commercialization of OPV has been addressed by a few companies with a view to integration into products (Krebs et al., 2011; Krebs, Fyenbo, et al., 2010; Krebs, Nielsen, et al., 2010), although grid-tied applications are foreseeable in a medium term, due to the fact that solar electricity costs are forecasted to decrease in the near future. The cost of solar electricity is typically compared to electricity produced by traditional sources with a levelized cost of energy (LCOE) calculation. Recent estimates of electricity cost generated by OPV have shown this to be possible (Azzopardi et al., 2011). It is surprising that for these solar cells based on ProcessOne under an average Mediterranean solar irradiance of 1700 kWh/m^2/year the LCOE ranges between 0.19 €/kWh and 0.50 €/kWh (Azzopardi et al., 2011; Kalowekamo et al., 2009; Powell et al., 2009), while a mature 19.7% efficiency 20MWp plant (depending on geography), yields LCOE values of around 0.05 to 0.07€/kWh[4].

[4] Own calculations with data from Rec group: http://www.recgroup.com/recgroup/operations/REC-in-Singapore/

Silicon technologies require a vast investment both in terms of energy and cost. OPV technologies need 10 times less energy and 3 times lower capital investment in comparison with the former as seen in Table 4.2.

Table 4.2. Investment cost comparison for current silicon PV technologies and OPV with a current 1% and a forecasted 10% efficiency module.

COSTS	Unit	Silicon PV	OPV (10%)	OPV (1%)
Monetary investment				
Annual capacity production	GW_p	365	365	365
Cost per W_p produced	€	1.76	0.63	6.32
Energy investment				
Equivalent Primary Energy	MJ/W_p	37.43	0.4511	4.51

4.3. Environmental impact of organic photovoltaics

Organic solar cells have intrinsically a low embedded energy when the organic compounds are deposited from solution in a medium scale. They have the potential to dramatically decrease the environmental impact of photovoltaics. Methodology of life cycle assessment as detailed above, together with the previous work on this field at UPCT -applied to organic solar cells at a laboratory scale (García-Valverde et al., 2010)-, has provided an excellent foundation to conduct the following studies on R2R semi industrial scale production of OSC at Risø, and has moreover served to establish the parameters that are critical for the beneficial use of polymer solar cells in society and to firmly demonstrate where the potential of the polymer solar cell technology is.

4.3.1. Flexible polymer modules by R2R: ProcessOne

The first life-cycle assessment performed during the PhD work was about ProcessOne, which is one of the first reported industrial manufacturing processes leading to flexible polymer solar cell modules that have been demonstrated. Manufacturing details were provided by Frederik C. Krebs from Risø DTU, and this work started a fruitful collaboration in this field.

4.3.1.1. Analytical frame

To start with, material inventory for the production of an organic solar module has been created, including solvents and other materials not present in the final module, but used during the manufacturing process. The energy embedded in the manufacture of materials from raw materials to initial input into the manufacture machinery, and energy embedded in the direct process, have been also compiled in order to calculate environmental parameters

Data compilation can benefit from our own previous studies on laboratory scale production using very similar materials as active layers and electrodes included in the device (García-Valverde et al., 2010), and also from available inventory data-bases (Jungbluth, 2005; Hammond et al., 2011; PlasticsEurope, 2010).

When a particular chemical process was not available, the use of grouping in similar chemical production categories has been useful in order to provide the figures needed for the LCA calculation.

Decommissioning and recycling procedures have not been taken into account in this LCA calculation. OPV is still a preliminary stage of deployment of the technology and a lack of solid knowledge of the recycling procedures for some of the materials included in the final organic module makes it unreliable to perform a calculation of the energy embedded in the decommissioning steps. Nevertheless, the recycling of some materials (especially solvents such as methanol) during manufacturing following ProcessOne has been taken into account in the calculations. Balance of System (BOS) analysis is also outside the purpose of the LCA calculation presented in this work; therefore the comparison with other PV technologies was performed at a module level.

The functional unit for the ProcessOne organic modules calculation has been the total processed area per 1 square meter of processed foil (305 mm width).

For calculating the energy yield, some assumptions have to be made: first, the efficiency of the produced organic PV modules is varied from 1.25 to 3% (efficiencies already obtained for laboratory cells), 5% and 10% (forecast for module efficiency on industrial level in 2020), secondly, the isolation level is set to 1700 kWh per square meter, typical of southern European countries and representative of a World average. Finally, we consider a 15 years life-time for the system, which is low compared with other PV technologies (usually 20-30 years), but realistic in terms of the aims for 2013 of the European Photovoltaic Technology Platform for organic photovoltaics (Photovoltaic Technology Research Advisory Council PV-TRAC, 2005).

The energy mix for Denmark was used to calculate the emissions released during manufacturing process (420.88 g-eqCO_2/kW_{el} in 2008).

4.3.1.2. Material inventory

Material Inventory is the amount of raw materials used to manufacture a functional unit of PV module. This calculation is the starting point for obtaining the energy embedded in a defined surface of the active solar cell, plus the non-active surface, which contributes to the total module surface. The subsequent energy calculations will take into account this material inventory.

Process One allows to prepare organic solar modules of 16 stripes of 13mm width and 562cm^2 of processed area. The manufacture of polymer solar cells by this route was made following the six steps shown in Figure 4.2.

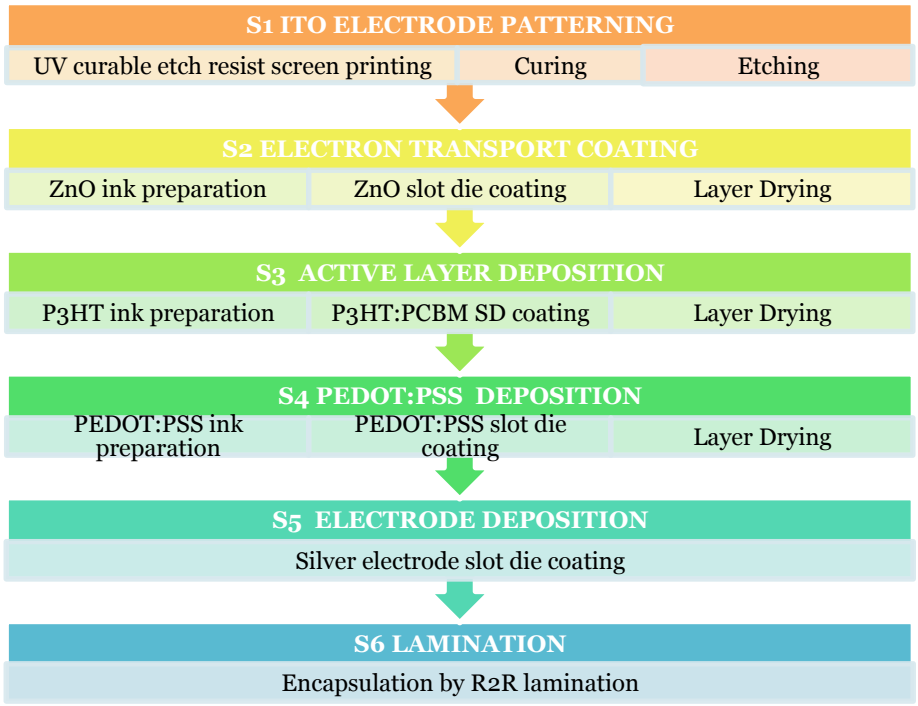

Figure 4.2. Steps and substeps during the ProcessOne PV module processing.

A roll PET substrate which has been sputtered with indium tin oxide (ITO) is patterned with a curable etch resist printing procedure. On the patterned ITO, three layers were deposited by slot die coating: ZnO, P3HT:PCBM and PEDOT:PSS, and finally, on top, the back electrode constituted by a silver mesh is screen printed. The encapsulation of the module is made using a polyester barrier material by a roll-to-roll lamination.

Conditions and material inventory for the fabrication processes -and subprocesses- of 1m² of processed surface, are based on previously reported studies (Krebs, 2009a; Krebs, Tromholt, et al., 2010) and they have been recently published in (Espinosa et al., 2011). They are presented below from Table 4.3 to Table 4.12. Those include the magnitudes of every step for ProcessOne described in Figure 4.2:

- Table 4.3. Screen printing conditions.
- Table 4.4. Curing process conditions.
- Table 4.5. Etching process conditions.
- Table 4.6. ZnO paste preparation equipment.
- Table 4.7. ZnO slot die coating and drying conditions.
- Table 4.8. Active layer blend preparation.
- Table 4.9. Active layer deposition.
- Table 4.10. PEDOT:PSS preparation, slot die coating conditions.
- Table 4.11. Silver electrode screen printing conditions.
- Table 4.12. Lamination conditions.

Table 4.3. Screen printing of UV curable substance conditions for a 1m² processed surface.

Conditions	
Speed	198 m/h
Working Printer Power	60000W
Equipment	
Description	Klemm line printer: unwinder, flat bed screen printer, UV curing oven and rewinder
Maximum Printer Power	150000W
Material inventory	
UV curable ink	3.28 g

Table 4.4. Curing process conditions for a 1m² processed surface.

Conditions	
Speed	198 m/h
Working Lamp Power	15000W
Equipment	
Description	The etch resist substance, deposited previously by screen printing, is hardened in a UV curing oven inside the printer. UV lamp includes also an air-fan to cool the water cooling for the lamp.
Maximum Lamp Power	15000W (incl. air fan cooler power)

Table 4.5. Etching process conditions for a 1m² processed surface.

Conditions	
Speed	198 m/h
Working Etcher Power	10000W
Working Dryer Power	20000W
Working Air Fan Power	20000W
Equipment	
Description	R2R etching machine: etching, stripping and washing baths.
Maximum Etcher Power	100000W
Maximum Dryer Power	20000W
Maximum Air Fan Power	20000W
Material inventory	
$CuCl_2$	0.25 g
Water	0.52 l
NaOH	1.66 g
Demineralized water	0.21 l

Table 4.6. ZnO paste preparation equipment for a 1m² processed surface.

Conditions	
Working Heater Power	150W
Equipment	
Maximum Heater Power	1000W
Material inventory	
$Zn(OAc)_2$	22.64 g
KOH	11.32 g
MeOH	0.09 l
Acetone	188.69 ml
MEA	2.26 g

Table 4.7. ZnO slot die coating and drying conditions for a 1m² processed surface.

Conditions	
Speed	120 m/h
Web Tension	80-90N
Drying temperature	140 ºC
Working Corona Treater Power	1500 W
Working Slot Die Power	2500 W
Working Oven Power	12000 W
Equipment	
Description	BC30 basecoater comprising: unwinder, corona treater, edge guide, double faced contact cleaning, antistatic system, coating roller, ink jet labeling printer, oven, cooling roller and winding station.
Maximum Corona Treater Power	1500 W
Maximum Slot die Coater Power	2500 W
Maximum Oven Power	40000 W
Material inventory	
ZnO ink	10 ml
Isopropanol (washing)	25.77 g

Table 4.8. Active layer blend preparation for a 1m² processed surface.

Conditions	
Heating temperature	120 ºC
Equipment	
Working Heater Power	100 W
Material inventory	
P3HT	0.1 g
PCBM	0.08 g
Chlorobenzene	6.56 ml

Table 4.9. Active layer deposition for a 1m² processed surface.

Conditions	
Speed	84 m/h
Working Slot Die Power	2500 W
Working Oven Power	12000 W
Equipment	
Description	BC30 basecoater comprising: unwinder, corona treater, edge guide, double faced contact cleaning, antistatic system, coating roller, ink jet labeling printer, oven, cooling roller and winding station.
Maximum Slot Die Power	2500 W
Maximum Oven Power	40000 W
Material inventory	
Active layer ink	6.56 ml

Table 4.10. PEDOT:PSS preparation, slot die coating conditions for a 1m² processed surface.

Conditions	
Stirrer	50 W
Speed	18 m/h
Working Slot Die Power	2500 W
Working Oven Power	12000 W
Equipment	
Description	BC30 basecoater comprising: unwinder, corona treater, edge guide, double faced contact cleaning, antistatic system, coating roller, ink jet labeling printer, oven, cooling roller and winding station.
Maximum Slot die Coater Power	2500 W
Maximum Oven Power	40000 W
Material inventory	
Isopropanol	14.75 g
PEDOT:PSS	29.51 g
Isopropanol (washing)	25.77 g
PEDOT:PSS ink	44.26 g

Table 4.11. Silver electrode screen printing conditions for a 1m² processed surface.

Conditions	
Speed	60 m/h
Resident time in oven	72 s
Drying temperature	130°C
Working Printer Power	15000W
Equipment	
Description	Alraum printer comprising unwinder, metering wheel, positioning camera, vacuum table, screen printer (AT701), hot air oven, transport rollers, dancing tensioning roller and rewinder
Maximum Printer Power	38000W
Material inventory	
Silver ink (PV410)	19.67 g

Table 4.12. Lamination conditions for a 1m² processed surface.

Conditions	
Speed	120 m/h
Working Laminator Power	1500W
Equipment	
Description	Laminator comprising unwinder, edge guide and cutting table, laminator, laminate unwinder, longitudinal cutting knifes and rewinder.
Maximum Laminator Power	1500W
Material inventory	
3M 467 MPF	50.60 g
PET	72.75 g

4.3.1.3. Energy inventory

Embedded energy in materials production

Estimation of energy requirements in the production of special chemicals is quite complex, since information on such production processes is scarce. Moreover, many of the chemical processes presented in this work are not yet in a full production scale. The estimation of energy in chemical synthesis for most of components was accomplished in previous works (García-Valverde et al., 2010). The processing energy for all components is listed in Table 4.13.

Table 4.13. Cumulative energy requirements for raw materials production.

Raw materials inventory	***Thermal energy (kJ_{th})***	***Electrical energy (kJ_{el})***	***References***
PET (1kg)	51314.56	5813.05	PET film (PlasticsEurope, 2010)
ITO ($1m^2$)	55.29	88632.86	(García-Valverde et al., 2010), calculated
NaOH (1kg)	8088.00	4175.50	(PlasticsEurope, 2010)
Demineralised Water ($1m^3$)	-	1080.00	(Tiyarov et al., 2004)
KOH (1kg)	8088.00	4175.50	(PlasticsEurope, 2010)
MeOH (1kg)	160.00	12705.53	(Atkins, 2008)
Acetone (1kg)	49552.00	1589.00	(PlasticsEurope, 2010)
Isopropanol	160.00	12705.53	(Atkins, 2008)
MEA (1kg)	33520.00	14665.00	(PlasticsEurope, 2010)
P3HT 99%HT (1kg)	1148.03	131.07	(García-Valverde et al., 2010)
PCBM (1kg)	6769.93	908.77	(García-Valverde et al., 2010)
Chlorobenzene (1 kg)	48552.00	1410.50	Grouping Benzene and Cl_2(PlasticsEurope, 2010)
Adhesive resin	69288.00	3055.50	Considered as PET (PlasticsEurope, 2010)
Barrier resin	51314.56	5813.05	(PlasticsEurope, 2010)

Once the material inventory and calculation of embodied energy in raw materials production have been accomplished, the embodied energy for input materials can be obtained. Finally, using the energy input of the cell fabrication method, the energy input required for the raw material processing, and the material inventory, the cumulative energy demand per square meter of processed surface can be obtained. This has been converted to Equivalent Primary Energy[5] (EPE), as it is recommended in the reference literature.

The share of energy consumed in the processing of each material is represented graphically in Figure 4.3. It provides a straightforward identification of the most energetically intensive materials processes.

Direct energy process

Embodied energy during direct energy process involves the energy consumption in the different steps during the processing of the module, from input materials to the final PV module, as shown in Table 4.14. All the considered energy inputs are

[5] For the conversion efficiency for electricity production we used a value of 0.35. For the conversion efficiency of thermal energy consumption to primary energy equivalent, we used a value of 0.8.

electrical; therefore the total embedded energy in Table 4.14 is expressed in electrical Wh, giving 7.48kWh per functional unit.

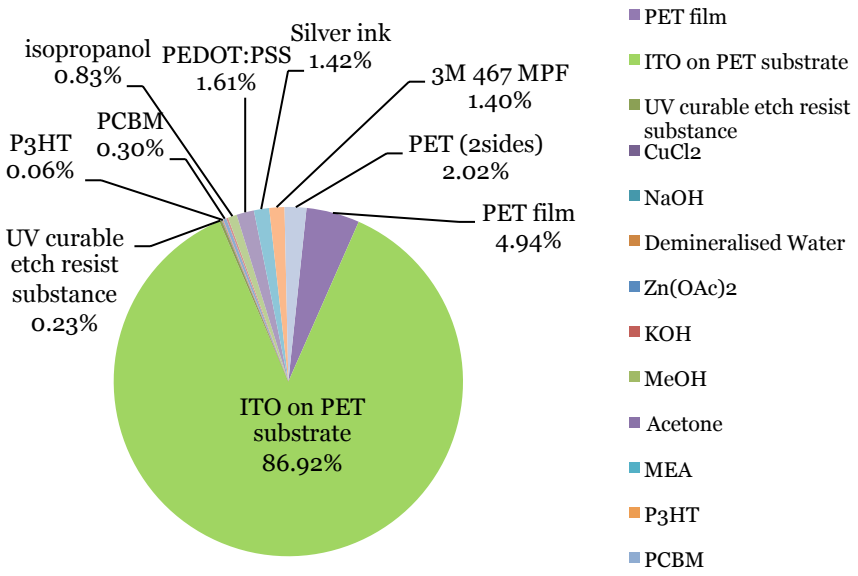

Figure 4.3. Calculated share of the embodied energy in the considered input materials to the direct production for the organic solar module.

In order to compare with other LCA studies it is convenient to know the value in Equivalent Primary Energy (EPE), here being 76.99MJ -assuming a 35% of efficiency of EPE to electrical energy-.

Table 4.14. Energy consumptions during R2R processing (ProcessOne) of a organic (P3HT:PCBM) PV modules.

	Electrical energy consumption (Wh_{el})	
S1 ITO ELECTRODE PROCESSING	***3050 cm²***	***1m² (67% active area)***
UV curable etch resist screen printing	303.03	993.54
Curing	75.76	248.39
Etching	151.52	496.77
S2 ET COATING		
ZnO ink preparation	51.80	169.82
ZnO coating SD	33.33	109.29
Layer Drying	100.00	327.87
S3 ACTIVE LAYER DEPOSITION		
P3HT ink preparation	2	6.56
P3HT:PCBM coating SD	20.83	68.31
Layer Drying	100.00	327.87
S4 PEDOT:PSS DEPOSITION		
PEDOT:PSS ink preparation	0.45	1.48
PEDOT:PSS slot die coating	138.89	455.37
Drying	666.67	2185.79
S5 ELECTRODE DEPOSITION		
Silver electrode slot die coating	636.67	2087.43
S6 LAMINATION		

Encapsulation by R2R lamination	2.04	6.68
SUBTOTAL (Wel)	2282.97	7485.16
SUBTOTAL (MJ EPE)	23.48	76.99

4.3.1.4. Life-cycle impact assessment

Energy impact assessment

Regarding the energy directly consumed in the manufacturing processes, PEDOT:PSS deposition is the more consuming step, accounting for more than one third of the total energy consumption during the manufacture (35.31%), followed from a short distance by both electrodes processing: silver deposition and ITO patterning (27.89% and 23.23% respectively). The electron transport layer deposition accounts for almost 10% of the total energy, and active layer is one of the less energy intensive processes (5.38%), as shown in the Figure 4.4.

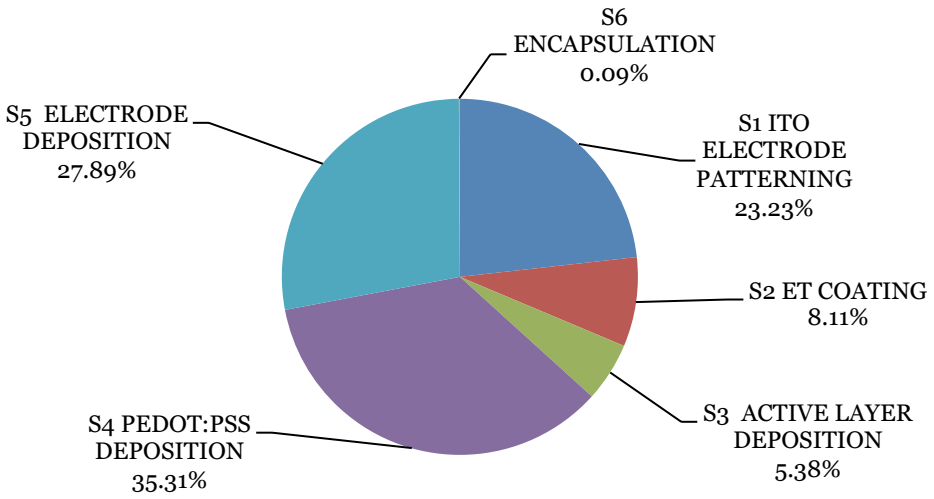

Figure 4.4. Calculated distribution of the energy consumption in the 'production steps' (direct process energy) for the organic solar module.

Important reductions of direct process energy in OSC fabrication have been achieved, as expected for a newly developed PV technology, the direct process energy accounts for about one quarter of the embedded energy in materials, 76.99MJ to 302.27MJ, as it is shown graphically in Figure 4.5.

Energy pay back time and GHG avoided emissions

The energy embedded in the production process of all the materials identified in the inventory has been calculated, and then the energy process of the organic solar cell fabrication and the module fabrication has been added. The output of the calculation is the energy embedded per surface of PV module. Figure 4.5 shows that 379.26MJ (EPE) are required to process 1m² surface of ProcessOne modules.

The Energy Pay Back Time (EPBT) for these modules is then calculated as the ratio of embodied energy to annual generated energy by the module, and the Energy Return Factor (ERF) as the ratio of lifetime to energy pay-back time ERF.

The generated energy is dependent on the final system performance. We assume a realistic performance ratio of 0.8.

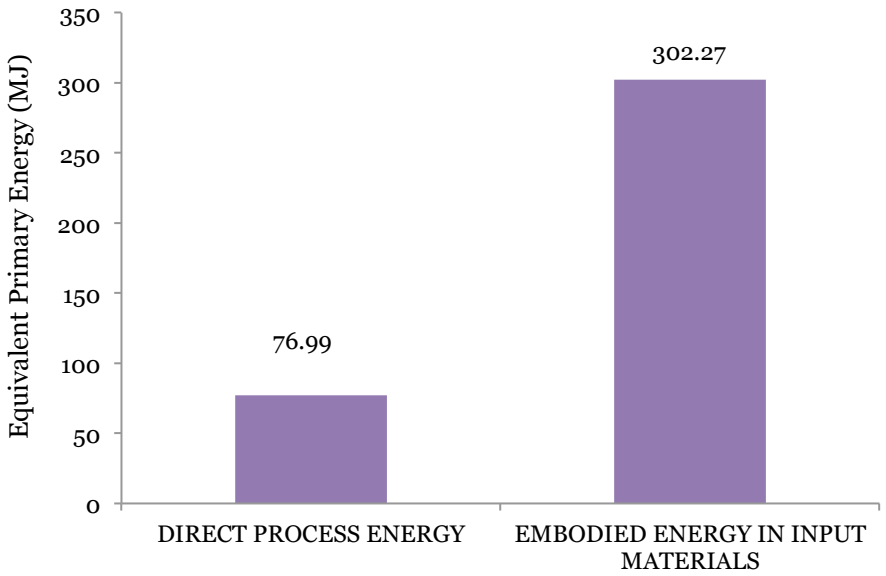

Figure 4.5. Embedded Energy in 1m² processed surface of an organic solar modules (67% of active area). The energy is given in Equivalent Primary Energy (EPE MJ).

The calculation for the saved EPE, EPBT and ERF, presented in Table 4.15, was made ranging active area from 50% to 85%, and efficiencies from 1.25 to 3% and forecasting efficiencies to 5 and 10%. It is clear the need for improving the ratio active/total area in OPV modules.

Table 4.15. EPBT and ERF for 1m² processed surface of organic PV modules, prepared by R2R processing with 15 years lifetime, for different efficiencies and percentages of active area.

Active area (%)	Efficiency (%)	$E_{generated}$ (MJ_{EPE}/year)	EPBT	ERF
50.00%	1.25%	87.43	4.34	3.46
	2.00%	139.89	2.71	5.53
	3.00%	209.83	1.81	8.30
	5.00%	349.71	1.08	13.83
	10.00%	699.43	0.54	27.66
67.00%	1.25%	117.15	3.24	4.63
	2.00%	187.45	2.02	7.41
	3.00%	281.17	1.35	11.12
	5.00%	468.62	0.81	18.53
	10.00%	937.23	0.40	37.07
85.00%	1.25%	148.63	2.55	5.88
	2.00%	237.81	1.59	9.41
	3.00%	356.71	1.06	14.11
	5.00%	594.51	0.64	23.51
	10.00%	1189.03	0.32	47.03

Photovoltaic systems do not generate green house gas (GHG) emissions during its electricity production stage, but if we consider the entire life cycle, then the pollutant emissions during the fabrication, transport, decommissioning and recycling stages should be taken into account. The method used here calculates the emissions using as starting point the embedded energy, which is one of the outputs of the previous energy pay-back time calculation. Then we assume a determined energy mix for the location of the facility where the modules are produced. As indicated previously, for ProcessOne we have used the energy mix for Denmark, 425.88 g-eq CO_2/KW_{el} in 2008, (*Danish Energy Agency*, 2011). This allows us to calculate the CO_2 emissions per square meter of module during the lifetime of the system, also called the embodied CO_2, which are presented in Table 4.16.

Table 4.16. CO_2 emission factor of organic photovoltaic modules. Two values of nominal efficiency are considered, the 1m² processed surface of modules has 67% of active area with its fabrication assumed to be in Denmark and its utilization is assumed in a Mediterranean location (1700kWh/m²/year of average irradiance). A lifetime of 15 years and a performance ratio of 0.8 are assumed.

Module efficiency	Embodied CO_2 (kg eq-CO_2)	E_{gen} during module life time (kWh_{el})	CO_2 emission factor (g eq-CO_2/kWh_{el})
2%	15.49	273.36	56.65
3%	15.49	410.04	37.77

4.3.1.5. Discussion

The results show that this technology has a low environmental impact in terms of embedded energy, GHG emissions and energy pay-back time. For a typical module of 3% efficiency, and an active area of 67% of module surface, the direct process energy is 76.96 MJ/m2 and the energy embedded in the materials is 302.27 MJ/m2, which delivers an energy pay-back time of 1.35 years. These values have also been calculated for other efficiencies and active area percentage. In all cases, the results compare well with other organic PV technologies. Since the energy involved in processing the ITO represents about 87% of the total, as seen in Figure 4.3, this material represents a bottleneck in the fabrication of organic solar modules and intensive research has to be carried out to find an alternative transparent conducting oxide or polymeric layer to be used as transparent electrode. No clear alternative has been pointed out so far, although several alternatives have been proposed, as will be illustrated in section 4.3.3.

4.3.2. Product integrated ProcessOne

It was the second analysis performed at Risø DTU, it is focused on a lamp that was manufactured in cooperation with Mekoprint A/S –a Danish company with large expertise in printing electronics-; it included solar cells produced by ProcessOne in conjunction with white light emitting diodes, polymer lithium ion batteries and flexible printed electronic circuits in lighting applications for the "Lighting Africa" initiative (Krebs, Nielsen, et al., 2010). This lamp sought to provide low cost reading light and simple rechargeable lighting in developing

countries without an electricity grid. Hence, its service will be compared versus other portable light applications.

4.3.2.1. Analytical frame

A life cycle analysis on a product integrated polymer solar module is carried out in this study. It was performed to assess the suitability of a light-weight lamp depicted in Figure 4.6 based on a plastic foil, a lithium-polymer battery, a polymer solar cell, printed circuitry, blocking diode, switch and a white light emitting semiconductor diode.

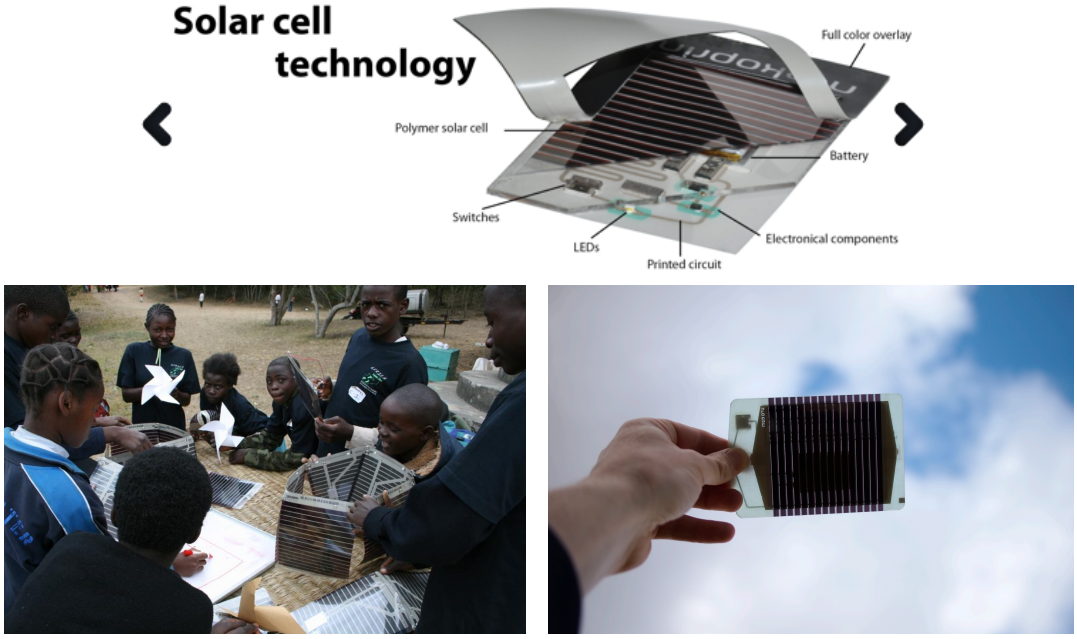

Figure 4.6. Photographs showing some of the lamps for the lighting Africa initiative (left) and exploded view of the lamp showing all different layers (right). Photographs from Mekoprint A/S and Mads Wadstrøm.

There are several functional units along the present study. One chosen functional unit, a 104cm² lamp, has served as the base of calculations of the energy embedded in the materials and for comparing with other lighting products. Another functional unit has served for comparisons for products that are investigated, therefore a functional unit in hours of daily operation over a period of one year was chosen.

Data for the specific lamp materials were gathered from different sources. Where possible, we have extracted data from manufacturers, free databases and literature. For some new materials and processes we had to create data by use of knowledge gathered for subcomponents. Calculations of the fabrication of the organic solar module process were based on our previous studies on organic solar cell module production, since the same materials have been used as active layer and for electrodes and buffer layers, that were included in this device (García-Valverde et al., 2010; Espinosa et al., 2011).

The production of the lamp was assumed to take place in Europe. For the OPV lamp, production of polymer solar cells is located in Denmark. The blocking

diode, the LED, the battery and all electric and electronic components are commonly manufactured in China or East Asia. However, since it is not possible to quantify the emissions in these locations, these components were assumed to be fabricated from a European energetic supply, adding the transport from these places to the location of the manufacturing and from there to the place of use.

Table 4.17. Technical specification details of the organic photovoltaic lamp.

Technical data		
OPV power	0.05-0.1	W_p
Nominal capacity battery	105	mAh
Battery voltage	3.7	V
LED Power	85	mW
Forward current LED	20	mA
Working time	3	h/day
Energy delivered by the battery in daily working time	255	mWh
Estimated Lifetime	2	years

4.3.2.2. Material and Energy inventories

The OPV lamp comprises several layers, which can be seen in Figure 4.6, and with the product specifications shown in Table 4.18.

Table 4.18. Inventory table of materials used in each subcomponent per unit of product, i.e one OPV lamp.

PROTECTIVE LAYERS (PET)			**BATTERY**		
Layer	**Thickness**	**Area (cm^2)**	**Component**	**Weight Content (%)**	**Material**
Overlay (frame)	50µm	39.48	Cathode	28.96	Lithium cobalt oxide
Adhesive (frame)	25µm	39.48	Cathode substrate	2.64	Aluminum foil
Adhesive (cell)	50µm	70.56	Anode	24.17	Graphite
Foil spacer	1.5mm	92.16	Anode substrate	6.13	Copper foil
Adhesive (Foil spacer)	25µm	104.16	Tab	3.37	Nickel tab/aluminum tab
Membrane Printed	130µm	104.16	Electrolyte	8.96	LiPF6+EC+PC
			Diaphragm	1.86	PP+PE
			Packaging	23.81	Aluminum plastic film
			Brown tap	0.10	PP+PE
SOLAR CELL			**OTHER COMPONENTS**		
Role	**Material**		**Component**	**Details**	
Front electrode	ITO 60 Ω/m^2 on PET		LED	Micro SIDELED LW Y87C (OSRAM)	
Electron conductor	MeOH based ZnO np		Metal dome	Stainless steel/gold	
Active	P3HT:PCBM		Button	Silicone rubber	
Hole conductor	PEDOT:PSS		Blocking Diode	1N4148W-V Vishay Semiconductors	
Back contact	Silver ink PV410		Printed circuit	5007E DUPONT	
Adhesive	3M 467 MPF		Vias contact	Copper adhesive	
Barrier Material	AMCOR barrier				

In this case each component of the lamp was analysed separately and all the materials were tracked back to the point of resource extraction, using cradle-to-gate data from manufacturers (Amcor, AEC, OSRAM), and all the energy consumed in these processes was accounted for separately as well. There was a phase of assembly where the electronic board was printed and every component was mounted on an automatized process. After that, the lamps were laminated, and cut into individual lamps by using a laser. Energy for materials, direct processing and transport will be disaggregated afterwards in Figure 4.10.

a. Protective layers

As can be observed in the exploded view of the OPV device shown in Figure 4.6, there are several layers for giving both protection and support structure to the lamp. All of them are considered as made of the same quality of Polyethylene terephthalate (PET) with different thicknesses listed in Table 4.18. This polymer is well studied from the industrial point of view and known to require 80.75 MJ/kg of primary energy for its manufacture (PlasticsEurope, 2010). A detailed material and energy inventory is shown in Table 4.19.

Table 4.19. Material and energy inventory for production of all protective layers of the OPV lamp.

Details	Amount	Unit
Overlay (frame)	0.27	g
Adhesive (frame)	0.14	g
Adhesive (cell)	0.48	g
Foil spacer	18.94	g
Adhesive (PET spacer)	0.36	g
Membrane Printed	0.36	g
Transport energy	43.67	kJ EPE
Total Energy requirements	1.70	MJ EPE

b. Battery

A lightweight lithium-polymer (Li-Po) battery was included in the OPV lamp. When compared to a lithium-ion battery, Li-Po has a greater life-cycle degradation rate. However, more than 500 charge-discharge cycles can be carried out before the capacity drops to 80% and these batteries are solid and have the safest design. Data about energy requirements for small and medium size electronic facilities, such as batteries, LEDs and diodes, are increasing as LCA studies are becoming widespread, but there are still little available data about these devices. For batteries, Rydh and Sanden made a complete energy analysis review of different technologies (Rydh et al., 2005a, 2005b). In a Li-Po battery, the common materials are shown in Figure 4.7 and materials content provided by the manufacturer was detailed in Table 4.18.

The anode is generally made of 14 μm thick graphite coated on copper foil (Gaines et al., 2000). The embodied energy in the anode materials was found to be 160MJ/kg of graphite (Pehnt, 2001) and 52 MJ/kg of copper foil (Papasavva et al., 2001). The diaphragm is made of equal proportions of polypropylene and polyethylene. These polymers are materials easily found in the PlasticsEurope database (PlasticsEurope, 2010) with energy requirements of 73.37 and 78.08 MJ/kg respectively.

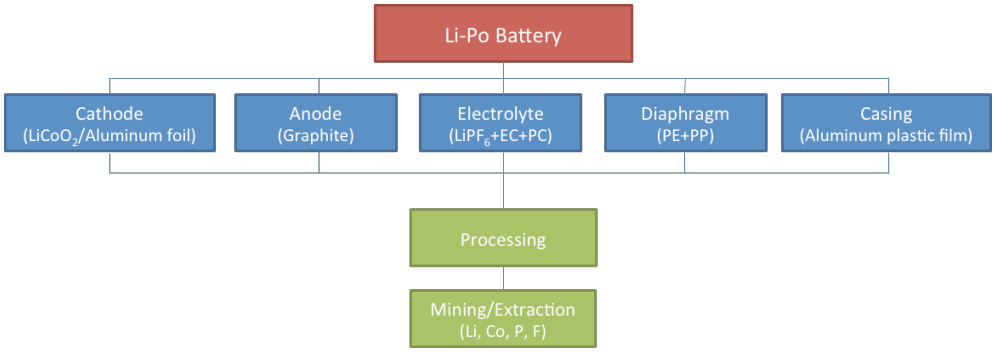

Figure 4.7. Components in the Li-Po Battery contained in the OPV lamp.

Lithium hexafluorophosphate ($LiPF_6$) is the most widely used salt in the electrolytes for this kind of battery. LCA data for lithium and the other ingredients (ethylene, and propylene) were found. However, the LCA data of $LiPF_6$ was not available in the literature and neither in the Ecoinvent database (Jungbluth, 2005). Therefore, the electrolyte has been modelled on the basis of its chemical synthesis with respect to industrial production requirements in terms of materials, energy, and catalysts, as shown below and in Table 4.20:

$$PCl_5 + 6\,LiF \rightarrow 5LiCl + LiPF_6$$

Table 4.20. Material and energy inventory for manufacturing of 1 kg of $LiPF_6$ electrolyte.

Detail	Amount	Unit
LiF_6	0.2 kg	kg
PCl_5	1.7 kg	kg
CaF_2	4.4 kg	kg
H_2SO_4	5.8 kg	Kg
Fuel oil	0.44 MJ	MJ
Electricity	23.6 kWh	kWh
Energy requirement	657.26	MJ EPE

The cathode is made of lithium cobaltite ($LiCoO_2$). The manufacturing process for the cathode salt needs energy for oxidation of pure $CoCl_2$ in a precise controlled furnace in which cobalt oxide (Co_3O_4) is produced. The cobalt oxide is then mixed with lithium containing compounds and transformed into $LiCoO_2$. Assuming the calculations of (Zackrisson et al., 2010), a total of 3 kJ electricity are needed per gram of $LiCoO_2$ produced.

For other components of the battery, valuable information for aluminium packaging was obtained from the manufacturer (Amcor) and from the PlasticsEurope Database. The energy needed for the nickel tab was obtained from (Norgate et al., 2002). This lead us to a material inventory and the energy required for the battery shown in Table 4.21.

Table 4.21. Material inventory and primary energy required for manufacturing a 105 mA Li-Po Battery.

Detail	Amount	Unit
CATHODE		
$LiCoO_2$	7.76E-01	g
Aluminum foil	7.07E-02	g
ANODE		
Graphite	6.48E-01	g
Copper foil	1.64E-01	g
ELECTROLYTE		
$LiPF_6$	0.13	g
Ethylene carbonate	8.04E-02	g
Polycarbonate	2.57E-02	g
OTHERS		
Tab (nickel tab/aluminum tab)	9.03E	g
Diaphragm (PP+PE)	4.98E	g
Packaging (aluminium plastic film)	6.38E	g
Brown tap (PP+PE)	2.68E	g
Material energy requirements	0.30	MJ EPE
Transport energy	5.71	kJ EPE
Total energy requirement	0.45	MJ EPE

c. Light Emitting Diode

Regarding the materials and the processes in manufacturing of opto-semiconductors devices, there is limited information. A detailed inventory of materials such as: Gallium nitride -and its starters: trimethyl gallium, ammonia precursors, high purity gases-, sapphire substrate and silicon, was not available; we have based our calculations, for energy needed in the production of the materials, on data from OSRAM: 0.41 kWh of primary energy are required per LED product (Finkbeiner et al., 2009). The manufacture of LEDs consists mainly in the steps shown in the frontend and backend processes shown in Figure 4.8.

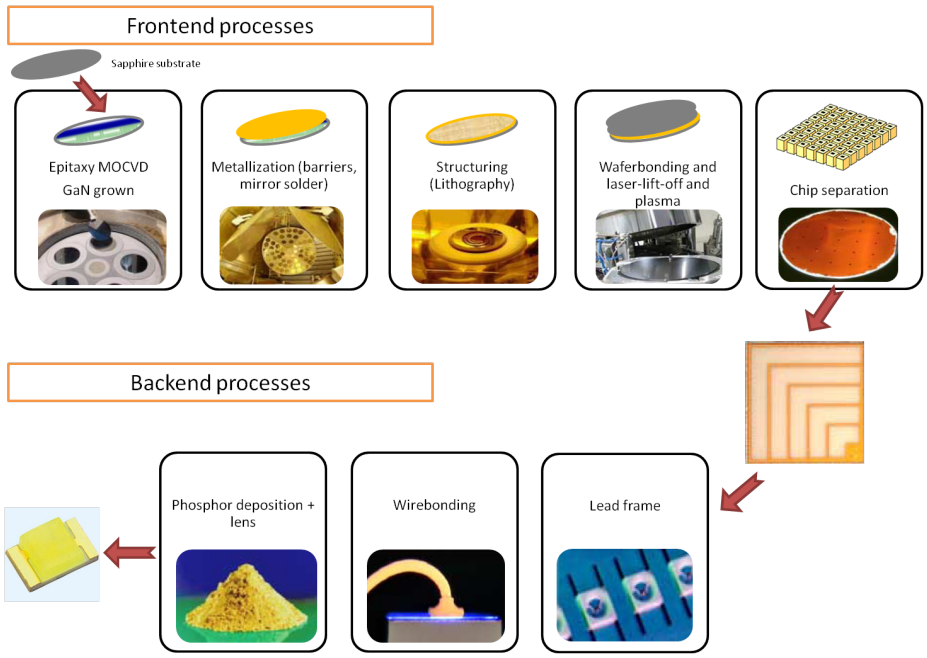

Figure 4.8. Basic front- and backend processing in opto-semiconductor manufacturing.

Including CVD, metal deposition, photolithography, etching and cleaning steps the energy in the manufacturing is ~30 kWh of primary energy per wafer (1000 LEDs) (Matthews et al., 2009), but there are no data available for bonding wafers, or laser lift-off, and neither for mounting, testing, packaging, phosphor coating or encapsulation processes.

The energy requirements for the rest of processes are listed in Table 4.22, giving a total embodied energy of 1.48MJ from which 1.17MJ are embodied in the materials, 0.31MJ in direct process, and the energy required for transport the LED from the manufacturing place to Denmark is 0.012kJ EPE.

Table 4.22. Energy requirements for the production of 1000 LED wafer and per LED.

Processing Step	**Technique**	**Estimated electricity per wafer (kWh)**
GaN Growth	MOCVD	4.3
Blanket metal deposition for p-contact	Average of chemical vapour deposition processes	7.5
Creation of n- contact	Photolithography	2.8
GaN surface Roughening	Photo-electrical- chemical etching	15
Die cleaning	Wafer cleaning	~0.4
Energy requirements per LED		
Transport Energy	0.012 KJ EPE	
Materials Energy	1.17 MJ EPE	
Total Energy required	1.48 MJ EPE	

d. Electronic board and assembly

An electronic circuitry comprising silver was printed on top of a PET membrane followed by semiautomatic mounting of discrete components to complete every lamp. These components such as blocking diode, white LED and a battery, were mounted after the printing on the back-side, using a fully automated SMD (surface mount device) process line with a consumption of 5.2kWh per 256 lamps in Mekoprint Electronics A/S. After component assembly the lamps were laminated and laser cut into individual lamps as shown in Figure 4.9.

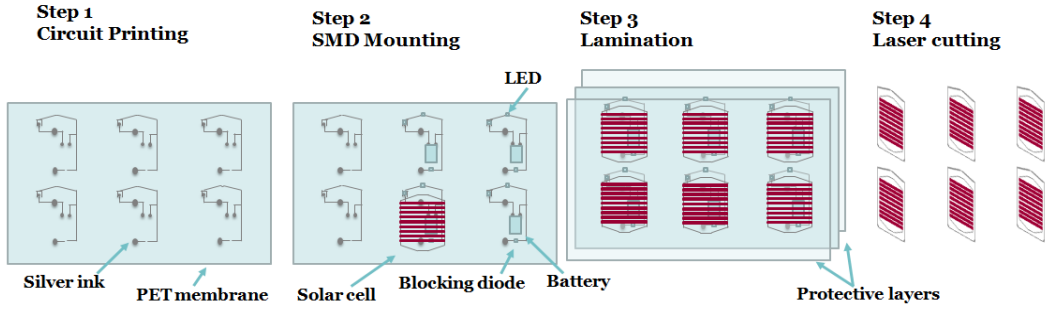

Figure 4.9. An illustration of how the electronic circuit is screen printed followed by component mounting, lamination with the OPV and protective layers and finally laser cut into individual lamps.

In Table 4.23 the material inventory for the electronic board is shown. For simplicity we have considered the same manufacturing energy input for both LED and blocking diode. For the copper tape and the metal dome made in stainless

steel and gold, we used the values proposed by (Norgate et al., 2002) on behalf of gross energy requirement for their production.

Table 4.23. Material inventory and energy requirements for electronic board of discrete components per OPV lamp

Details	Amount	Unit
Stainless Steel dome	0.56	g
Gold cover dome	2.78E-04	g
Silicone rubber Button	1.12	g
Blocking Diode	1	-
Silver ink	0.04	g
Copper foil	1.97E-03	g
Adhesive copper tape	1.27E-04	g
Material energy	1.31	MJ EPE
Electricity	20.31	Wh
Transport energy	39.26	kJ EPE
Total energy requirement	2.17	MJ EPE

4.3.2.3. Life-cycle impact assessment

EPBT is calculated assuming a best thermoelectric efficiency of $\eta_{th\text{-}el}$ of 35%, and the estimated embodied energy for the OPV lamp, which is equivalent to 178Wh_{el}. The OPV device must supply a load, which follows a daily constant pattern of 3 hours per day leading to a daily average energy consumption of 255 mWh. This means that the annual electrical production is 93.075Wh_{el}/year. According to that an EPBT of 9.98 years is obtained for the lamp. Therefore, the OPV device will generate less energy than the energy embodied in it by the end of its lifetime (estimated in 2 years).

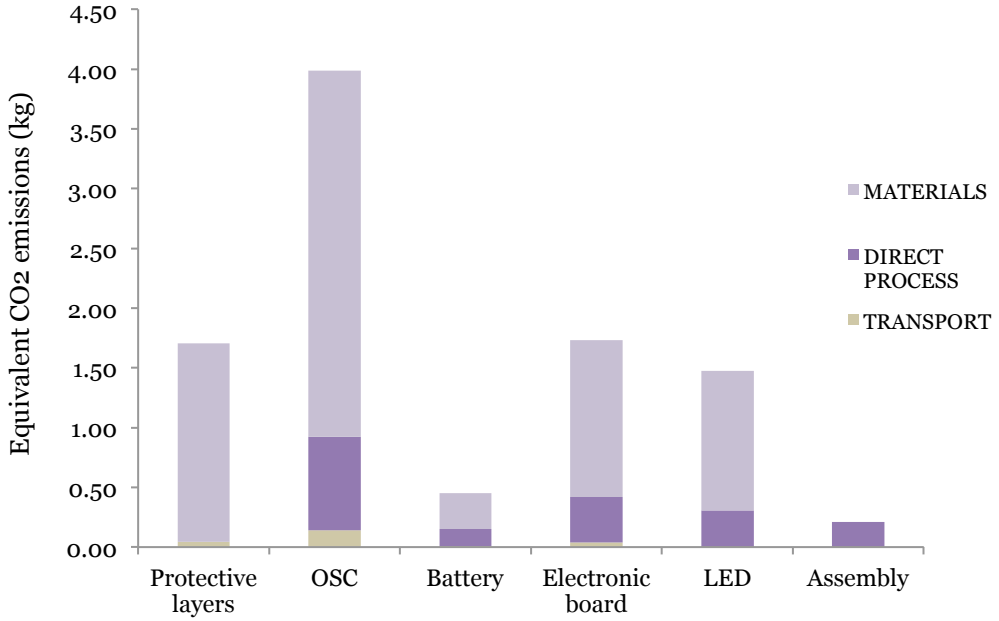

Figure 4.10. Total embodied CO_2 share for transport, direct process and materials in each component or process, in the manufacturing of an OPV lamp.

The amount of 0.39kg of embodied CO_2 for the given OPV lamp has been calculated in the life cycle GHG emissions study and shown in Figure 4.10. The

electricity generated by the OPV device in its lifetime can be estimated to be 186Wh_{el}. For this OPV device the CO_2 emission factor is about 2.18g/Wh_{el}.

4.3.2.4. Discussion

When looking at the share of the energy used per components and process for manufacturing the lamp depicted in Figure 4.11, the solar cells are responsible for the 42%(4MJ) of the entire energy, followed by the electronic board and the protective layers, both around a 18% each (or 1.73 and 1.70MJ correspondingly). Production of materials, processing and transport of the LED contribute 15%(1.48MJ) to the energy requirements, and the battery accounts for just 5% (0.44MJ) in the manufacturing phase. The assembly of the components takes 2% (0.21MJ) of the embodied energy.

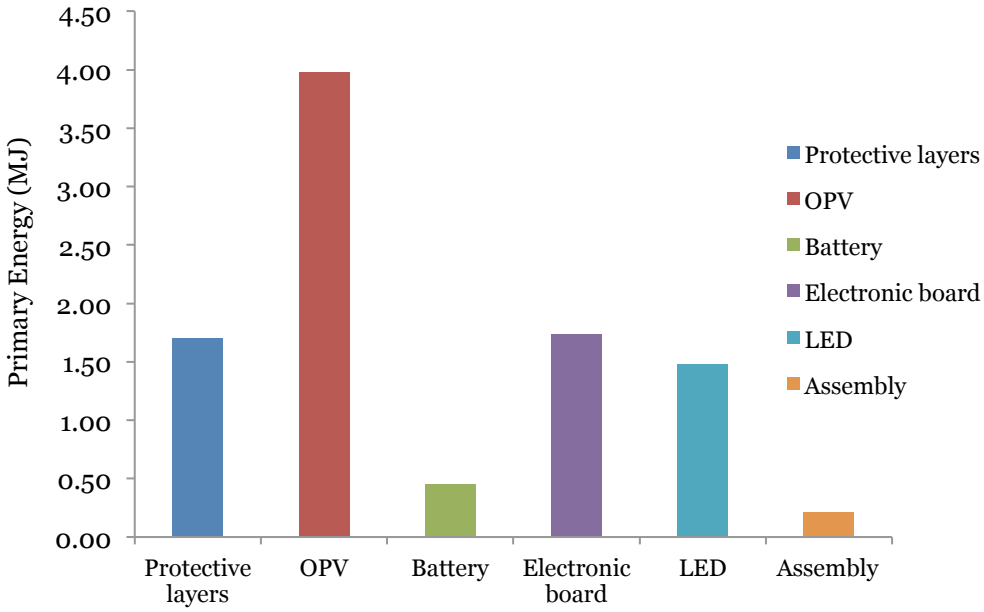

Figure 4.11. Energy input in the manufacturing of the OPV lamp including energy embedded in the materials, in direct process energy and transport per component

Comparison with other portable power products

The environmental impacts of the OPV lamp can only be evaluated properly by comparing it to other alternative options, because avoided emissions depend on the electricity, or lighting supply in this case, by the source or device that the OPV lamp would be replacing. In order to compare the lamp with another light source, the energy embedded in the OPV system, E_{EMB}, and the energy "saved", $E_{avoided}$ during the lifetime of the replaced lighting product, L (Eq 4.3, both in primary energy) should be taken into account.

Eq 4.3

$$EPBT = \frac{E_{EMB} \cdot L}{E_{avoided}}$$

That is the energy that is saved every year by not using the alternative to the OPV lamp. Several scenarios are then used for this comparison, we have considered four alternatives for lighting devices detailed below and listed in Table 4.24.

Firstly, the OPV lamp would be used in a remote area as a replacement for a kerosene lamp. We have chosen Ethiopia where excellent solar conditions exist, well above 2,000 kWh/m²/yr (Huld et al., 2005). Ethiopia would thus be an excellent place to make use of a solar powered lamp since most of the inhabitants live in rural areas (85%) and where the average electrification rate is only 1% (*World Energy Outlook*, 2010). As a result, Ethiopians experiences numerous limitations at nighttime. Once the Sun sets between 6pm and 7pm, the only source of light in most parts of rural Ethiopia is a dim kerosene lamp producing health-hazardous smoke and presents a significant fire hazard. Therefore, the substitution of the poor kerosene lamps with solar powered LED lights, could not only solve lighting needs, but would also provide environmental, social and economical benefits.

Table 4.24. Products evaluated in comparison with OPV lamp.

	OPV lamp	**Kerosene lamp**	**PV silicon lamp**	**Torch**	**BCS**
Light system	1 LED	Kerosene tin lamp	6 LED	7W CFL bulb	7W CFL bulb
Light strength	14lm/W	7lm/kJ	14lm/W	6lm/W	6lm/W
Battery type and capacity (Ah)	Li-Pol, 0.105	-	NiCd, 2	Lead acid, 4.5	Lead acid, 100
PV type and power (W_p)	OPV, 0.31	n.a	a-Si, 0.7	n.a.	n.a.
Maximum daily operation (h)	3	n.a. (0.035l/h)	3.5	3	60[6]
Emission factor (g/Wh_{el})	2.18	15.77	2.70	1.06	2.34
Energy consumption (MJ/lamp) Reference	9.56 This study	162.28 (Mills, 2003; Optis, 2008; Dave, 2009)	73.91 (Alsema et al., 2000; Rydh et al., 2002)	397.69 (Finkbeiner et al., 2009; Dave, 2009)	1087.55[7] (Alsema, 2000; Dave, 2009)

An EPBT of 0.12 years is obtained when a kerosene lamp is substituted by the OPV lamp meaning that the OPV device would need to operate just 1.46 months in order to earn back its invested energy. In case the OPV lamp replaces a torch lead acid battery or either a Battery Charging Station (BCS) as light supply, it will require only 0.09 years of operation. All EPBTs are shown in **¡Error! No se encuentra el origen de la referencia.**. In Table 4.24, all the emission factors for the lanterns or systems are also shown. Despite the fact that the torch and the BCS are the most energy intensive systems, the emission factors are not so high because they are used in combination with a compact fluorescent lamp (CFL) bulb of 7W. For a diesel generator the considered emissions are 1.27kg of

[6] All electricity in the battery will be supplied for lighting services.
[7] For the total Battery Station: diesel generator, lead acid battery and CFL.

CO_2/kWh_{el} (Alsema, 2000). This figure includes emissions during fuel combustion, the fuel extraction and refining, manufacturing of the generator itself and fuel transport (over 100 km). And 2.56 kg CO_2-eq per kerosene litre have been estimated from the literature (Mills, 2003).

The analysis reveals that the OPV lamp has a significant advantage provided that some of the challenges facing this novel technology are efficiently met such that it can enter the market of portable lighting devices.

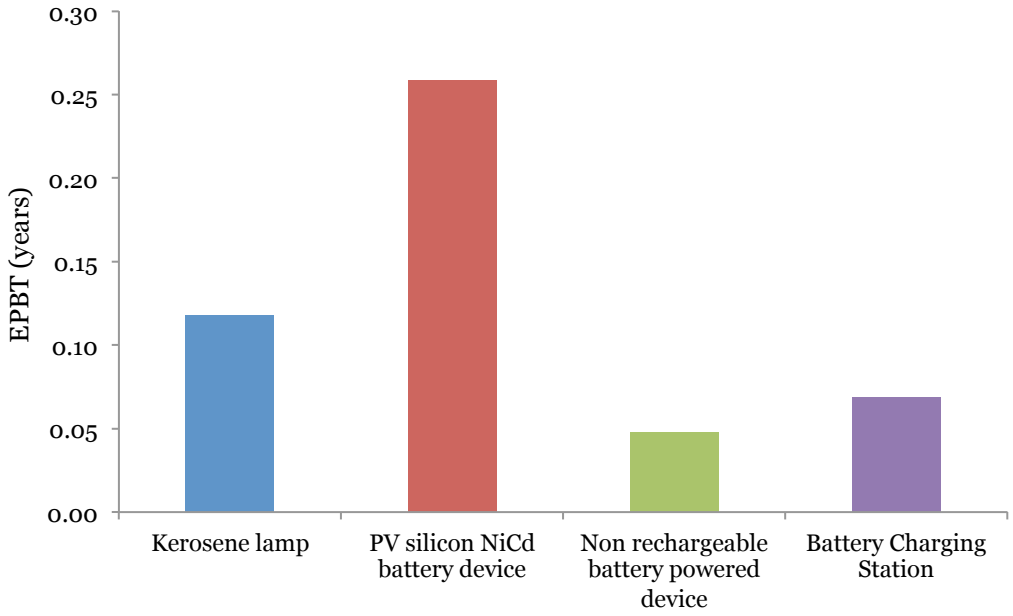

Figure 4.12. Energy Pay-Back Times obtained when switching to an OPV lamp from different lighting systems.

4.3.3. Indium Tin Oxide free solar cells

In this study a complete life cycle assessment that was performed on innovative ITO-free polymer solar cell architecture is presented. As already discussed in section 3.2.2 in this thesis, ITO main constituent, indium, is an scarce and high energy demanding element that should be replaced in case a large-scale production of OSC is launched. This process was demonstrated to be fully roll-to-roll (R2R) compatible and had been reported previously a couple of times by the same group (Krebs, 2009b, 2009c), but the corresponding devices showed significantly poorer performance than ITO-based devices (Krebs, 2009a; Krebs, Tromholt, et al., 2010). There have been however a few reports on ITO free device architectures with similar performance to the ITO-based devices, although it has not been demonstrated they can be fully R2R fabricated (Zimmermann et al., 2007; Niggemann et al., 2008; Galagan, de Vries, et al., 2011; Galagan, J.M. Rubingh, et al., 2011). The most promising ITO-free approach was transferred, following a device structure developed at Fraunhofer ISE (Zimmermann et al., 2009), to a R2R process at Risø DTU (Manceau et al., 2011). The process follows the steps shown in Figure 4.15 and while the performance was compromised to some extent by the up-scaling, an improvement in performance, as compared to prior reports, was achieved.

4.3.3.1. Analytical frame

The main goal of this work is to study to what extent the LCA outcome is affected by the replacement of a cost intensive electrode by an ITO-free one. In order to avoid ITO, one layer of aluminium and a subsequent layer of chromium were sputtered on polyimide film (Kapton). This is used as initial input in the main process. The choice of Kapton was only for the purpose of development and to avoid problems with thermal instability of the substrate during the sputtering -as explained in Chapter 3 when dealing with Materials in section 3.2.1 Substrate. The assumption of a PET substrate -since it is envisaged that PET would be used in the final version of this solar cell-, also facilitates the comparison of our study with previous LCA studies, mostly based on this material.

The system boundary demarcates which processes are considered in the analysis, as it is presented in Figure 4.13. So that in this case the analysis incorporates also direct energy to process and direct energy to produce materials used in the manufacturing -primary and ancillary-; but leaving the energy used for manufacturing the equipment outside.

Energy requirements due to transportation of materials to the manufacturing place have been also neglected. It can be quite safely assumed to be of low significance per module. Typical values, as given in SimaPro, range from 0.23 MJ/kg, for road transport to 0.47 MJ/kg when it is rail freight. One module weighs much less than 1 kg/m² and the required chemicals including bottles etc. also weigh less than 1 kg, so the total contribution of transport should be below 2 MJ/m².

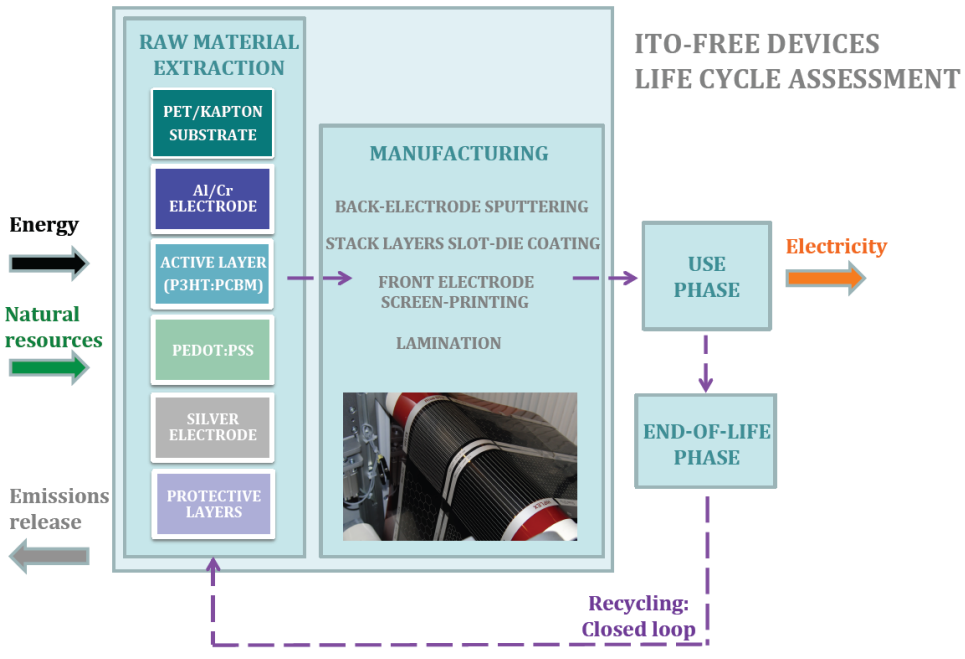

Figure 4.13. Life–cycle stages of the ITO-free PV modules. The green line demarcates a box representing the system boundaries applied in this study.

Balance of System (BOS) components are not considered at this stage. Nevertheless, since OPV technologies are aiming at very low-cost processing,

both environmental and monetary costs, the importance of the relative share of the BOS in both cases will have to be taken into account in the future. Furthermore, since light weight and highly flexible OPV designs may be particularly well suited for building integration, it is expected that this BOS impact could be reduced significantly compared with other conventional PV technologies.

The functional unit for the ITO-free organic module calculation is 1 square meter of processed area (290 mm width). When processing 1 square meter of foil in the facility under consideration (the roll-to-roll equipment at Risø DTU), several modules are produced, with 68.1% of active area of the total Hiflex OPV module area. We note that only 54% of this 1m² processed area is covered by PV modules, i.e., there are some blank areas due to spatial limitations by some processing steps, such as screen-printing. The processed, module and active areas are shown in Figure 4.14.

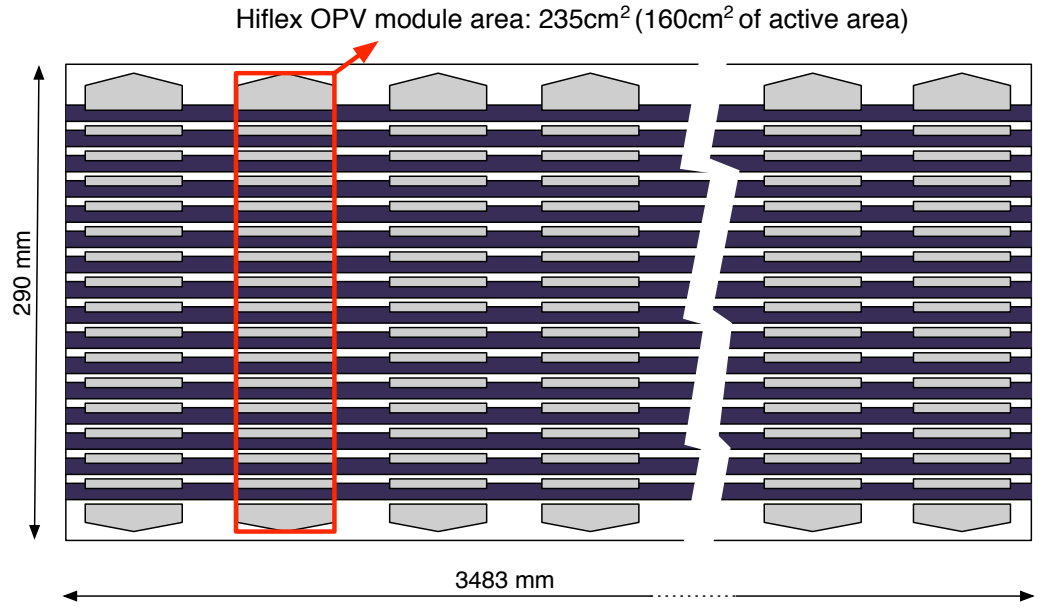

Figure 4.14. Representation of the considered functional unit: 1m² of processed area (290 mm x 3483 mm). Note that the OPV modules area only covers 54% of the processed area, and from this latter percentage, 68.1% corresponds to active area. The drawing is not at scale.

4.3.3.2. Material inventory

The input materials in the manufacturing steps are shown in Figure 4.15 per functional unit; i.e. per 1m² of OPV processed surface. First, the stripes are directly patterned masking the foil. Then, on the patterned cathode, the process follows as in the ITO-based OPV module fabrication (known as ProcessOne described in previous section 4.3.1). Two more layers are deposited by slot-die coating: the photoactive layer made of a blend of P3HT:PCBM, and a PEDOT:PSS layer as hole transport layer. Finally, on top, the front electrode constituted by a silver mesh is screen-printed. The encapsulation of the module is made with a polyester barrier material applied by a roll-to-roll lamination procedure. In Figure 4.15, the main fabrication processes are presented, and further detail described below each of these steps, which together with equipment and material inventory have been reported (Krebs et al., 2009; Krebs, Tromholt, et al., 2010).

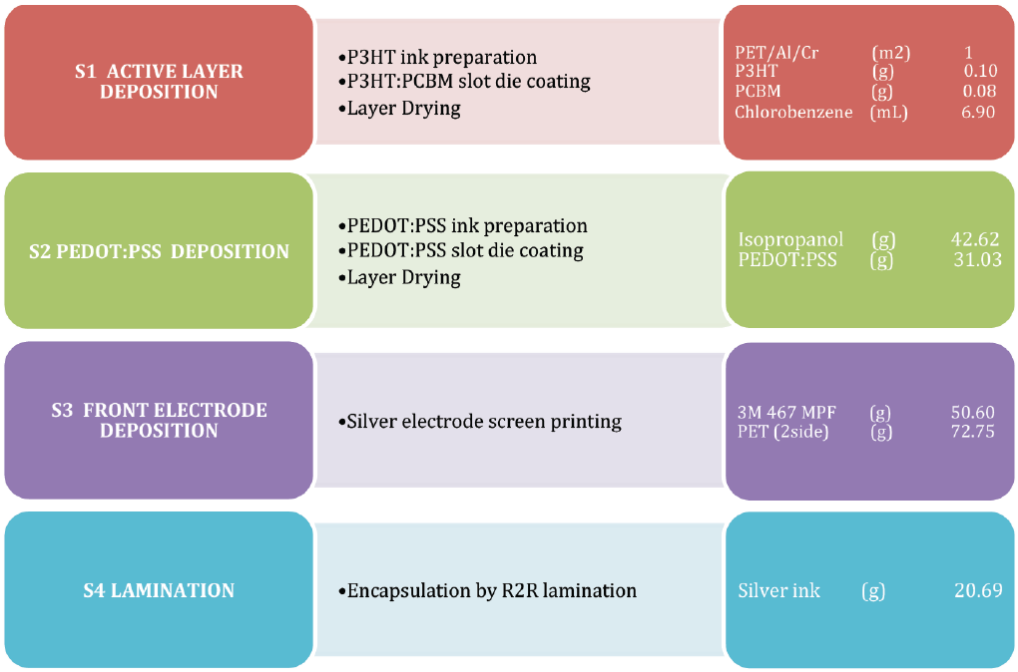

Figure 4.15. Manufacturing process steps and material inventory for ITO-free modules with 1m² of processed substrate.

4.3.3.3. Energy inventory

Embedded energy in materials production

The life cycle of the raw materials used in the preparation of the cells must be analysed in order to calculate the full-embedded energy per square meter of module. Table 4.25, summarizes the energy consumption in the raw materials production. The information about R2R electrode processing, as applied in the ITO-free fabrication process of this study (Manceau et al., 2011), has been directly collected from manufacturers and is further detailed in the following paragraphs.

Table 4.25. Cumulative primary energy requirements for raw materials production in MJ EPE units.

Raw materials inventory	Primary energy (MJ/kg)	References	Certainty in energy data
Sputtered patterned PET/Al/Cr (1m²)	421.97	This study	++
P3HT 99%HT (1kg)	1809.52	(García-Valverde et al., 2010)	+
PCBM (1kg)	11061.31	(Anctil et al., 2011; García-Valverde et al., 2010)	+
PEDOT:PSS (1kg)	64.72	(García-Valverde et al., 2010)	+
Isopropanol (1kg)	36.50	(Espinosa et al., 2011)	++
Chlorobenzene (1 kg)	159.41	(Espinosa et al., 2011)	++
Silver ink (1kg)	210.00	(Espinosa et al., 2011)	0
Adhesive resin (1kg)	200.00	(Hammond et al., 2011)	+
Barrier resin (1kg)	80.75	(Espinosa et al., 2011)	+

a. Preparation of ITO-free cathode (back electrode)

The main processes from cradle-to-gate in the preparation of the electrode are presented in Figure 4.16.

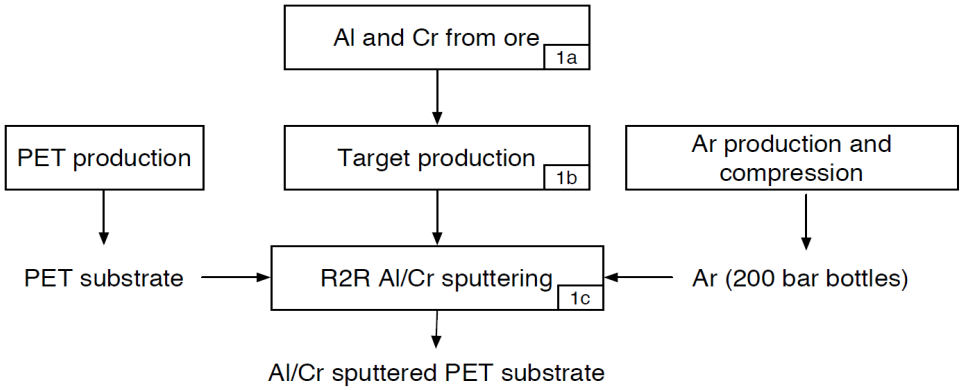

Figure 4.16. ITO-free cathode (back-electrode) production scheme.

The plastic roll (8-13m length by 290 mm width) is loaded into the vacuum chamber, which is pumped down overnight (12h). The foil is then rolled through the machine while sputtering at a rate of 1 cm/min. Two layers are sputtered: first, 100 nm aluminium is deposited at 4.4Å/s, followed by a chromium layer of 15nm at 0.66Å/s. The process is based on room temperature magnetron sputtering, with an argon flow rate of 300sccm. The manufacturer estimates the efficiency of the target use, i.e. the percentage of the target transferred to the substrate through the mask, to be ~ 10%. All the energy consumption is electrical power. Other conditions and assumptions are specified in Table 4.26.

Table 4.26. Equipment conditions and energy and material inventories in the sputtering process (material and energy inputs are related to the functional unit) directly gathered from supplier.

Process Conditions	
Sputtering system	R2R magnetron sputtering
Targets	Sintered Al and Cr
Substrate width (cm)	29
Vacuum pump power (W)	20800
Working Pressure (mbar)	0.007
Substrate temperature	Room
Sputtering power Al (W)	4000
Sputtering power Cr (W)	200
Argon flow rate (sccm)	300
Web Speed (cm/min)	1
Al Deposition rate (Å/min)	264
Cr Deposition rate (Å/min)	39.60
Al layer thickness (nm)	100
Cr layer thickness (nm)	15
Efficiency of the sputtering (%)	10
Maximum roll length (m)	100
Material Inputs	
Sintered Al target (kg)	2.7E-3
Sintered Cr target (kg)	1.08E-3
Argon (Nm^3)	0.10
Energy inputs	
Vacuum (MJ EPE)	88.53
Sputtering (MJ EPE)	248.28

The electrode is deposited by a roll-to-roll sputtering procedure onto a plastic foil substrate (i.e. Kapton, PET), following a scheme illustrated further below in Figure 4.17.

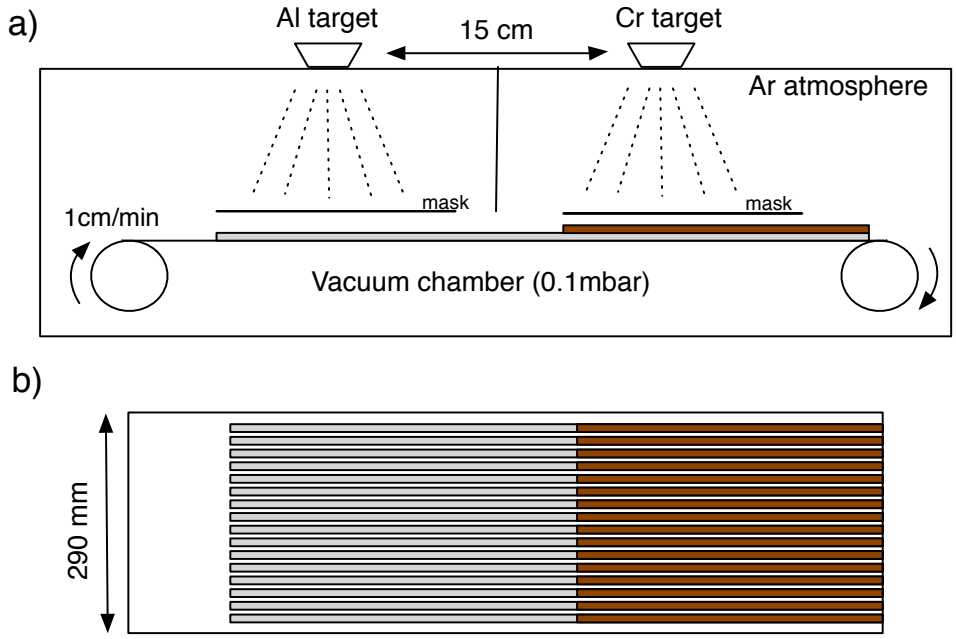

Figure 4.17. Schematic view of the sputtering process for aluminium and chromium forming the cathode (machines and top view of the layers).

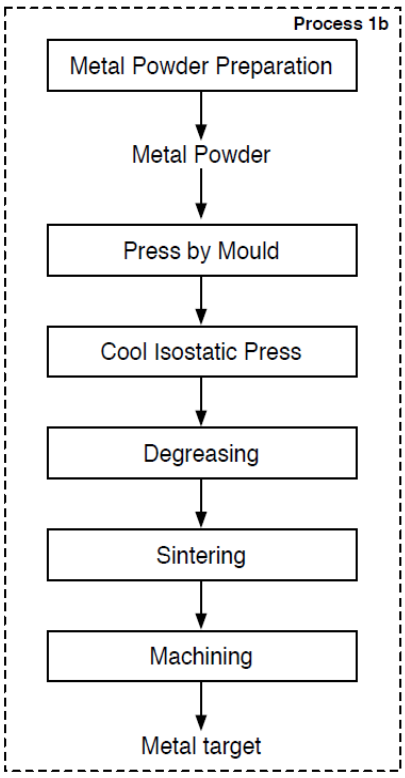

Figure 4.18. Manufacturing of metal targets for sputtering systems.

Metal targets are usually prepared by sintering metal powder following the general scheme presented in Figure 4.18. Metal powders are hot pressed; isostatically cool pressed or slip casted and sintered. Although these processes can differ slightly from one material to another, for the sake of simplicity, energy requirements of chromium and aluminium targets have been considered to be similar to the ITO ceramic target production processes in China (assumed as a cap value). In analogy to the corresponding information from Hunan Boyun New Materials Co. Ltd (Hunan Boyun New Materials Co. Ltd.; www.itocn.net, 2011).

The energy requirements for metal powder preparation are therefore estimated to be 72 MJ_{el}/kg, and the target production energy 108 MJ_{el}/kg where for simplicity; no losses of processed metals have been included- i.e. 100% material efficiency-.

The most common processing stages for aluminium production are alumina refining (Bayer process) and aluminium smelting (Hall–Heroult process). The Hall–Heroult electrolytic process is the only process for Al production in commercial use today. The energy consumption for Al production from pristine metals is found to range from 208 to 211MJ/kg (White, 1998; Hammond et al., 2011). The last version of the inventory of the University of Bath (UK) accounts 62 records for virgin Al production with an average of 224MJ/kg. However, the recycling rates of Al are quite high: the worldwide average is 33% of recycled content (based on information from the International Aluminium Institute, IAI). This latter value was therefore assumed here, resulting in a value of 157.1MJ/kg for the Al production. With the aim to prove whether the recycled content of aluminium can affect the results, a sensitivity study was conducted, varying from 0 to 100% the values for this parameter, and no significant influences were founded (below 0.2%).

Main products of chromium ore refining are ferrochromium and metallic chromium. For the production of pure chromium, the iron has to be separated from the chromium in a two-step roasting and leaching process. The chromite ore is heated with a mixture of calcium carbonate and sodium carbonate in the presence of air. The chromium is oxidized to the hexavalent form, while the iron forms the stable Fe_2O_3. The subsequent leaching at higher elevated temperatures dissolves the chromates and leaves the insoluble iron oxide. The chromate is converted by sulphuric acid into the dichromate (White, 1998), and the dichromate is finally converted to the chromium (III) oxide by reduction with carbon and then reduced in an aluminothermic reaction to chromium. The energy required per kg of metallic chromium was found to be 83 MJ (White et al., 2000; Papp et al., 2006).

The energy requirements for the PET substrate and argon were taken from our own previous studies (Garcia-Valverde et al., 2009) and in section 4.3.1, resulting in 80.75MJ/kg and 662.08MJ/m^3 respectively. The latter value includes full air distillation and compression to commercial 200 bar in argon bottles. Table 4.27 summarizes the energy requirements during the main steps of the ITO-free electrode production, per square meter, and a qualification on the certainty level in these data.

Table 4.27. Energy requirements per square meter of ITO-free electrode (functional unit of sputtered Al/Cr on PET) and certainty levels od the data.

Sub-process	***Equivalent Primary Energy (MJ EPE)***	***References***	***Certainty in energy data***[8]
Al/Cr sputtering	320.24	This study (personal communication with manufacturer data)	++
Al target production	1.39	(Hammond et al., 2011)	o
Al production	0.26	(Norgate et al., 2002)	+
Cr target production	0.55	(Hammond et al., 2011)	o
Cr production	0.09	(White, 1998; White et al., 2000)	+
Argon production	65.12	(Garcia-Valverde et al., 2009)	++
PET substrate	14.38	(Espinosa et al., 2011)	++
TOTAL	402.03		

The share of the total energy requirement in sputtering is shown in Figure 4.20a. The sputtering processes have an intrinsic problem, as presented in the figure, the R2R sputtering of the Al and Cr layers is the main contribution to the overall energy consumption (nearly 80% of the total). Given that the contribution of the argon is also considerable, it seems clear that future improvements must be also addressed in order to reduce Ar consumption by reusing or recycling it. Finally, the use of targets must be addressed, because on average, only around 10% of the material of the target is finally transferred to the manufactured samples. Therefore a recycling process for the production of new targets from the used ones is compulsory if the ultimate aim is to improve the process at this particular step.

b. Other raw materials

The remaining input materials in the Hiflex process have been described in detail in previous studies that were referenced in Table 4.25. In the case of the adhesive used for encapsulation, the embedded energy has been reconsidered; adopting the maximum value recorded for sealants and adhesives at University of Bath inventory (Hammond et al., 2011).

The share of embodied material energies is represented graphically in Figure 4.20b1). It allows us the identification of the most energetically intensive materials. The overwhelming importance of the PET substrate including the sputtered Al/Cr electrode is evident: it represents almost 94% of the total embodied materials energy (of 430.47MJ EPE per functional unit) and we have not reduced the energy, which was 302.27 MJ/m^2 for our ITO-based cells. We can solve the problem of the scarcity of indium with this new approach, but since it still has a high-energy consumption for producing the electrode, our work shows that vacuum processing should be avoided.

[8] *Notation for certainty of data: ++ very good, + good, o fair,- low, --very low. The qualifications refer to all preceding data in the same row.*

Direct energy process

Direct process energy involves the steps that were shown in Figure 4.15. All the considered energy inputs are electrical; therefore the total embedded energy is expressed in electrical Wh_{el}, giving a total of 5.4 kWh_{el} per square meter. This corresponds to 55.57MJ Equivalent Primary Energy (EPE) assuming a 35% of efficiency of primary energy to electrical energy conversion as seen in Table 4.28, where every consumption per manufacturing step are listed.

Table 4.28. Energy consumptions during R2R processing of ITO-free OPV modules of $1m^2$ processed surface.

	Electrical energy consumption (Wh_{el})
S1 ACTIVE LAYER DEPOSITION	
P3HT ink preparation	6.90
P3HT:PCBM coating SD	71.84
Layer Drying	344.83
S2 PEDOT:PSS DEPOSITION	
PEDOT:PSS ink preparation	1.55
PEDOT:PSS slot die coating	478.93
Drying	2298.85
S3 FRONT ELECTRODE DEPOSITION	
Silver electrode printed	2195.40
S4 LAMINATION	
Encapsulation by R2R lamination	4.31
SUBTOTAL (W_{el})	5402.60
SUBTOTAL (MJ EPE)	55.57

As expected for a newly developed PV technology, important reductions in terms of direct process energy have been achieved in this OPV fabrication when one moves from one generation to the next one. The embedded energy in materials accounts for almost ten times of the direct process energy, 430.47MJ versus 55.57MJ, as shown graphically in Figure 4.19.

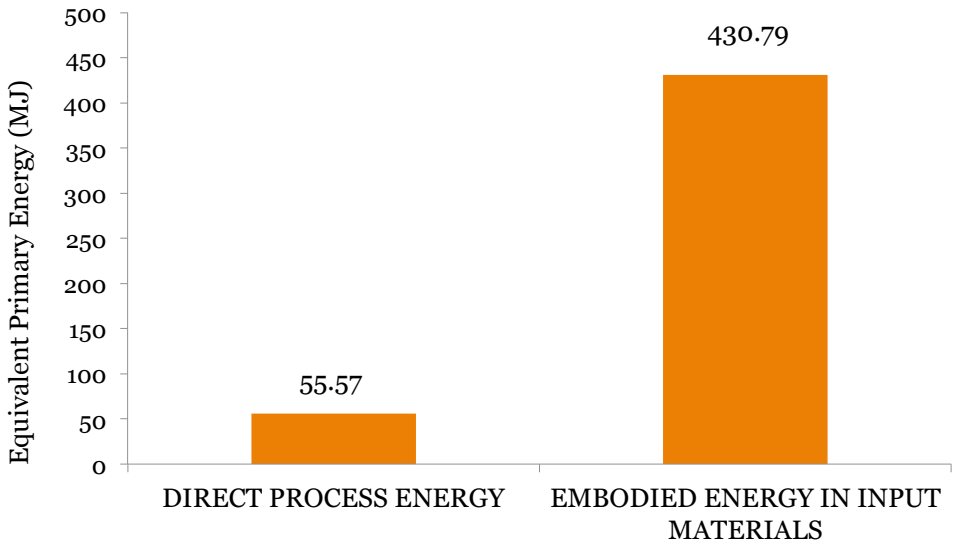

Figure 4.19. Resulted share of total embodied energy per OPV module functional unit produced.

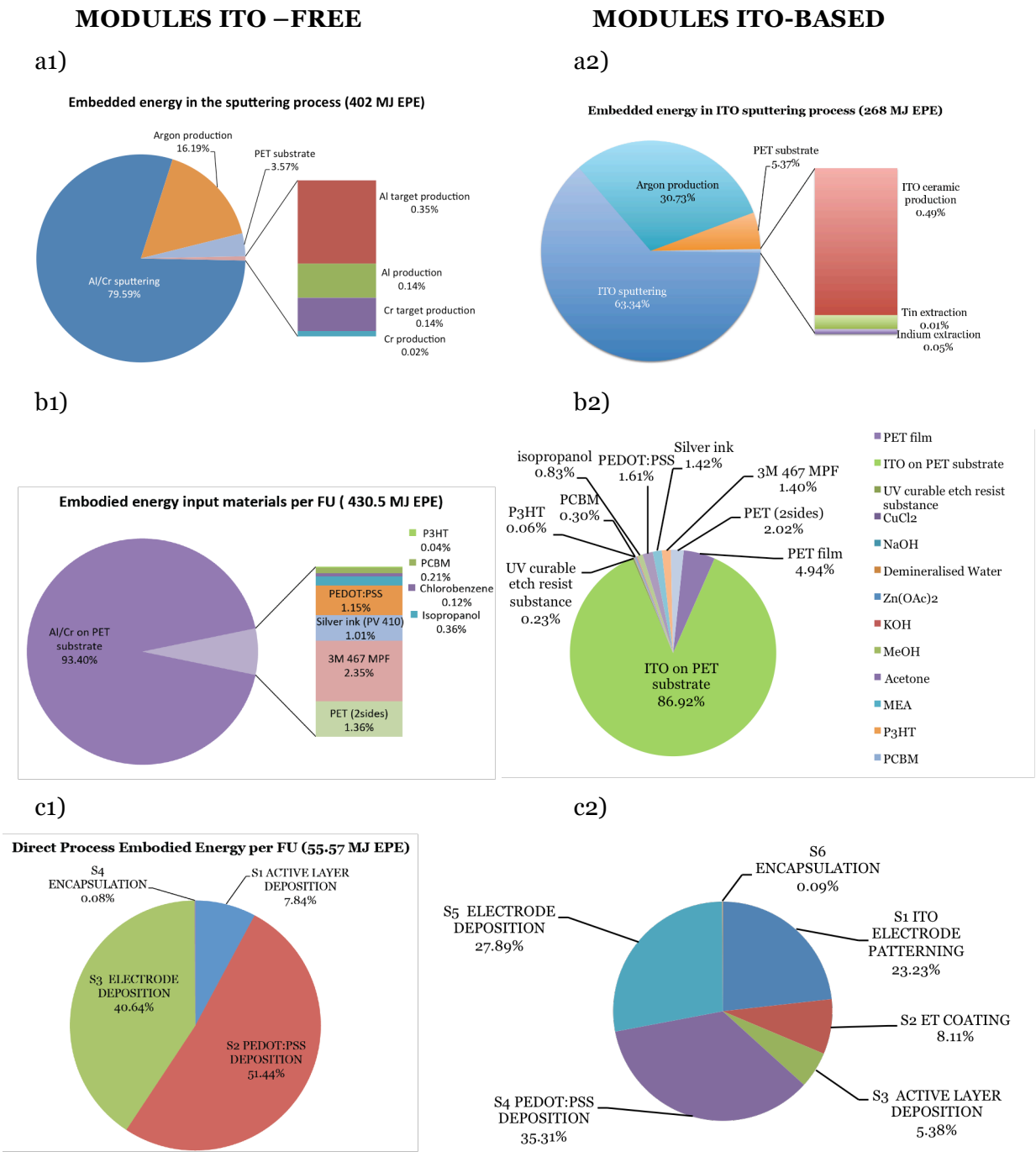

Figure 4.20. Share of the embedded energies for ITO-free OPV modules on the left, and corresponding energies for ITO-based modules, a1), a2) Energy used in the sputtering process for both, electrodes, b1), b2) calculated share of the embodied energy in the considered input materials, used for the direct production of the OPV module, c1), c2) represent the share of the energy consumption in the 'production steps' (direct process energy).

Regarding the energy directly consumed in the manufacturing processes, the breakdown of the processing energies into the different manufacturing steps is illustrated in Figure 4.20 c1) and c2). Note that we have neither an electrode patterning process nor an electron transport layer deposition. PEDOT:PSS

deposition –mainly the drying step- is still the most consuming stage, as it was for the ITO-based OPV cells, accounting for about half of the total energy consumption during the manufacture (51% in comparison with 35.31%), followed by the silver electrode processing (41% versus a 28% in the reference process). The active layer is still one of the least energy intensive processes (8%), as obtained for previous processes.

4.3.3.4. Life-cycle impact assessment

The environmental quality indicators (EPBT, GHG) are calculated on the basis of the material and energy inventories of the production process. Combining the information from Table 4.25, Table 4.26 and Table 4.27, total embodied energy of 486 MJ (EPE) was found for processing 1m² total surface area of organic PV modules by R2R Hiflex processing.

Energy pay back time and GHG avoided emissions

The generated energy by the OPV module is very much dependent on the final system performance. We assume a realistic performance ratio (equal to real output/nominal output of a PV system) of 0.8. Energy generated by the module (in EPE), EPBT and ERF are shown in Table 4.29 as a function of active area coverage (%) and module efficiency.

Table 4.29. EPBT and ERF for 1m² processed surface of organic PV modules prepared by R2R processing for different efficiencies and percentages of active area.

Active area (%)	Efficiency (%)	$E_{generated}$ per year (MJ_{EPE}/year)	EPBT	ERF
36.78%	1.00	51.45	9.45	1.59
	3.00	154.36	3.15	4.76
	5.00	257.26	1.89	7.94
	10.00	514.52	0.94	15.88
68.10%	1.00	95.26	5.31	2.94
	3.00	285.79	1.77	8.82
	5.00	476.31	1.06	14.70
	10.00	952.62	0.53	28.24
85.00%	1.00	118.90	4.09	3.67
	3.00	356.71	1.36	11.01
	5.00	594.51	0.82	18.35
	10.00	1189.03	0.41	36.70

The pollutant emissions during the fabrication, transport, decommissioning and recycling phases of a PV system are accounted for as embodied CO_2, which are presented in Table 4.30. At the present development stage the GHG emissions are quite high (137.68 g eq-CO_2/kWh_{el}) compared with other PV technologies (20-40 g/kWh). However, slight efficiency increments will lead to considerable environmental impact reduction.

Table 4.30. CO_2 emission factor of organic photovoltaic modules for 1m² processed surface. Three values of nominal efficiency are considered.

Module efficiency	Embodied CO_2 (kg eq-CO_2)	E_{gen} during module life time (kWh_{el})	CO_2 emission factor (g eq-CO_2/kWh_{el})
1%	20.66	150.06	137.68
3%	20.66	225.09	91.79
5%	20.66	375.15	55.07

4.3.3.5. Discussion

EPBT results for the two R2R OPV processes realised at Risø DTU have been compared. Present values of EPBT for a process referred to as ProcessOne reach 1.94 years with 3% efficiency and 45% active area (67% on module area); the corresponding value for the ITO-free Hiflex process is 9.45 years with 1% efficiency and 36.7% active area.

The main reasons for this significantly poorer value are the lower efficiency (1% vs. 3%) and to a lesser extent the lower active/total area ratio (36.7% vs. 68.1%). The forecasted values depicted in Figure 4.21, show that both processes could still have their EPBT reduced by improvements of the active area and the efficiency.

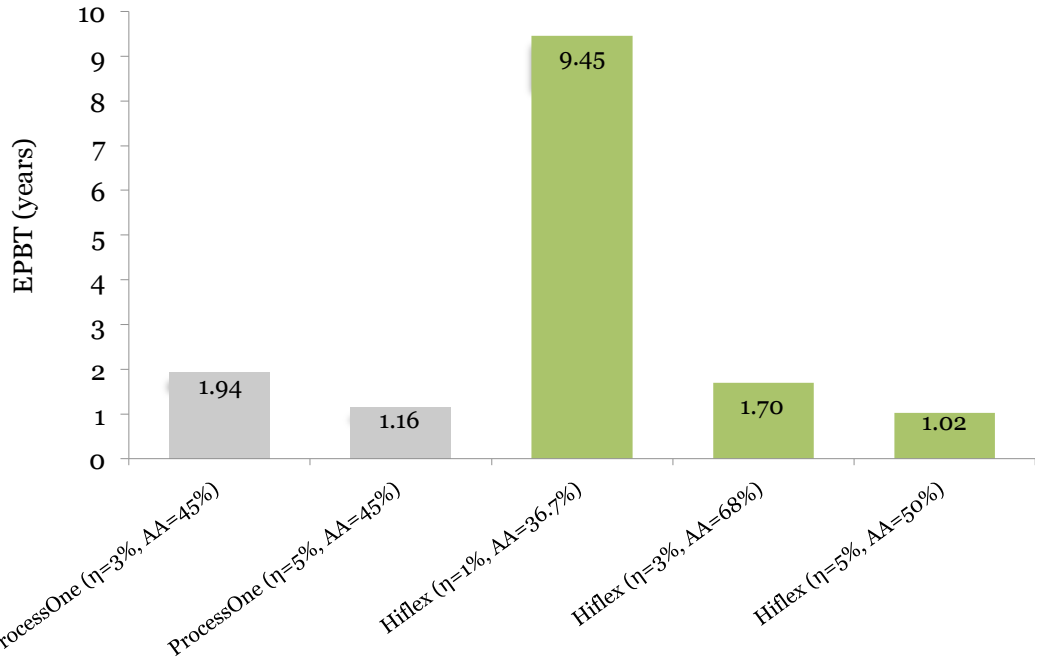

Figure 4.21. EPBT for 1m²-processed substrate in two OPV R2R manufacturing accomplished at Risø DTU. Present state and some realistic forecasted values. AA stands for the active area related to the total processed substrate).

Figure 4.22 shows the EPBT as a function of the active area coverage for different efficiencies. As also shown in the figure the EPBT with the current Hiflex module efficiency is 9.45 years.

Note that with the same efficiency and lifetime, the environmental impact could be significantly reduced by nearly half to EPBT≈5 years when an optimized active

area ratio could be realized. Moreover, a further improvement of the efficiency to 5% would set the EPBT in 1 year.

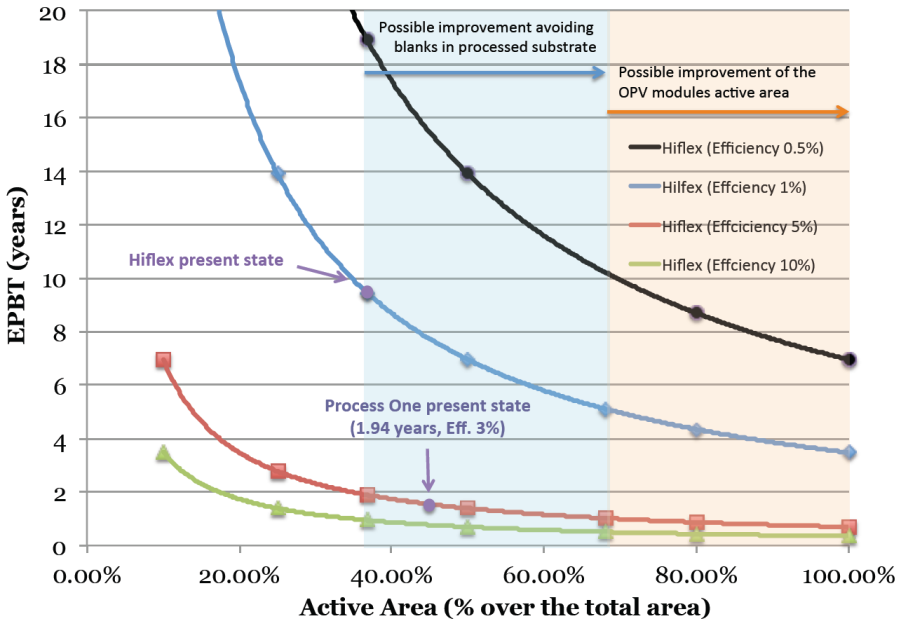

Figure 4.22. EPBT prospective for different scenarios of module efficiency and active areas.

The reference process ProcessOne, shows a significantly lower EPBT of only ~2 years, which is due to a better module efficiency (3% vs. 1%) and a more optimized active area ratio (45 vs. 37%).

It must be emphasized that Hiflex processing that follows Al/Cr application is entirely accomplished at ambient conditions, avoiding the use of special atmosphere and further emissions related to vacuum systems. Used chemicals (mainly solvents) during R2R processing are naturally released to the atmosphere by evaporation during the drying steps. A detailed assessment of these emissions cannot be done at this stage; however, compared to ProcessOne the number of coating steps has been reduced, and correspondingly the number of involved solvents.

4.3.4. Towards 1 day energy payback time

A dozen of new approaches were analysed, guided by the previous studies to accomplish the goals of low energy budgets and avoiding the use of critical materials as ITO (European, 2010; Haxel et al., 2002). As a result, the most successful route was identified by deliberate minimisation and balancing of the equivalent primary energy. For assessing the environmental impacts, SimaPro (PRé Consultants), an LCA software was used and it allowed us to identify which materials have a detrimental effect on different environmental categories.

4.3.4.1. Analytical frame

For this calculation we use 1m² of *processed* area (290 mm width) as functional unit, from where 45% is photoactive area. The ratio active/total area is a critical issue and has been discussed earlier in section 4.3.3.

Energy consumption related to these materials and upstream processes were obtained from databases such as Ecoinvent 2.1 ("Swiss Centre for Life Cycle Inventories," 2011), through SimaPro (a commercial software widely used for LCA studies) and from the literature. Both thermal and electrical budgets were converted to equivalent primary energy (MJEPE) at a later stage. The conversion efficiency depends on the technology mix of the electricity supply system and may vary considerably between different countries and also with time. An average of 35% has been considered, and in case of thermal energy consumption was given separately, a European average factor of 85% has been used to obtain the primary energy equivalent (Alsema, 1998).

Data used in the assessment are experimental as already stated; it is not estimation. However, a weakness of this approach is that it is based on some assumptions, as there would otherwise be too many uncertainties to allow for a plausible assessment of the product's environmental merits. We have estimated this uncertainty by introducing the following qualifications: ++ very good, + good, 0 fair, - low, --very low; as previously explained in section 4.1.2.

The emissions inventory presented here is, as in the other LCA studies presented in this thesis, only focused on emissions of CO_2 equivalents related to the energy consumption during the manufacturing. For the electricity mix of Denmark these emissions amount to 493.80 g-eqCO_2/kW_{el} in 2010 (*Danish Energy Agency*, 2011).

4.3.4.2. Material inventory

Data about the OPV processing were acquired in situ from materials consumption and equipment specifications for building up the inventories, which are shown in the following tables (Krebs, Fyenbo, et al., 2010; Krebs, Tromholt, et al., 2010):

- Table 4.31. Slot die coating processes, drying conditions and material inventory for processing several layers of 1m² OPV modules.
- Table 4.32. Flat bed Screen Printing process, including drying conditions and material inventory for printing the electrodes of 1m² OPV modules.
- Table 4.33. Rotary screen printing process, including drying conditions and material inventory for printing the electrodes of 1m² OPV modules.
- Table 4.34. Encapsulation processes, including drying conditions and material inventory for 1m² OPV modules.

Table 4.31. Summary of the slot die coating process, including drying conditions and material inventory for processing several layers of 1 m² OPV modules.

Conditions			
Speed	0.02-2.5 m/min		
Web Tension	80-90N		
Drying temperature	140 °C		
Working Corona Treater Power	1500 W		
Working Slot Die Power	1500 W		
Working Oven Power	12000 W		
Equipment			
Description	R2R printing and coating machine from Grafisk Maskinfabrik A/S comprising unwinder, corona treater, edge guide, Rotary screen printer, flexo unit, coating roller, oven, cooling roller and winding station.		
Maximum Corona Treater Power	1500 W		
Maximum Slot die Coater Power	1500 W		
Maximum Oven Power	12000 W		
Material inventory			
Front electrode layer		Active layer	
PEDOT:PSS	39.34 g	P3HT	0.08 g
Silver nanoparticle ink full	3.68 g	PCBM	0.07 g
Silver ink (18% Ag)	0.26 g	Chlorobenzene	6.19 g
Butanol	1.29 g		
Graphene ink	1.97 ml		
ELT layer		HTL layer	
$ZnO(OAc)_2$	3.71 g	PEDOT:PSS	26.23 g
KOH	1.86 g	Isopropanol	38.89 g
MeOH	12.24 g		
Acetone	24.50 g		
MEA	0.37 g		
$ZnO(OAc)_2$	0.30 g		
Water	2.95 g		
Back electrode layer			
Silver for interconnections	0.63 g		

Table 4.32. Summary of Flat bed Screen Printing process, including drying conditions and material inventory for printing the electrodes of 1 m² OPV modules.

Conditions	
Speed	1 m/min
Residence time in oven	72 s
Drying temperature	140 °C
Working Screen Printer Power	1500 W
Equipment	
Description	Alraun printer comprising unwinder, metering wheel, positioning camera, vacuum table, screen printer (AT701), hot air oven, transport rollers, dancing tensioning roller and rewinder.
Maximum Screen Printer Power	38000 W
Material inventory	
Back electrode layer	
Silver ink PV410 full	19.67 g
Graphite full	19.67 g

Table 4.33. Summary of Rotary screen printing process, including drying conditions and material inventory for printing the electrodes of 1 m² OPV modules.

Conditions	
Speed	3 m/min
Drying temperature	140 °C
Working RS Printer Power	600 W
Working Oven Power	12000 W
Equipment	
Description	R2R printing and coating machine from Grafisk Maskinfabrik A/S comprising unwinder, corona treater, edge guide, Rotary screen printer, gravure unit, coating roller, oven, cooling roller and winding station.
Maximum RS Printer Power	1500 W
Maximum Oven Power	21000 W
Material inventory	
Front and back electrode layer	
Graphite full	4.59 g
Graphite interconnections	0.79 g

Table 4.34. Summary of encapsulation process, including drying conditions and material inventory for 1 m² OPV modules.

Conditions	
Speed	120 m/h
Working laminator power	1500 W
Equipment	
Description	Laminator comprising unwinder, edge guide and cutting table, laminator, laminate unwinder, longitudinal cutting knifes and rewinder.
Maximum Power	1500 W
Material inventory	
Adhesive (3M 467 MPF)	20.24 g
PET encapsulation	61.65 g

4.3.4.3. Energy inventory

Embedded energy in materials production

By using the materials specified in the above tables, the energy needed for manufacturing the materials was computed for Process A to K, and for Process Two.

When the cumulative energy demand (CED) for a specific material was not available in the Ecoinvent database, it was necessary to calculate the energy content of a raw material or ink from scratch; i.e. from its basic components. Silver for the transparent electrodes is a non-particle conductive ink, which contains in its formula 18% of silver. It has been estimated to require as much as 275 MJ/kg of energy for its production, and as low as 126 MJ/kg, thus resulting in 200.5 MJ/kg in average. This is very close to estimations that were done for PV 410 silver ink (from Dupont®) in previous study in section 4.3.1. The silver ink was then diluted in butanol 1:5 (v/v); the energy embedded in butanol is 81.02 MJ/kg according to Ecoinvent database. Printable graphite conductive ink was estimated to embed 174.82 MJ/kg. Since the solid content in its formula can vary from 34 to 37%, an average of 36.5% was estimated (as shown in Table 4.35). With the aim to prove whether the solid content of the ink can affect the results, a

sensitivity study was conducted, by varying this parameter from 0 to 100%, and no significant influences were found. Even if the embodied energy would increase by 200%, the variation of EPBT would remain below 3% of its initial value.

The graphene ink was prepared according to method described by Hummers and Offerman (Hummers et al., 1958) from natural graphite, and found to range from 200 to 400 MJ/kg.

With regard to the ETL, Zinc oxide ink, and HTL, PEDOT:PSS, had already been studied in the LCA studies for ProcessOne (Espinosa et al., 2011), as well as Photoactive inks, solvents and other Chemicals (potassium hydroxide, acetone, chlorobenzene, etc.).

Table 4.35. Detailed material inventory and CED for raw materials production in MJ_{EPE} units for Process H, with Notation for certainty of data: ++ very good, + good, 0 fair,- low, --very low.

	Embedded energy (MJ_{EPE})	**Units**	**Embedded energy (MJ_{EPE})**	**Certainty in energy data**
	Per kg/m²	**Per FU**	**Per FU**	
PET substrate	80.75	0.0616500	4.98	++
Electrode ink (graphite)	174.82	0.0045902	0.80	0
$Zn(OAc)_2$	42.07	0.0002951	0.01	++
P3HT	1809.52	0.0000836	0.15	+
PCBM	11061.31	0.0000669	0.74	+
Chlorobenzene	61.58	0.0061869	0.38	++
Isopropanol	62.74	0.0388852	2.44	++
PEDOT:PSS	159.41	0.0262295	4.18	+
Back electrode (silver)	309.22	0.0006330	0.20	+
Adhesive	200.00	0.0202400	4.05	+
PET encapsulation	80.75	0.0616500	4.98	++
SUBTOTAL			**22.91**	

The contribution to the embodied energy for each process is shown in Figure 4.23. The electrode ink appears to have a greater contribution for process A, and B, which is due to the fact that PEDOT:PSS has a large embodied energy (159.41 MJ_{EPE}/kg) and it is used in large amounts for those two processes.

Direct energy process

The R2R techniques that have been used for the production of solar cells are: slot-die coating, screen printing and rotary screen printing. Thus, the energy requirements at the R2R line are purely electrical. By computing the manufacturing time per functional unit (1 m^2) we can calculate the electrical consumption for all the equipment involved as shown in Table 4.36.

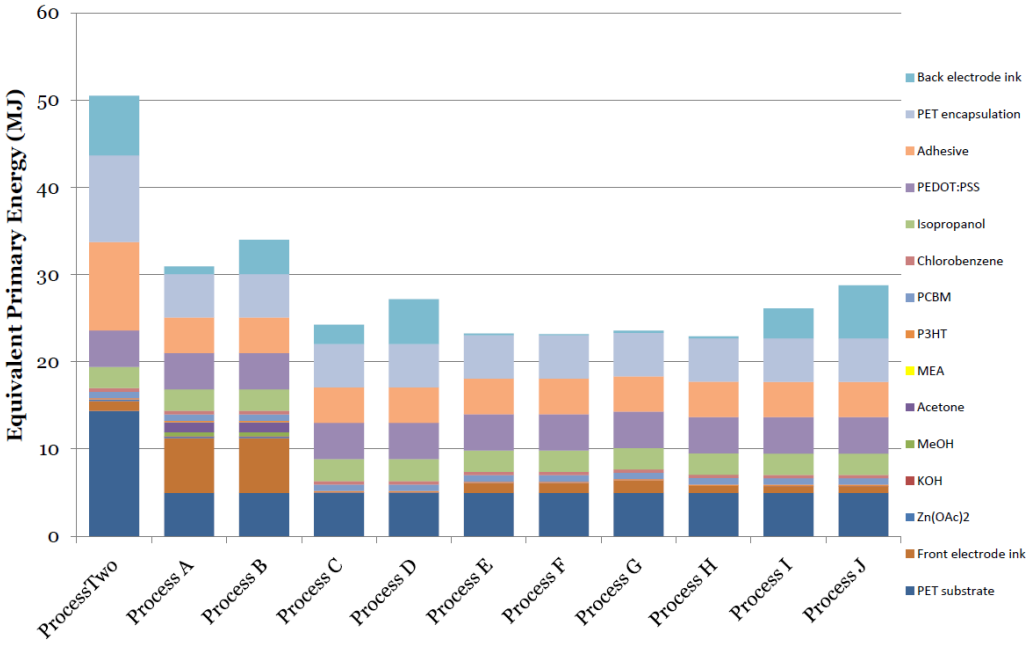

Figure 4.23. Embodied energy in the materials per functional unit (m²) in processes from A to J (MJ$_{EPE}$), ITO processes (ProcessOne and Process K) are not depicted for being out of scale.

When comparing the share of the direct process energy in the manufacturing steps for processes from A to K, with ProcessOne and ProcessTwo (Figure 4.24), we find that an enormous decrease is attainable, although the use of PEDOT:PSS as HTL is still figuring as the most energy demanding step. This is also observed when PEDOT:PSS acts as front electrode (e.g. the green coloured part of the bar chart for Process A and B in Figure 4.24) because of the low web speed employed and the consequently higher thermal input for drying.

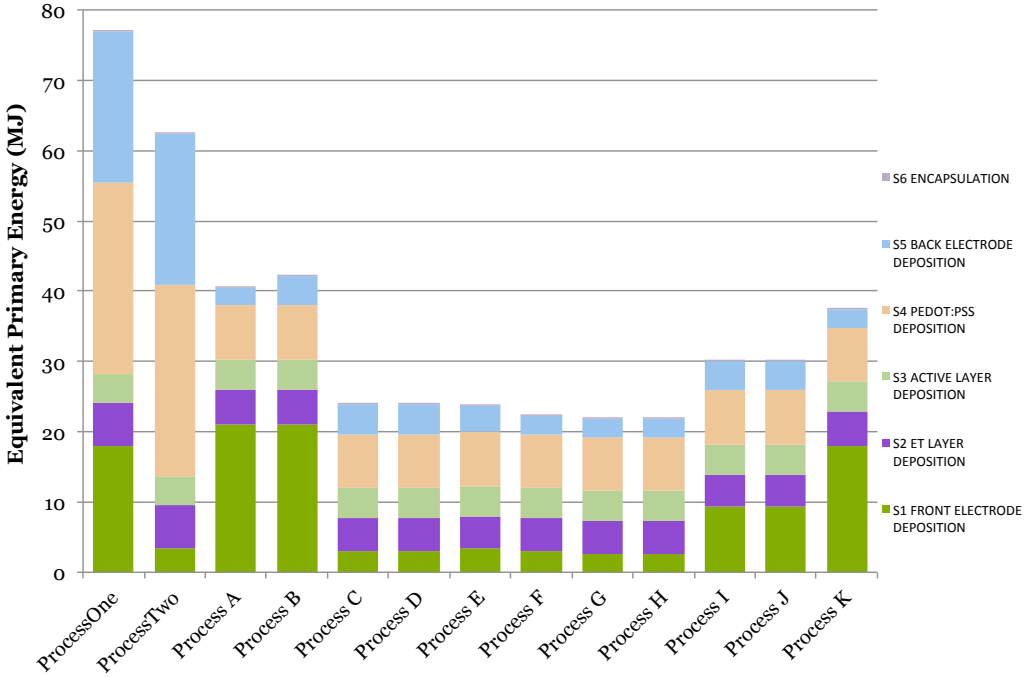

Figure 4.24. Direct process energy employed for different steps in the manufacturing of OPV modules by routes A to K, and by ProcessOne and ProcessTwo.

Table 4.36. Electrical energy consumptions in Wh_{el} of 1 m^2 of OPV module processed surface in new all solution ITO-free routes from A to J.

	A	B	C, D	E	F	G, H	I, J
S1 FRONT ELECTRODE DEPOSITION							
Electrode coating	204.92	204.92	32.79	65.57	32.79	32.79	163.93
Drying	1844.2	1844.2	262.30	262.30	262.30	245.90	737.70
S2 ET LAYER DEPOSITION							
ZnO ink preparation	27.83	27.83	0	0	0	0	0
ZnO coating SD	81.97	81.97	81.97	81.97	81.97	81.97	81.97
Drying	368.85	368.85	368.85	368.85	368.85	368.85	368.85
S3 ACTIVE LAYER DEPOSITION							
P3HT:PCBM ink preparation	5.57	5.57	5.57	5.57	5.57	5.57	5.57
P3HT:PCBM coating SD	40.98	40.98	40.98	40.98	40.98	40.98	40.98
Drying	368.85	368.85	368.85	368.85	368.85	368.85	368.85
S4 PEDOT:PSS DEPOSITION							
PEDOT:PSS ink preparation	1.31	1.31	1.31	1.31	1.31	1.31	1.31
PEDOT:PSS slot die coating	74.52	74.52	74.52	74.52	74.52	74.52	74.52
Drying	670.64	670.64	670.64	670.64	670.64	670.64	670.64
S5 BACK ELECTRODE DEPOSITION							
Slot die coating	10.93	5.46	5.46	65.57	10.93	10.93	5.46
Drying	245.90	409.84	409.84	295.08	245.90	245.90	409.84
S6 LAMINATION							
Encapsulation by R2R lamination	4.10	4.10	4.10	4.10	4.10	4.10	4.10
SUBTOTAL (W_{el})	3950.6	4109.1	2332.6	2305.3	2168.7	2152.3	2933.7
SUBTOTAL (MJ_{EPE})	40.64	42.27	23.94	23.71	22.31	22.14	30.18

The process with a semitransparent silver-based electrode, named Process H, has the lowest embedded energy. The energy balance for Process H has been shown in Figure 4.25. When examining Figure 4.25 it is clear that the equivalent primary energy has been balanced both in terms of energy embedded in the materials and in the direct process energy.

4.3.4.4. Life-cycle impact assessment

The environmental impact of PET used as substrate and barrier encapsulation in these routes, shown in Figure 4.26, is particularly high since it is being produced by polymerization of two petroleum-based raw materials. This causes depletion of fossil fuel resources. Electricity consumed by the manufacturing equipment during manufacture also has a strong effect on fossil fuels since electrical input is produced to a large extent from fossil fuels in Denmark (80% of them in the electricity mix, 20% of the mix comes entirely from renewable sources).

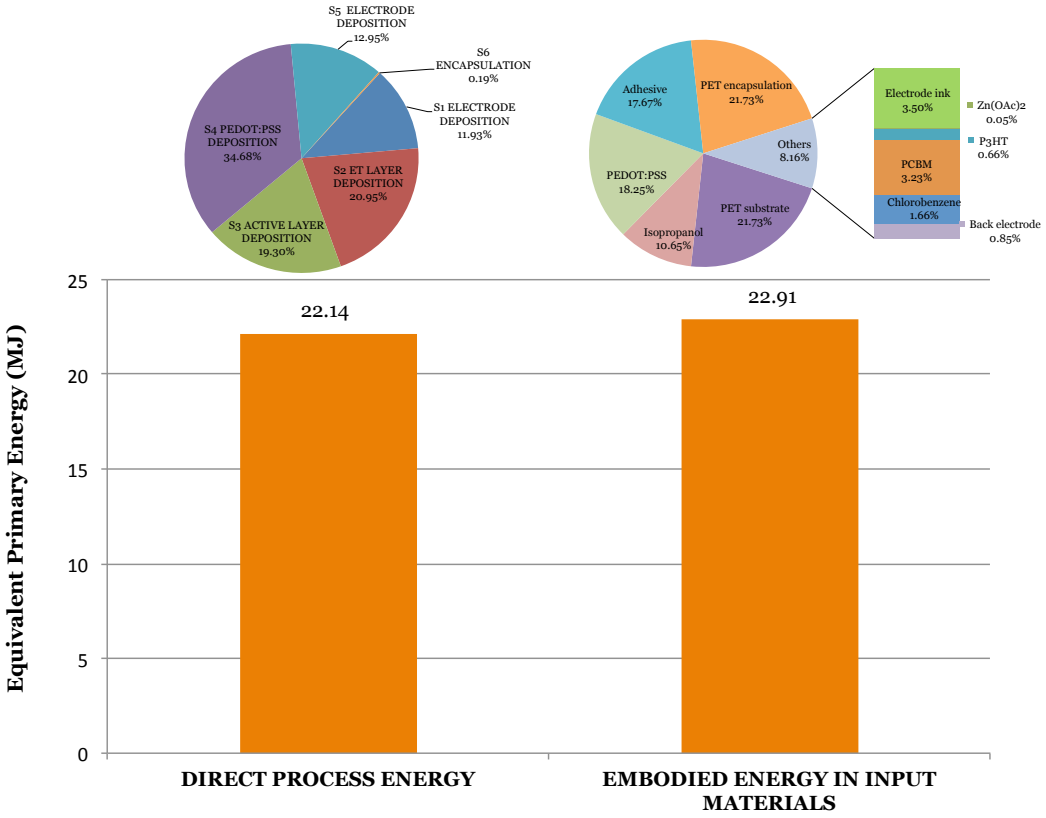

Figure 4.25. Materials inventory share and direct process energy in Process H, both given in Equivalent Primary Energy (MJ EPE).

Nonetheless, when comparing damaging environmental impacts of ProcessOne, ProcessTwo and Process H (Figure 4.27), there is a trend in the way of generally diminishing impacts, even in the high impacted fossil fuels category. One can thus conclude that the methodology has allowed for the successful development of a process that is more efficient at all levels.

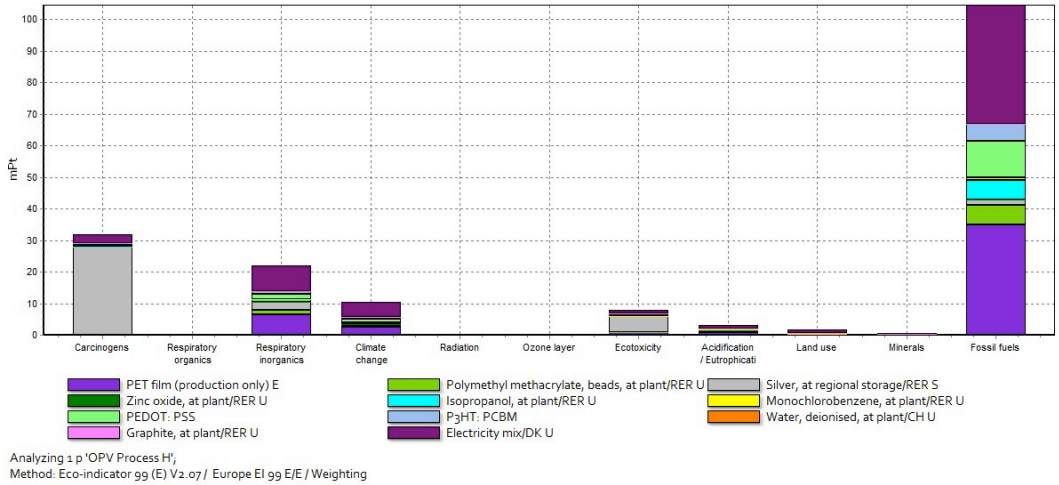

Figure 4.26. Impact categories assessment weighted according to the raw materials used in the production of polymer solar cells by Process H. The methodology employed has been Eco-indicator 99, implemented in the SimaPro software, and developed under the Dutch NOH Programme by PRé Consultants.

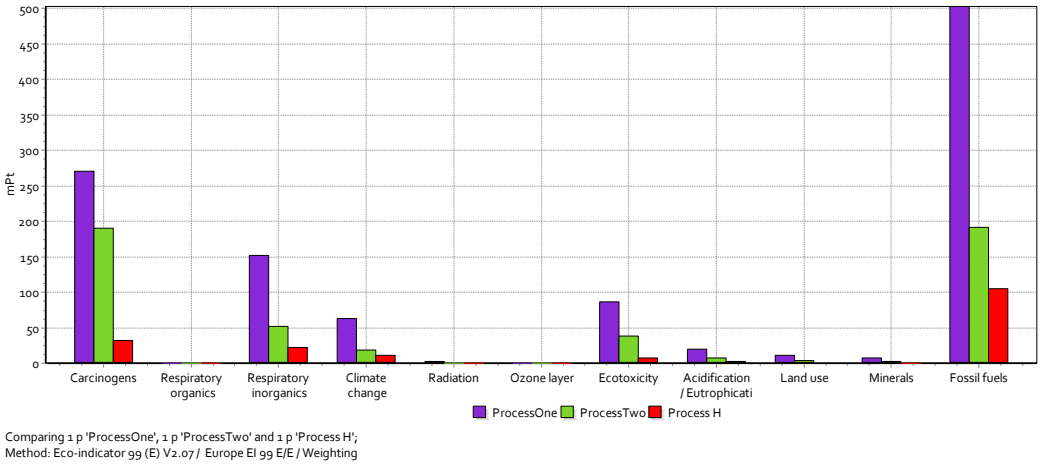

Figure 4.27. Impact categories assessment corresponding to ProcessOne, ProcessTwo and Process H, weighted according Eco-indicator 99, implemented in the SimaPro software, and developed under the Dutch NOH Programme by PRé Consultants.

Energy pay back time and GHG avoided emissions

The processes under study have a significantly shorter energy payback time than the reference process, ProcessOne. With this new route, Process H, an EPBT of 1.42-0.71 years is achievable with a power conversion efficiency of 0.5-1%. In comparison to ProcessOne with and energy payback time of 2.02-1.35 years for 2-3 % efficiency this is a great leap forward, and shows that it is possible to achieve a shorter energy payback time for a solar cell that at least in terms of efficiency is a poorer performer.

4.3.4.5. Discussion

When comparing the share of the direct process energy in the manufacturing steps for processes from A to K, with ProcessOne and ProcessTwo (Figure 4.24), we find that it is possible to obtain enormous decrease in environmental impacts, although the use of PEDOT:PSS as HTL is still appearing as the most energy demanding step. This is also observed when PEDOT:PSS acts as front electrode (e.g. the green coloured part of the bar chart for Process A and B in Figure 4.24) because of the low web speed employed and the consequently higher thermal input for drying.

Table 4.37. EPBT in days for Process H in its existing form, in comparison with reference route, ProcessOne.

EFFICIENCY	**0.25%**	**0.5%**	**0.7%**	**1%**	**2%**	**3%**	**5%**	**10%**	**15%**
ProcessOne	5939	2969	2120	148	742.0	494.8	296.9	148.5	98.9
Process H	1039	520	371	260	130	87	52	26	17

The feasible improvements

Further improvements, over an already refined Process H as seen in Figure 4.25, should obviously address the individual slices in the pie charts without leading to a large unbalance. In terms of the direct process energy it is possible to introduce renewable energy sources very easily due to the fact that the low temperatures involved imply that a polymer solar cell production plant can easily be operated using solar electricity and solar thermal energy for drying and curing (the drying steps account for almost 90% of the total direct energy). By carefully examining the embodied energy it can be seen that the thickness of the barrier and the adhesive can easily be also reduced. It should be possible to make an entirely functional encapsulated device with a thickness of 50-70 micron thus reducing the embedded energy significantly. These improvements are obvious and the only reason they were not implemented in this work is due to the fact that a laboratory/pilot line was employed. As seen in Chapter 3, where processing widths up to a meter were cited to be commonly used in packaging industry, therefore using 305 mm with a working width of 250 mm is a constraint but a trivial one. Experiments with larger working widths have been shown to be very feasible.

The challenging improvements

There are several realistic improvements that would require some innovation and therefore they represent valuable research targets. As shown in Table 4.38, these will lead to only smaller improvement as compared to the feasible improvements described above. Of those, the simultaneous formation of several layers in the solar cell stack would (provided that the technical yield is not compromised) lead to both reductions in energy usage and an improvement in overall processing speed. We also applied the projections for efficiency and lifetime set forward by the European Community. Finally, recycling or end of use handling was also considered. The beneficial effects of recycling are difficult to estimate, and we considered the energy gained by combustion of the solar cell and recovery of the metals (Ag and Zn) from the ashes.

Table 4.38. EPBT in days for Process H in its existing form and when improving following both feasible and challenging developments.

EFFICIENCY	0.25%	0.5%	0.7%	1%	2%	3%	5%	10%	15%
ProcessOne	5939	2969	2120	148	742.0	494.8	296.9	148.5	98.9
Process H	1034	517	369	259	129	86	52	26	17
Feasible Assumptions	211	105	75	53	26	18	11	5	4
Challenging Assumptions	83	41	30	21	10	7	4	2	1

4.4. Conclusions

Solar modules produced at a medium-scale by R2R methods (ProcessOne) have been analysed with LCA methodology. When analysing these polymer solar cells it was found that energy pay-back times ranging from 1.35 to 2.02 years was possible (corresponding 3% and 2% efficiency, respectively). Before the first life cycle analysis on a well-settled roll-to-roll process for manufacturing OPV cells was performed, no precise information about which parameters the are likely to affect the future scale up of manufacturing was available. This first study concluded that 90% of the total energy was embedded in the transparent conducting oxide.

Secondly, in order to know the balance of these cells when integrated in a lamp, this product was also analysed. The analysis revealed that the OPV lamp can provide a significant advantage if some improvements are made in the components and in the OPV module itself, although the EPBT is high (9.8 years) and longer than its lifetime, the use of the OPV lamp can be environmentally beneficial when compared to available alternatives for lighting in developing countries.

Then, a new approach of architecture that tried to solve the indium scarcity problem was evaluated. The starting point of this work was then to get rid of indium but it would seem that the entire processing of OPV has to be redefined at least so that vacuum coating steps are entirely avoided. The problem should be viewed from a larger distance and new developments should be made on those assumptions. One additional point is that if there is a problem with the use of indium, there will also be a problem with silver. Even if the latter is a more accessible element, exhibits approximately the same abundance as indium -around $7x10^8$ kg per kg of silicon-; it can be thus a silver problem in the context of large-scale manufacture of OPV.

Finally, in view of all previous results, Risø team started to develop a new collection of routes for processing polymer solar cells beating all known marks in terms of use of energy and materials so far. When looking at material inventory share and direct process energy in Process H -in Figure 4.25- it is clear that the equivalent primary energy has been balanced, both in terms of energy embedded in the materials and in the direct process energy, in comparison with ProcessOne and ITO-free modules -plotted in Figure 4.20. Moreover there has been a reduction in the equivalent primary energy by a factor of ~10 with respect to reference processes.

The developments made from ProcessOne through Process H enable one to transcend EPBT-efficiency plot in Figure 4.28; i.e. to achieve significantly lower EPBT with lower efficiency and further improvements can be made through easily applicable and more challenging improvements. The LCA directed improvements led to yield better EPBT, despite the trade-off in performance; i.e. jumping from ProcessOne to Process H and further again by assuming straightforward and more demanding challenges means going down and left in the plot.

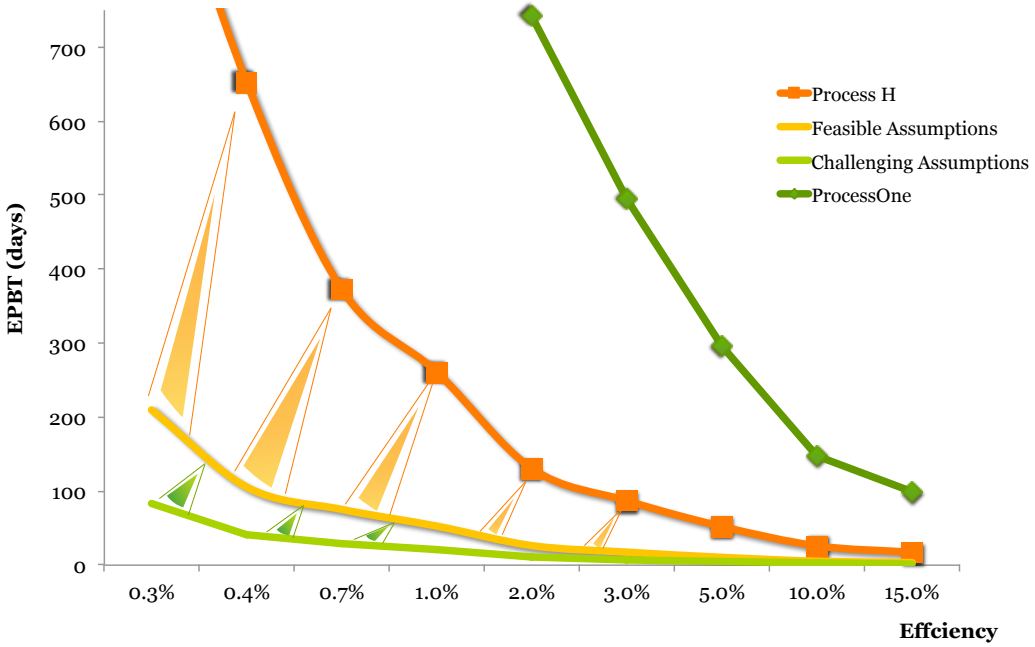

Figure 4.28. An evolution of the EPBT guided by analysis (note that the scale is not linear).

The major conclusion that one can draw from these analyses is that OPV is seemingly a promising technology that however will require significant development before it can be viewed as a technology that solves more problems than it creates. The most relevant question to ask is then what these developments are and as we clearly show here there can be no doubt that processes employing both vacuum and inert gasses should be avoided.

Life cycle assessments have proven to be a very useful tool for the identification of the roadmaps in which the developments for the future OPV should be. Future developments should thus seek processes that does not involve silver, indium, vacuum, or complex processes and should maximize the usage of the processed area and water-based solvents.

References

Alsema, E. A. (1998). Energy requirements of thin-film solar cell modules:a review. *Renewable and Sustainable Energy Reviews*, *2*(4), 387–415.

Alsema, E. A. (2000). Environmental life cycle assessment of solar home systems. *Department of Science Technology and Society, Utrecht University, Utrecht, The Netherlands*, 89.

Alsema, E. A., & de Wild-Scholten,M.J. (2005). The real environmental impacts of crystalline silicon PV modules: an analysis based on up-to-date manufacturers data. Presented at the 20th European Photovoltaic Solar Energy Conference and Exhibition, Barcelona, Spain.

Alsema, E. A., & Nieuwlaar, E. (2000). Energy viability of photovoltaic systems. *Energy Policy*, *28*(14), 999–1010.

Anctil, A., Babbitt, C. W., Raffaelle, R. P., & Landi, B. J. (2011). Material and Energy Intensity of Fullerene Production. *Environmental Science & Technology*, *45*(6), 2353–2359.

Atkins, S. (2008). Methanol Energy Analysis. *Report, Northern Arizona Univ., available at http://ses. nau. edu/AZSynFuels/literature-refs/Methanol.*

Azzopardi, B., Emmott, C. J. M., Urbina, A., Krebs, F. C., Mutale, J., & Nelson, J. (2011). Economic assessment of solar electricity production from organic-based photovoltaic modules in a domestic environment. *Energy & Environmental Science*, *4*(10), 3741–3753.

Azzopardi, B., & Mutale, J. (2010). Life cycle analysis for future photovoltaic systems using hybrid solar cells. *Renewable and Sustainable Energy Reviews*, *14*(3), 1130–1134.

Azzopardi, B., Mutale, J., & Kirschen, D. (2008). Cost boundaries for future PV solar cell modules. *Sustainable Energy Technologies, 2008. ICSET 2008. IEEE International Conference on* (pp. 589–594).

Danish Energy Agency. (2011).http://www.ens.dk/.

Dave, S. H. (2009). *Life cycle assessment of off-grid lighting applications: kerosene vs. solar lanterns*. Massachusetts Institute of Technology.

Emmott, C. J. M., Urbina, A., & Nelson, J. (2012). Environmental and economic assessment of ITO-free electrodes for organic solar cells. *Solar Energy Materials and Solar Cells*, *97*(0), 14–21.

Espinosa, N., García-Valverde, R., Urbina, A., & Krebs, F. C. (2011). A life cycle analysis of polymer solar cell modules prepared using roll-to-roll methods under ambient conditions. *Solar Energy Materials and Solar Cells*, *95*(5), 1293–1302.

Espinosa, N., García-Valverde, R., Urbina, A., Lenzmann, F., Manceau, M., Angmo, D., & Krebs, F. C. (2012). Life cycle assessment of ITO-free flexible polymer solar cells prepared by roll-to-roll coating and printing. *Solar Energy Materials and Solar Cells*, *97*(0), 3–13.

Espinosa, N., Hösel, M., Angmo, D., & Krebs, F. C. (2012). Solar cells with one-

day energy payback for the factories of the future. *Energy Environ. Sci.*, *5*(1), 5117–5132.

European, C. (2010). *Critical raw materials for the EU: Report of the Ad-hoc Working Group on defining critical raw materials*. European Commission.

Finkbeiner, M., Olsen, S., & Hesselbach, J. (2009). *Life Cycle Assessment of Illuminants. A Comparison of Light Bulbs, Compact Fluorescent Lamps and LED Lamps*. OSRAM Opto Semiconductors GmbH,.

Gagnon, L., Bélanger, C., & Uchiyama, Y. (2002). Life-cycle assessment of electricity generation options: The status of research in year 2001. *Energy Policy*, *30*(14), 1267–1278.

Gaines, L., & Cuenca, R. (2000). *Costs of lithium-ion batteries for vehicles* (No. ANL/ESD-42). Argonne National Laboratory.

Galagan, Y., de Vries, I. G., Langen, A. P., Andriessen, R., Verhees, W. J. H., Veenstra, S. C., & Kroon, J. M. (2011). Technology development for roll-to-roll production of organic photovoltaics. *Chemical Engineering and Processing: Process Intensification*, *50*(5-6), 454–461.

Galagan, Y., J.M. Rubingh, J.-E., Andriessen, R., Fan, C.-C., W.M. Blom, P., C. Veenstra, S., & M. Kroon, J. (2011). ITO-free flexible organic solar cells with printed current collecting grids. *Solar Energy Materials and Solar Cells*, *95*(5), 1339–1343.

García-Valverde, R., Cherni, J. A., & Urbina, A. (2010). Life cycle analysis of organic photovoltaic technologies. *Progress in Photovoltaics: Research and Applications*, *18*(7), 535–558.

Garcia-Valverde, R., Miguel, C., Martínez-Béjar, R., & Urbina, A. (2009). Life cycle assessment study of a 4.2 kWp stand-alone photovoltaic system. *Solar Energy*, *83*(9), 1434–1445.

Greijer, H., Karlson, L., Lindquist, S.-E., & Anders Hagfeldt. (2001). Environmental aspects of electricity generation from a nanocrystalline dye sensitized solar cell system. *Renewable Energy*, *23*(1), 27–39.

Guinée, J. (2002). *Handbook on Life Cycle Assessment*. Eco-Efficiency in Industry and Science, (Vol. 7).

Hammond, G., & Jones, C. (2011). *Inventory of Carbon & Energy (ICE) Version 2.1*. Department of Mechanical Engineering, University of Bath, UK.

Haxel, G., Hedrick, J. B., Orris, G. J., & (US), G. S. (2002). *Rare Earth Elements: Critical Resources for High Technology*. US Department of the Interior, US Geological Survey.

Hohenstein, W. G., & Wright, L. L. (1994). Biomass energy production in the United States: an overview. *Biomass and Bioenergy*, *6*(3), 161–173.

Huld, T., Suri, M., Dunlop, E., Albuisson, M., Wald, L., & others. (2005). Integration of Helioclim-1 database into PV-GIS to estimate solar electricity potential in Africa. Presented at the 20th European Photovoltaic Solar Energy Conference, Barcelona, Spain.

Hummers, W. S., & Offeman, R. E. (1958). Preparation of Graphitic Oxide. *Journal of the American Chemical Society*, *80*(6), 1339.

Hunan Boyun New Materials Co. Ltd.; www.itocn.net. (2011).

International Organisation for Standardisation (ISO). (1997). *ISO 14040: Environmental management – Life cycle assessment – Principles and framework*. Geneve, Switzerland.

Jungbluth, N. (2005). Life cycle assessment of crystalline photovoltaics in the Swiss ecoinvent database. *Progress in Photovoltaics: Research and Applications*, *13*(5), 429–446.

Kalowekamo, J., & Baker, E. (2009). Estimating the manufacturing cost of purely organic solar cells. *Solar Energy*, *83*(8), 1224–1231.

Kato, K., Hibino, T., Komoto, K., Ihara, S., Yamamoto, S., & Fujihara, H. (2001). A life-cycle analysis on thin-film CdS/CdTe PV modules. *Solar Energy Materials and Solar Cells*, *67*(1-4), 279–287.

Knapp, K., & Jester, T. (2001). Empirical investigation of the energy payback time for photovoltaic modules. *Solar Energy*, *71*(3), 165–172.

Krebs, F. C. (2009a). Polymer solar cell modules prepared using roll-to-roll methods: Knife-over-edge coating, slot-die coating and screen printing. *Solar Energy Materials and Solar Cells*, *93*(4), 465–475.

Krebs, F. C. (2009b). All solution roll-to-roll processed polymer solar cells free from indium-tin-oxide and vacuum coating steps. *Organic Electronics*, *10*(5), 761–768.

Krebs, F. C. (2009c). Roll-to-roll fabrication of monolithic large-area polymer solar cells free from indium-tin-oxide. *Solar Energy Materials and Solar Cells*, *93*(9), 1636–1641.

Krebs, F. C., Fyenbo, J., & Jørgensen, M. (2010). Product integration of compact roll-to-roll processed polymer solar cell modules: methods and manufacture using flexographic printing, slot-die coating and rotary screen printing. *Journal of Materials Chemistry*, *20*(41), 8994–9001.

Krebs, F. C., Fyenbo, J., Tanenbaum, D. M., Gevorgyan, S. A., Andriessen, R., van Remoortere, B., Galagan, Y., et al. (2011). The OE-A OPV demonstrator anno domini 2011. *Energy & Environmental Science*, *4*(10), 4116–4123.

Krebs, F. C., Gevorgyan, S. A., & Alstrup, J. (2009). A roll-to-roll process to flexible polymer solar cells: model studies, manufacture and operational stability studies. *Journal of Materials Chemistry*, *19*(30), 5442–5451.

Krebs, F. C., Nielsen, T. D., Fyenbo, J., Wadstrøm, M., & Pedersen, M. S. (2010). Manufacture, integration and demonstration of polymer solar cells in a lamp for the "Lighting Africa" initiative. *Energy & Environmental Science*, *3*(5), 512–525.

Krebs, F. C., Tromholt, T., & Jørgensen, M. (2010). Upscaling of polymer solar cell fabrication using full roll-to-roll processing. *Nanoscale*, *2*(6), 873–886.

Leung, D. Y. C., Yin, X. L., & Wu, C. Z. (2004). A review on the development and

commercialization of biomass gasification technologies in China. *Renewable and Sustainable Energy Reviews*, *8*(6), 565–580.

Manceau, M., Angmo, D., Jørgensen, M., & Krebs, F. C. (2011). ITO-free flexible polymer solar cells: From small model devices to roll-to-roll processed large modules. *Organic Electronics*, *12*(4), 566–574.

Matthews, D., Jaramillo, P., Matthews, H., McMichael, F., & Weber, C. (2009). DOE Solid-State Lighting Life Cycle Assessment. *DOE SSL Market Introduction Workshop Presentation, Chicago, IL*.

Mills, E. (2003). Technical and economic performance analysis of kerosene lamps and alternative approaches to illumination in developing countries. *Lawrence Berkeley National Laboratory Report*.

Nanomarkets. (2011). *Materials, Applications and Opportunities in Organic Photovoltaics*. Virginia, USA.

Niggemann, M., Zimmermann, B., Haschke, J., Glatthaar, M., & Gombert, A. (2008). Organic solar cell modules for specific applications--From energy autonomous systems to large area photovoltaics. *Thin Solid Films*, *516*(20), 7181–7187.

Norgate, T. E., & Rankin, W. J. (2002). The role of metals in sustainable development. *Proceedings, Green Processing*. Presented at the International Conference on the Sustainable Processing of Minerals, Queensland, Australia.

Optis, M. B. (2008). *Incorporating Life Cycle Assessment into the LEED Green Building Rating System*. University of Victoria.

Papasavva, S., Kia, S., Claya, J., & Gunther, R. (2001). Characterization of automotive paints: an environmental impact analysis. *Progress in Organic Coatings*, *43*(1–3), 193–206.

Papp, J. F., & Lipin, B. R. (2006). Chromite. *Industrial Minerals & Rocks: Commodities, Markets, and Uses* (7th ed.). Society for MIning, Metallurgy and Exploration, Inc.

Pehnt, M. (2001). Life-cycle assessment of fuel cell stacks. *International Journal of Hydrogen Energy*, *26*(1), 91–101.

Pehnt, M. (2006). Dynamic life cycle assessment (LCA) of renewable energy technologies. *Renewable Energy*, *31*(1), 55–71.

Photovoltaic Technology Research Advisory Council PV-TRAC. (2005). *A vision for photovoltaic technology*.

PlasticsEurope, A. (2010). LCA process inventories for refining and plastic production databases.

Powell, C., Bender, T., & Lawryshyn, Y. (2009). A model to determine financial indicators for organic solar cells. *Solar Energy*, *83*(11), 1977–1984.

Raugei, M., Bargigli, S., & Ulgiati, S. (2007). Life cycle assessment and energy pay-back time of advanced photovoltaic modules: CdTe and CIS compared to poly-Si. *Energy*, *32*(8), 1310–1318.

Roes, A. L., Alsema, E. A., Blok, K., & Patel, M. K. (2009). Ex-ante environmental and economic evaluation of polymer photovoltaics. *Progress in Photovoltaics: Research and Applications*, *17*(6), 372–393.

Rydh, C. J., & Karlström, M. (2002). Life cycle inventory of recycling portable nickel–cadmium batteries. *Resources, Conservation and Recycling*, *34*(4), 289–309.

Rydh, C. J., & Sandén, B. A. (2005a). Energy analysis of batteries in photovoltaic systems. Part I: Performance and energy requirements. *Energy Conversion and Management*, *46*(11-12), 1957–1979.

Rydh, C. J., & Sandén, B. A. (2005b). Energy analysis of batteries in photovoltaic systems. Part II: Energy return factors and overall battery efficiencies. *Energy Conversion and Management*, *46*(11-12), 1980–2000.

Schleisner, L. (2000). Life cycle assessment of a wind farm and related externalities. *Renewable Energy*, *20*(3), 279–288.

Swiss Centre for Life Cycle Inventories. (2011). Ecoinvent Centre.

Tiyarov, M. A., Konstantinova, N. A., Sharov, Y. V., & Sobolev, G. V. (2004). Modern Equipment Sets for Production of Demineralized and Deionized Water. *Chemical and Petroleum Engineering*, *40*(7/8), 379–383.

White, S. W. (1998). *Net energy payback and CO2 emissions from 3He fusion and wind electrical power plants. Ph.D. Dissertation*. University of Wisconsin-Madison.

White, S. W., & Kulcinski, G. L. (2000). Birth to death analysis of the energy payback ratio and CO2 gas emission rates from coal, fission, wind, and DT-fusion electrical power plants. *Fusion Engineering and Design*, *48*(3-4), 473–481.

World Energy Outlook. (2010). International Energy Agency.

Zackrisson, M., Avellán, L., & Orlenius, J. (2010). Life cycle assessment of lithium-ion batteries for plug-in hybrid electric vehicles – Critical issues. *Journal of Cleaner Production*, *18*(15), 1519–1529.

Zimmermann, B., Glatthaar, M., Niggemann, M., Riede, M. K., Hinsch, A., & Gombert, A. (2007). ITO-free wrap through organic solar cells--A module concept for cost-efficient reel-to-reel production. *Solar Energy Materials and Solar Cells*, *91*(5), 374–378.

Zimmermann, B., Würfel, U., & Niggemann, M. (2009). Longterm stability of efficient inverted P3HT:PCBM solar cells. *Solar Energy Materials and Solar Cells*, *93*(4), 491–496.

CHAPTER 5
Conclusions

5.1. The need of changing energy models

Modern societies that want to be preserve an ecological balance, in view of the energy panorama, are urged to rethink and redesign the energy model into a more sustainable one; starting from seeking for secure resources, followed by using of low-carbon technologies and the use of more efficient technologies. Renewable energies as low-carbon technologies can tackle climate change targets. Sunlight is in particular the most abundant resource and sustainable resource, and this is a reason for including it as part of the solution.

Among the existing PV technologies, organic photovoltaics (OPV) has evolved in an exponential way in the last five years exhibiting a large potential. Despite there are still important challenges to overcome, there is an active research in this subject that has enabled for example that the efficiency of the devices has increased by a factor of 10 during the last decade. The progress has been delivered by the developments and steps forward such as the discovery of the semiconducting polymers, the use of bulk heterojunction in the active layer, the inverted geometry structure, the introduction of interfacial layers, and the continuous fabrication; all of which lead to expect fast, cheap and low environmental impact production methods.

5.2. Film forming techniques and materials for OPV

Promising materials have been presented as potential ingredients for OPV devices. The fabrication of small devices at a lab scale, with the most successful combination of them has been realized in this thesis. Replacement of some materials though, as PEDOT:PSS, due to hygroscopic issues, was attempted; although moderate PCE has been achieved.

Due to the fact that mostly of the materials involved in the fabrication of the polymer solar cells are susceptible to be deposited from solution, a wide range of possibilities emerge for the massive fabrication of OPV. Moreover, inverted geometry that provides advantages as humidity stability and the possibility of using less reactive materials (such as silver instead of aluminium), has been developed. This has been treated in Chapter 3.

In terms of going towards an environmentally friendly roll-to-roll processing of polymer solar cells, there is a semi industrial scale pilot plant at Risø DTU, where some printing and coating techniques have been already tested with good results in functional devices.

The most used film-forming technologies, but not massively explored in the context of polymer solar cells, have been herein gathered. Since the number of different techniques can rise up to 1000, analysis grounded on a multi-criteria decision making methodology has been used to assess of the most suited coating and printing technologies. Three groups appear in which the technologies have similar score: a first group, formed by Gravure, Flexography, Offset, Inkjet, Curtain and Screen, revealing a certain predominance of printing techniques over coating ones. A second score group, which include Slot die, Doctor Blade, Knife

over edge. And finally a third group where Slide coating scored as the worst technique for the purpose of organic layers deposition, mainly due to the low score in criteria such as Thickness control, Reproducibility and Maximum throughput, which are parameters with high weights in the criteria selection process.

The characterization of materials and devices is an important step to check whether the limitations are and improve the performance of the devices. There are challenges still with the understanding of the links between the nanoscale behaviour and the performance at a device scale. AFM experiments were conducted, as well as DSC or GIWAXS, that provided useful information, e.g. to investigate the degradation of the devices due to morphology changes induced by UV irradiation and ozone exposure. If the production of solar cells is realized in a continuous way, in line characterization techniques should be developed.

5.3. Life-cycle Assessment applied to OPV

The life cycle assessments of several OPV systems have been investigated to evaluate the potential of OPV. This methodology was initially applied to evaluate solar modules produced at a medium-scale by a R2R method known as ProcessOne. Energy payback times (EPBT) ranging from 1.35 to 2.02 years, were found corresponding to 3% and 2% efficiency, respectively. The study pointed out as well that 90% of the total energy was embedded in the ITO, the transparent conductor oxide.

Then, a new approach of architecture that tried to solve the indium scarcity problem was evaluated. In this case, the EPBT value for the ITO-free Hiflex process is 9.45 years, for 1% efficiency and 36.7% active area. The main reasons for this significantly poorer value with respect to ProcessOne are the lower efficiency (1% vs. 3%) and, to a lesser extent, the lower active/total area ratio (36.7% vs. 68.1%).

The starting point of this work was then to get rid of indium but it would seem that the entire processing of OPV had to be redefined at least so that vacuum coating steps are entirely avoided. One additional point is that if there is a problem with the use of indium, there will also be a problem with silver. Even if the latter is a more accessible element, exhibits approximately the same abundance as indium, thus it can be a silver problem in the context of large-scale manufacture of OPV.

In order to calculate the balance of OPV cells when they are integrated in a lamp, this product was also analysed. The analysis revealed that although it had not a good energy payback time (it was 9.8 years), the OPV lamp could provide a significant advantage for remote applications from an environmental point of view. However, if minor improvements are made in the components, and in the OPV module itself, this could lower substantially its EPBT.

The major conclusion that can be drawn from these three first analyses - ProcessOne modules, ITO free modules and an OPV lamp- is that OPV future developments should thus seek processes that do not involve silver, indium,

vacuum, or inert gases; they should maximize the usage of the processed area, and if possible use water-based solvents.

Grounded on these previous statements, a new collection of routes for processing polymer solar cells were assessed, beating therefore all known marks in terms of use of energy and materials so far. Among them a route called Process H is the win option. Significantly shorter EPBT than the reference process, ProcessOne, of 1.42-0.71 years was achieved just with a power conversion efficiency of 0.5-1%. An outstanding consequence of the new routes concepts is that material inventory share and direct process energy, are balanced in equivalent primary energy, in comparison with ProcessOne and ITO-free modules.

All the previous LCAs were focused on energy consumption and energy related impact categories, whereas for Process H chemical related impact categories covering ecotoxicity and human toxicity were investigated as well. The most impacted categories by the production of OPV modules by Process H are Fossil fuels, Carcinogens, Respiratory inorganics and Climate change. The pressure on fossil fuels depletion is mainly due to PET production and electricity directly used in the manufacturing. Both raw materials have significant impact as well on respiratory inorganics category. Silver has the highest score in Carcinogenics category, due to the potentially carcinogenic damage from the upstream materials production, i.e. in its extraction.

General conclusions

The main goal of this work has been to study routes and materials typically used in the production of polymer solar cells, to quantify the environmental impacts for all mass and energy flows within its production, in order to provide a better understanding of the way the technology is impacting the environment. This has thus allowed proposing improvements in order that OPV modules fabrication is optimized and has a lower carbon footprint.

Laboratory production of PV devices at small scale at the UPCT and in a R2R pilot plant at Risø DTU, has made possible to carry out these LCA studies with a great detail. Life cycle assessment methodology has proven to be a very useful tool for the identification of the premises in which the developments for the future OPV should be.

The developments made from ProcessOne to Process H enable to make a breakthrough in the EPBT-efficiency ratio; i.e. to achieve significantly lower EPBT –even with lower efficiency- and further improvements can be made through easily applicable and more challenging improvements. The LCA directed improvements led to yield better EPBT, despite the trade-off in performance. Moreover there was a reduction in the equivalent primary energy by a factor of ~10 with respect to reference processes.

The aim of the present thesis has been to establish the parameters that are critical for the beneficial use of polymer solar cells in society, as well as provide a supported basis for making the improvements, towards this technology can be a productively disruptive alternative.

Future and Outlook

OPV has grown at an accelerated pace, but there are some problems to undertake. New materials for active layer are needed since the existing limitations of the present materials in terms of degradation and stability. With regard to electrode materials, discrepancies of sputtering energy consumption have to be solved as well as the search of alternative materials for electrodes have to be pursued.

There are some questions that will remain open since OPV has still some restraints, like low efficiency and limited lifetime expectancy due to mentioned degradation mechanisms. Despite flexible materials are inherently beneficial when it comes to sustainability and eco-friendliness (light weight, initial source reduction, lower energy costs and easy disposal compared to rigid alternatives), applications lifetime should match with the OPV module lifetime.

At the end of their lifetime, the OPV systems will have to be decommissioned. The possible scenarios as incineration to recover part of energy, or landfill can be easily performed, although it would be desirable that OPV cells will be recycled. A carefully material selection, that accounts for abundance and end of life stages, should be addressed in the future s. As an example, biodegradable materials could play an important role if they can be used as substrate.

Another topic derived from this work in the pursuit of lower the energy embedded in the OPV manufacturing, is the need of specifically designing patterns for the available deposition techniques. Those patterns would enable on the one hand to configure at will the cells interconnexion (series-parallel) what it can fulfil the requirements of the application (higher voltage or higher currents), and on the other hand to optimize material usage.

Beyond the scope of this thesis are as well economy and markets for OPV, which have not been treated in depth in this work but that will be critical for a successful deployment of this technology.

List of scientific contributions

JCR publications

1. Espinosa, N., Hösel, M., Angmo, D., & Krebs, F. C. (2012). Solar cells with one-day energy payback for the factories of the future. *Energy Environ. Sci.*, *5*(1), 5117–5132.
2. Espinosa, N., García-Valverde, R., Urbina, A., Lenzmann, F., Manceau, M., Angmo, D., & Krebs, F. C. (2012). Life cycle assessment of ITO-free flexible polymer solar cells prepared by roll-to-roll coating and printing. *Solar Energy Materials and Solar Cells*, *97*(0), 3–13.
3. Abad, J., Espinosa, N., Ferrer, P., García-Valverde, R., Miguel, C., Padilla, J., Alcolea, A., et al. (2012). Molecular structure of poly(3-alkyl-thiophenes) investigated by calorimetry and grazing incidence X-ray scattering. *Solar Energy Materials and Solar Cells*, *97*(0), 109–118.
4. García-Valverde, R., Espinosa, N., & Urbina, A. (2012). Simple PEM water electrolyser model and experimental validation. *International Journal of Hydrogen Energy*, *37*(2), 1927–1938.
5. García-Valverde, R., Espinosa, N., & Urbina, A. (2011). Optimized method for photovoltaic-water electrolyser direct coupling. *International Journal of Hydrogen Energy*, *36*(17), 10574–10586.
6. Reese, M. O., Gevorgyan, S. A., Jørgensen, M., Bundgaard, E., Kurtz, S. R., Ginley, D. S., Olson, D. C., et al. (2011). Consensus stability testing protocols for organic photovoltaic materials and devices. *Solar Energy Materials and Solar Cells*, *95*(5), 1253–1267.
7. Espinosa, N., García-Valverde, R., Urbina, A., & Krebs, F. C. (2011). A life cycle analysis of polymer solar cell modules prepared using roll-to-roll methods under ambient conditions. *Solar Energy Materials and Solar Cells*, *95*(5), 1293–1302.

8. Abad, J., Espinosa, N., García-Valverde, R., Colchero, J., & Urbina, A. (2011). The influence of UV radiation and ozone exposure on the electronic properties of poly-3-octyl-thiophene thin films. *Solar Energy Materials and Solar Cells*, *95*(5), 1326–1332.
9. Espinosa, N., Dam, H. F., Tanenbaum, D. M., Andreasen, J. W., Jørgensen, M., & Krebs, F. C. (2011). Roll-to-Roll Processing of Inverted Polymer Solar Cells using Hydrated Vanadium(V)Oxide as a PEDOT:PSS Replacement. *Materials*, *4*(1), 169–182.
10. Espinosa, N., García-Valverde, R., & Krebs, F. C. (2011). Life-cycle analysis of product integrated polymer solar cells. *Energy & Environmental Science*, *4*(5), 1547–1557.

International conference contributions

11. Espinosa, N., García-Valverde, R. , Urbina, A., Krebs, F.C. (2011). Life-cycle assessment of polymer solar cells prepared by roll to roll techniques. Oral Presentation in at the *Global Organic Photovoltaic Conference* (GOPV), Hangzhou, CHINA.
12. J. Abad, N. Espinosa, A. Urbina, J. Colchero. (2011) Morphology, contact potential and electrical properties of P3HT/PCBM organic solar cells studied by scanning probe microscopy. Visual Presentation at the *Symposium on Functional π-Electron Systems (Fπ10)*, Beijing, CHINA
13. Lenzmann, F., Kroon, J., Andriessen, R., Espinosa, N., Garcia-Valverde, R., & Krebs, F. (2011). Refined life-cycle assessment of polymer solar cells (Vol. 2011, p. 2010). Presented at the *26th European Photovoltaic Solar Energy Conference and Exhibition (EUPVSEC)*, Hamburg, GERMANY.
14. N. Espinosa, C. Emmott, R. García-Valverde, B. Azzopardi, J. Mutale, F.C. Krebs, A. Urbina and J. Nelson. An environmental life-cycle analysis of polymer solar cells. Visual Presentation at Hybrid and Organic Photovoltaics Conference (HOPV11), Valencia, SPAIN.
15. N. Espinosa, R. García-Valverde, A. Urbina, F.C. Krebs. (2010). Life-cycle analysis of product integrated polymer solar cells. Visual Presentation at International Summit on OPV Stability (ISOS-3). Roskilde, DENMARK.
16. N. Espinosa, R. García-Valverde, A. Urbina, F.C. Krebs. (2010). Life-cycle assessment in polymer solar cells. Visual Presentation at *International Summit on OPV Stability (ISOS-3)*, Roskilde, DENMARK.

17. J. Abad, N. Espinosa, A. Urbina, J. Colchero. (2010). Nanoscale ultraviolet and ozone degradation of P3OT thin films studied by scanning probe microscopy and related techniques. Visual Presentation at *International Summit on OPV Stability (ISOS-3)*, Roskilde, DENMARK.
18. N. Espinosa, R. García-Valverde, M.S. García-Cascales, A. Urbina. (2010). Multi-criteria decision method applied to film forming techniques in polymer solar cells. Visual Presentation at the 4th *Technologies for polymer electronics Conference*. Rudolstadt, GERMANY.
19. J. Abad, N. Espinosa, A. Urbina, J. Colchero. (2010). Nanoscale ultraviolet and ozone degradation of P3OT thin films studied by scanning probe microscopy and related techniques. Visual Presentation at the 4th *Technologies for polymer electronics Conference*. Rudolstadt, GERMANY.
20. N. Espinosa, F. Henao, R. García-Valverde, L. Serrano, A. Hernández-Ortega, J.A. Cherni, A. Urbina. (2010). Rural Electrification in Ethiopia: An Assessment of Photovoltaic Technologies Using SURE-DSS, a Decision-Support System. Visual Presentation at the *25th European Photovoltaic Solar Energy Conference and Exhibition (EU PVSEC) / 5th World Conference on Photovoltaic Energy Conversion (WCPEC-5)*, Valencia, SPAIN.
21. R. García-Valverde, N. Espinosa, R. Martínez-Béjar, A. Urbina. (2010). Performance: Modelling from datasheets for dynamic anomaly detection at monitorised on-grid and stand-alone PV facilities. Visual Presentation at the *25th European Photovoltaic Solar Energy Conference and Exhibition (EU PVSEC) / 5th World Conference on Photovoltaic Energy Conversion (WCPEC-5)*, Valencia, SPAIN.
22. Espinosa, N., García-Valverde, R., García-Cascales, M. S., & Urbina, A. (2010). Towards low-cost manufacturing of organic solar cells: multi-criteria assessment of fabrication technologies. Presented at the *International Conference on Renewable Energies and Power Quality*, Granada, SPAIN.
23. Sánchez-Lozano, J. M., García-Cascales, M. S., Espinosa, N., & Urbina, A. (2010). Multi-criteria decision methods applied to the assessment of photovoltaic technologies. Presented at the *International Conference on Renewable Energies and Power Quality*, Granada, SPAIN.

National conference contributions

24. N. Espinosa-Martínez, C. Romojaro. (2008) La Energía Solar en la Región de Murcia. Poster at *Congreso Nacional de Medio Ambiente (CONAMA)*. Libro de Abstract. ISBN: 978-84-613-1481-2. Madrid, SPAIN.
25. C. Romojaro, N. Espinosa-Martínez. (2008). Reducción Voluntaria y Compensación de las Emisiones. Poster at *Congreso Nacional de Medio Ambiente (CONAMA)*. Libro de Abstract. ISBN: 978-84-613-1481-2, Madrid, SPAIN.